Department of Mechanical and
Aerospace Engineering

Rotor Dynamics Laboratory

SCHOOL OF ENGINEERING AND APPLIED SCIENCE

RESEARCH CONTRACT
[FINAL REPORT]

DESIGN STUDY OF MAGNETIC EDDY-CURRENT VIBRATION SUPPRESSION DAMPERS FOR APPLICATION TO CRYOGENIC TURBOMACHINERY

For

NATIONAL AERONAUTICS AND SPACE ADMINISTRATION
LEWIS RESEARCH CENTER
NAG-3-263

By

E. J. Gunter
Professor

R. R. Humphris
Research Professor

and

S. J. Severson
Research Assistant

December 1983

UVA/528210/MAE84/101

University of Virginia
Charlottesville, Virginia 22901

RESEARCH CONTRACT

[FINAL REPORT]

DESIGN STUDY OF MAGNETIC EDDY-CURRENT VIBRATION SUPPRESSION DAMPERS FOR APPLICATION TO CRYOGENIC TURBOMACHINERY

For

NATIONAL AERONAUTICS AND SPACE ADMINISTRATION

LEWIS RESEARCH CENTER

NAG-3-263

By

E. J. Gunter
Professor

R. F. Humphris
Research Professor

and

S. J. Severson
Research Assistant

December 1983

UVA/528210/MAE84/101

TABLE OF CONTENTS

Page

Nomenclature

Vector flux per unit length	$\vec{A}$	
Magnetic flux density	$\vec{B}$	tesla = w/m^2
Electric flux density	$\vec{D}$	$coulomb/m^2$
Electric field intensity	$\vec{E}$	volt/m
Magnetic field intensity	$\vec{H}$	ampere/m
Electric current density	$\vec{J}$	$ampere/m^2$
Magnetization	$\vec{M}$	ampere/m
Area	A	m^2
Permittivity of free space	ε_o	farad/m
Dielectric constant or permittivity	ε	
Electric charge density	ρ_s	c/m^3
Conductivity	σ	mhos/m
Permeability of free space	μ_o	henry/m
Relative permeability	μ	
Resistivity	ρ	ohm-m

I. Introduction

Cryogenic turbomachinery of the type used to pump high pressure fuel (liquid H_2) and oxidizer (liquid O_2) to the main engines of the Space Shuttle have experienced rotor instabilities. Subsynchronous whirl, an extremely destructive instability, has caused bearing failures and severe rubs in the seals (1,2). These failures have resulted in premature engine shutdowns or, in many instances, have limited the power level to which the turbopumps could be operated. The labyrinth seals originally used in these pumps were initially indicated as a source of subsynchronous vibration (2). Other principal sources of self-excited instabilities in the hydrogen pump, in addition to the seals, are aerodynamic cross coupling turbine and impeller forces and internal shaft hysteresis and friction forces caused by relative motion between surfaces. All of these mechanisms can induce self-excited rotor non-synchronous whirl motion in a pump (3-6). The hydrogen pump, for example, has all three instability mechanisms present because of its built-up structure of spline fits and high energy density level (7). The SSME oxygen pump as well as the hydrogen pump is susceptible to self-excited whirl motion (8).

The occurrence of self excited instability can be extremely dangerous because the whirl amplitude of motion may increase rapidly with increasing energy input. Unlike synchronous vibrations whose amplitudes reduce as the critical speed is traversed, subsynchronous whirl orbits may spiral out until metal to metal contact occurs in the impellers and seals. The occurence of metallic rubs on the oxygen pump is particularly serious as catastrophic fires may occur (9). High synchronous vibrations in a pump may be controlled by proper balancing and by avoiding operation near the critical speeds. However, with self-excited whirl motion, improvement of balance has little or no effect. In fact, it may even aggravate the situation (10).

The large rotor orbits caused by self-excited whirl induce high bearing loads. Since rolling element bearing life varies approximately inversely as the third power of loading, an increase in bearing loading can lead to a dramatic reduction in bearing life. Current turbopump designs do not include provisions for multiplane trim balancing of the built-up rotor after final assembly in the pump casing. Although the impellers, turbine wheels, seal runners and the shaft may be individually balanced, a satisfactorily balanced assembly is not always guaranteed.

The need for dissipating vibrational energy in high performance turbomachines has long been recognized. Many of today's turbojet engines in both civilian and military aircraft incorporate vibration dampers at or near bearing supports (11).

With the availability of bearing lubricating oils in aircraft engines, a device known as a "squeeze film" damper has been used quite successfully in attenuating potentially large and damaging forces (11). Over the years, numerous investigators have produced both analyses and test results on squeeze film dampers (12-21). Because of these efforts, it is possible to design such dampers with the assurance that they will perform reliably in many different applications. Viscous "squeeze film" dampers have successfully attenuated both synchronous and nonsynchronous whirling if properly designed.

In the Space Shuttle Main Engine (SSME) turbopumps, liquid H_2 and LOX are used to cool the rolling element bearings. Because of the extremely low viscosity of the liquids (liquid H_2 has a viscosity approximately equal to air at room temperature), they cannot be considered as adequate in providing a damping media for either viscous shear or squeeze film damping. Unless suitable energy dissipating devices can be developed, future generation turbopumps may be susceptible to the same potentially destructive vibrations as have been encountered in the current generation of cryogenic turbomachinery (9).

The objective is to examine one of the damping mechanisms that might be suitable for the development of a practical discrete cryogenic machinery

damper. Listed below are the more common damping mechanisms available.

1. Viscous shear and squeeze film bearings
2. Visco-elastic material dampers, such as rubber isolation pads
3. Coulomb-friction dampers
4. Turbulent flow close clearance seals
5. Eddy-current or magnetic dampers

The first and probably most common damping mechanism is viscous damping; here the damping force is directly proportional to velocity. The constants of proportionality differ however, in the case of "squeeze-film" damping, as compared to viscous shear damping. "Squeeze-film" coefficients vary directly with viscosity and as the cube of damper length while varying inversely as the cube of the clearance. To obtain any effective damping with very low viscosity fluids such as liquid H_2 and O_2 either the size of the damper must be made quite large and/or the clearance between moving and stationary members should be made quite small. The damping coefficient for a shear film damper is directly proportional to the fluid viscosity and the shear area and again inversely proportional to the first power of the clearance. This type of damper would provide very little damping unless made prohibitively large and would not be acceptable in a compact turbomachine.

A second type of damping, visco-elastic or hysteresis damping, is generally produced by elastic materials. Almost all materials exhibit some sort of damping when strained repeatedly. Visco-elastic materials such as rubber, and used in machinery, provide a sizeable amount of damping and are generally quite effective. Obviously rubber would not be suitable at cryogenic temperatures since it would lose its visco-elastic properties, i.e., become very brittle (22).

A third type of damping used in machinery isolators is friction or coulomb damping. In a friction damper the force is directly proportional to the coefficient of friction of the contacting surfaces, the area, and the pressure applied to bring the plates into contact. The damping force in this case is not proportional to the velocity. The problem with using this type of damper in rotating machinery is the inability to

predict the amount of damping available for any given situation. Values of the coefficient of friction are unreliable. The contacting surfaces under too little pressure, slip relative to one another or, with too great a pressure, do not move at all and therefore provide little, if any, damping. A considerable effort was expended by Rocketdyne to incorporate a colomb-friction damper into the SSME hydrogen pump bearing supports. This effort was unsuccessful.

The stability of the hydrogen pump was eventually improved by incorporating close clearance seals and stiff bearing supports based on design recommendations of the Rotor Dynamics Laboratory of the University of Virginia. The turbulent flow seals produce both principal and cross-coupling stiffness and damping coefficients. Under proper selection of bearing support stiffnesses and seal clearances, the seal effects can promote rotor stability. However, critical speeds are now placed in the operating speed range, and when clearance seal wear occurs, this stabilizing effect is lost.

A fifth damping mechanism is the eddy-current or magnetic damper. Many devices based on this type of damping are currently being used. Most of these applications are in instruments where the damping forces required are quite small.

The damping force is velocity or frequency dependent but more importantly, the damping coefficient varies inversely as the resistivity of a conductor moving in the magnetic field. If such a damper were to be used in a liquid H_2 pump, for example, the extremely low temperatures encountered would significantly decrease the resistivity of the conductor material, thereby producing a reasonable value of damping.

This report outlines the efforts of a preliminary study of the feasibility of using an eddy-current type of damping mechanism for the SSME.

II. Fundamental Design Equations for Eddy Current Damper

The fundamental electromagnetic field equations, pertaining to the design and analysis of an eddy current cryogenic pump damper, are derived from Maxwell's equations.

These equations are as follows:

2.1. Electro-Static Field Equation. The displacement current density J is related to the charge density ρ_s per unit volume by

$$\vec{J} = \rho_s \vec{V} \quad , \tag{2.1.1}$$

where $\vec{V}$ is the average velocity.

The electric current across a surface S is defined as the rate at which charge crosses that surface.

The current flow across this surface is given by

$$I = \int_S \vec{J} \cdot \vec{dS} = \int_s \vec{J} \cdot \vec{n} dS \quad . \tag{2.1.2}$$

The gradient of the displacement field is equal to the charge density

$$\nabla \cdot \vec{D} = \rho_s \tag{2.1.3}$$

where $\vec{D}$ is the density of electric flux passing through a given area. This relationship is the differential form of Gauss' Law.

2.2 Electro-Magnetic Field Equation - Ampere's Law (Maxwell's First Law). The ampere-turn drop around a closed circuit equals the current enclosed

$$I = \oint_c \vec{H} \cdot \vec{dl} \tag{2.2.1}$$

where $\vec{H}$ = magnetization vector.

From Equation (1.1.2),

$$I = \oint_c \vec{H} \cdot d\vec{l} = \iint_S \vec{J} \cdot d\vec{S} \qquad (2.2.2)$$

By Stokes Law

$$\oint_c \vec{H} \cdot d\vec{l} = \iint_S (\nabla \times \vec{H}) \cdot d\vec{S}$$

Hence $$\nabla \times \vec{H} = \vec{J} \qquad (2.2.3)$$

By replacing $\vec{J}$ by the total current density which is the sum of the conduction current density and the displacement current density, then Equation (2.2.3) can be written as

$$\nabla \times \vec{H} = \vec{J}_c + \frac{\partial \vec{D}}{\partial t} . \qquad (2.2.4)$$

The above is called Maxwell's first equation.

2.3 Faraday's Law of Induction (Maxwell's Second Law). The Faraday law of induction states that the voltage V (induced) is equal to

$$V \text{ induced} = -N \frac{d\phi}{dt} \qquad (2.3.1)$$

Where N = number of turns in coil

ϕ = flux linked

Let $\vec{E}$ be called the electric field and be defined as the gradient of a voltage (scaler function) by

$$\vec{E} = \nabla V . \qquad (2.3.2)$$

The voltage is defined by the contour integral of the electric field by

$$V = \oint_c \vec{E}\cdot\vec{dl} , \tag{2.3.3}$$

By Stoke's theorem

$$V = \oint_c \vec{E}\cdot\vec{dl} = \iint_S (\nabla \times \vec{E})\cdot\vec{dS} \tag{2.3.4}$$

From Equation 1.3.1 for one turn

$$V = -\frac{d\phi}{dt} .$$

If we define the quantity $\vec{B}$ as the flux density or magnetic induction, then

$$\vec{B} = \nabla_S \phi . \tag{2.3.5}$$

We can write

$$\iint_S (\nabla \times \vec{E})\vec{dS} = -\frac{\partial}{\partial t} \iint_S \vec{B}\cdot\vec{dS} . \tag{2.3.6}$$

Dropping the integral sign, we have

$$\nabla \times \vec{E} = -\frac{\partial \vec{B}}{\partial t} . \tag{2.3.7}$$

This is the Maxwell's second equation.

2.4 Divergence of the Magnetic Field (Maxwell's Third Law). If we consider the flux passing through a pie-shaped section radial to a current I in a conductor, then the flux entering the section also emerges from the section and the net flux build-up is zero.

$$\phi_{enter} - \phi_{emerge} = 0 \tag{2.4.1}$$

or

$$\vec{B}_{enter}\cdot\vec{dS} - \vec{B}_{emerge}\cdot\vec{dS} = 0 , \tag{2.4.2}$$

but Equation 2.4.2 represents a closed surface integral,

$$\oiint_S \vec{B}\cdot d\vec{S} = 0, \tag{2.4.3}$$

and by use of the divergence theorem,

$$\oiint_S \vec{B}\cdot d\vec{S} = \iiint_u (\nabla\cdot\vec{B})\, du = 0 \tag{2.4.4}$$

or

$$(\nabla\cdot\vec{B}) = 0 . \tag{2.4.5}$$

This is Maxwell's third equation and simply states that magnetic fields neither emerge from nor close at a point.

2.5 Constitutive Relations. To the above differential equations are added the constitutive relationships describing the macroscopic properties of the medium being dealt with in terms of permittivity ε, permeability μ and conductivity σ. The quantities ε, μ, and σ are not necessarily simple constants. For example, in the case of ferromagnetic materials, the B-H relationship may be highly nonlinear. These constitutive relations are given by

$$\vec{D} = \varepsilon\vec{E} \tag{2.5.1}$$

$$\vec{B} = \mu\vec{H} \tag{2.5.2}$$

$$\vec{J} = \sigma\vec{E} . \tag{2.5.3}$$

2.6 Simplified Equations for an Eddy-Current Damper*

Magnetic Induction - $\vec{B}$

The flux ϕ_B in webers for a magnetic field can be defined in exact analogy with the flux ϕ_E for the electric field, namely

$$\phi_B = \int \vec{B} \cdot \vec{dS} \ , \tag{2.6.1}$$

where $\vec{B}$ is the basic magnetic field vector called the magnetic induction in gauss or webers/meter^2 and the integral is taken over the surface for which ϕ_B is defined.

The definition of $\vec{B}$ is as follows: If a positive test charge q_o is fired with velocity $\vec{v}$ through a point P and if a (sideways) force $\vec{F}$ acts on the moving charge, a magnetic induction $\vec{B}$ is present at point P, where $\vec{B}$ is the vector that satisfied the relation

$$\vec{F} = q_o \vec{v} \times \vec{B} \ , \tag{2.6.2}$$

$\vec{v}$, q_o, and $\vec{F}$ being measured quantities. The magnitude of the magnetic deflecting force $\vec{F}$, according to the rules for vector products, is given by

$$F = q_o \, v \, B \sin \theta \tag{2.6.3}$$

where θ is the angle between $\vec{v}$ and $\vec{B}$. The magnetic field always acts at right angles to the direction of motion.

The units of B are:

1 tesla = 1 weber/m^2 = 10^4 gauss = 1 newton/coul(m/sec) = 1 newton/amp-m

Faraday's Law of Electromagnetic Induction

Faraday's Law of Induction says that the induced emf ξ in a circuit is equal to the negative rate at which the flux through the circuit is changing. If the rate of change of flux is in webers/sec, the emf ξ will be in volts. In equation form,

$$\xi = - \frac{d\phi}{dt} \ . \tag{2.6.4}$$

The minus sign is an indication of the direction of the induced emf. Lenz's Law states that the induced current resulting from the induced emf will appear in such a direction that it opposes the change that produced it.

*From material and relations found in D. Halliday and R. Resnick, Physics, John Wiley & Sons, Inc., 1965.

As an example, consider Figure 1 which shows a rectangular loop of wire of width L, one end of which is in a uniform magnetic field $\vec{B}$ pointing at right angles to the plane of the loop. This field of $\vec{B}$ may be produced in the gap of a large permanent magnet or an electromagnetic. The dashed lines show the assumed limits of the magnetic field. The experiment consists of pulling the loop to the right at a constant speed v. The flux ϕ_B enclosed by the loop is

$$\phi_B = BLx \tag{2.6.5}$$

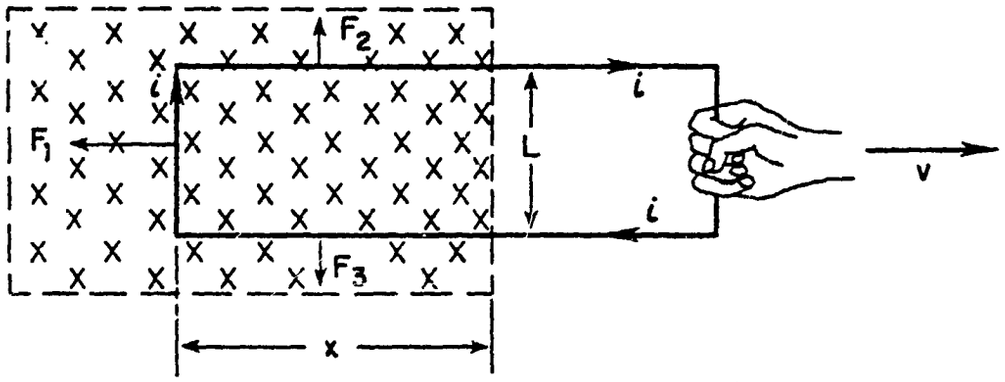

Figure 1. A rectangular loop is pulled out of a magnetic field with velocity v.

From Faraday's Law the induced emf is

$$\xi = -\frac{d\phi}{dt} = -\frac{d(BLx)}{dt} = -BL\frac{dx}{dt} = BLv, \tag{2.6.6}$$

where $-\frac{dx}{dt}$ was made equal to the speed v at which the loop is pulled out of the magnetic field. This induced emf sets up a current in the loop, determined by the loop resistance R,

$$i = \frac{\xi}{R} = \frac{BLv}{R} \quad . \tag{2.6.7}$$

From Lenz's Law, this current must be clockwise in the above figure since it opposes the change (the decrease in ϕ_B) by setting up a field that is parallel to the external field within the loop.

The current in the loop will cause forces $\vec{F}_1$, $\vec{F}_2$, and $\vec{F}_3$ to act on the three conductors, as given by equation 2.6.3. Because $\vec{F}_2$ and $\vec{F}_3$ are equal and opposite, they cancel each other. $\vec{F}_1$, which is the force that opposes any effort to move the loop, is given in magnitude from equations 2.6.3 and 2.6.7 as

$$F_1 = i\ L\ B \sin 90° = \frac{B^2L^2v}{R} \text{ (newton)}. \qquad (2.6.8)$$

For completeness, a check of equation 2.6.8 for units is as follows:

$$i \text{ (amp)} = \frac{\xi}{R} \left(\frac{\text{volts}}{\text{ohm}}\right) = \frac{BLv}{R} \left(\frac{\text{weber}}{\text{meter}^2} \times \text{meter} \times \frac{\text{meter}}{\text{sec}} \times \frac{1}{\text{ohm}}\right)$$

$$= \frac{BLv}{R} \left(\frac{\text{weber}}{\text{sec-ohm}}\right)$$

or

$$\text{ohm} = \left(\frac{\text{weber}}{\text{amp-sec}}\right)$$

Thus,

$$F = \frac{B^2L^2v}{R} \left(\frac{\text{weber}^2}{\text{meter}^4} \times \text{meter}^2 \times \frac{\text{meter}}{\text{sec}} \times \frac{\text{amp-sec}}{\text{weber}}\right)$$

$$= \frac{B^2L^2v}{R} \left(\frac{\text{weber-amp}}{\text{meter}}\right),$$

and since

$$1 \text{ (weber)} = \left(\frac{\text{newton-meter}}{\text{amp}}\right),$$

then

$$F = \frac{B^2L^2v}{R} \left(\frac{\text{newton-meter}}{\text{amp}} \times \frac{\text{amp}}{\text{meter}}\right)$$

or

$$F = \frac{B^2L^2v}{R} \text{ (newton)}$$

The resistivity, ρ, is a characteristic of a material rather than of a particular specimen of a material and has the units of ohm-meter. Since the resistance of an electrical conductor is directly proportional to the length of the conductor and is inversely proportional to the cross sectional area, it is related to the resistivity as follows:

$$R = \rho \frac{L}{A} \left(\text{ohm-meter } \frac{\text{meter}}{\text{meter}^2}\right) \tag{2.6.9}$$

Thus, substituting this relation for the resistance R into equation (2.6.9) yields

$$\boxed{F = \frac{B^2 LA}{\rho} v \text{ (newton)}} \tag{2.6.10}$$

This force, $\vec{F}$, is directly opposite to the direction of motion of the conductor and could be considered as the eddy-current damping force.

It is noted that the eddy-current damping force is directly proportional to the velocity, $F \propto v$, and by introducing a constant of proportionality called the damping coefficient, C_d, then

$$\vec{F} = C_d \vec{v} \tag{2.6.11}$$

It is obvious, then, that the damping coefficient would be

$$\boxed{C_d = \frac{B^2 LA}{\rho} \left(\frac{\text{newton-sec}}{\text{meter}}\right)} \tag{2.6.12}$$

where B = magnetic flux density in webers/meter^2, L = length of conductor in meters, A = cross section of conductor in meters^2, and ρ = resistivity of conductor material in ohm-meters.

The mks system and the English system of units for the damping coefficient are related as follows:

$$1 \frac{\text{newton-sec}}{\text{meter}} = 1 \frac{\text{newton-sec}}{\text{meter}} \times \frac{\text{lb}}{4.448 \text{ newton}} \times \frac{\text{meter}}{39.37 \text{ in}} = 5.710 \times 10^{-3} \frac{\text{lb-sec}}{\text{inch}}$$

$$\boxed{\begin{aligned} 1 \frac{\text{newton-sec}}{\text{meter}} &= 5.710 \times 10^{-3} \frac{\text{lb-sec}}{\text{inch}} \\ 1 \frac{\text{lb-sec}}{\text{inch}} &= 1.751 \times 10^{2} \frac{\text{newton-sec}}{\text{meter}} \end{aligned}}$$

Sample Calculation - Damping Coefficient (C_d)

Assume a circular 4 inch diameter copper conductor with a cross-sectional area of 0.0625 $inch^2$ is immersed in pressurized liquid H_2 at 27°K and the magnetic flux density is 7,000 gauss or 7×10^{-1} webers/$meter^2$. A value of $\rho = 2 \times 10^{-9}$ ohm-meters for copper is very conservative. For a high purity copper at 27°K, the resistivity can be as low as 0.14×10^{-9} ohm-meters.*

$$C_d = \frac{B^2LA}{\rho} = \frac{(7\times10^{-1})^2 \times (\pi\ 10.2 \times 10^{-2}) \times (0.64\ 10^{-2})^2}{2 \times 10^{-9}} \qquad (2.6.13)$$

$$\boxed{C_d = 3220 \frac{\text{newton-sec}}{\text{meter}} = 18.4 \frac{\text{lb-sec}}{\text{inch}}}$$

Sample Calculation - Stiffness (k)

Assume the same constants and conditions as above and determine k when the peak-to-peak amplitude of motion, is 0.005 inches at a whirl frequency of 190 Hz. The stiffness k is

$$k = \frac{\Delta F}{\Delta e} = \frac{B^2LA}{\rho e}\frac{de}{dt} = \frac{B^2LA}{\rho e} \times \frac{ew}{2} \quad \left(\frac{\text{newtons}}{\text{meter}}\right) \qquad (2.6.14)$$

$$= \frac{(7\times10^{-1})^2 \times \pi(10.2\times10^{-2}) \times (0.64\times10^{-2})^2}{2 \times 10^{-9} \times 1.27 \times 10^{-4}} \times \frac{1.27\times10^{-4}}{2} \times 1194$$

$$\boxed{k = 1.92 \times 10^6 \frac{\text{newtons}}{\text{meter}} = 11{,}000 \frac{\text{lb}}{\text{inch}}\ .}$$

* R. Barron, Cryogenic Systems, McGraw-Hill Book Co., 1966.

III. FINITE ELEMENT GALERKIN ANALYSIS OF EDDY-CURRENT LOSSES USING TWO-DIMENSIONAL POTENTIAL VECTOR FORMULATIONS

INTRODUCTION

In this report, the method of solution of the eddy-current problem is presented. The report presents two formulations used in the solutions of two-dimensional eddy-current problems: These formulations are called the magnetic vector potential method (MVP) and the electric vector potential method (EVP). Both methods generate a second order Helmholtz type complex differential equation. The formulation presented here is taken from J. M. Schneider in his Ph.D. Thesis on "The Finite Element-Boundary Integral Hybrid Method and Its Application to Two-Dimensional Electromagnetic Field Problems", R.P.I., 1982, under the direction of Dr. Scheppard J. Salon, Department of Electrical Engineering, Rensselaer Polytechnic Institute, Troy, New York.

For the case of the eddy-current damper moving in a magnetic field, the EVP formulation is applicable rather than the MVP formulation. The partial differential equation is multiplied by a weighting function and the Galerkin method is applied to generate a finite element approximation.

3.1 Derivation of Maxwell's Sinusoidally Time-Varying Field Equations

1. $\vec{\nabla} \times \vec{H} = \vec{J}_c + \frac{\partial \vec{D}}{\partial t}$ (3.1.1)

or in integral form

$$\oint \vec{H} \cdot d\vec{l} = \int_s \left(\vec{J}_c + \frac{\partial \vec{D}}{\partial t} \right) \cdot ds \quad (3.1.2)$$

The first Maxwell equation is referred to as Ampere's Law and

$\vec{H}$ = magnetic field.

2. $\vec{\nabla} \times \vec{E} = - \frac{\partial \vec{B}}{\partial t}$ (3.1.3)

or in integral form

$$\oint \vec{E} \cdot d\vec{l} = \int_s \left(- \frac{\partial \vec{B}}{\partial t} \right) \cdot \vec{ds} \quad (3.1.4)$$

The above equation is called Faraday's Law.

3. $\vec{\nabla} \cdot \vec{D} = \rho$ (3.1.5)

or in integral form

$$\oint \vec{D} \cdot \vec{ds} = \int \rho dv \quad \text{(Gauss's Law)} \quad (3.1.6)$$

4. $\vec{\nabla} \cdot \vec{B} = 0$ or $\oint_s \vec{B} \cdot \vec{ds} = 0$ (3.1.7)

(nonexistance of monopole)

Note that the point and integral forms of the first two equations are equivalent under stokes theorem, while the point and the integral forms of the last two equations are equivalent under the divergence theorem. For free space, where there are no charges ($\rho = 0$) and no conduction currents ($J_c = 0$), Maxwell's point equations assume the following form (1):

$$\vec{\nabla} \times \vec{H} = \frac{\partial \vec{D}}{\partial t} \quad (3.1.8)$$

$$\vec{\nabla} \times \vec{E} = - \frac{\partial \vec{B}}{\partial t} \quad (3.1.9)$$

$$\vec{\nabla} \cdot \vec{D} = 0 \quad (3.1.10)$$

$$\vec{\nabla} \cdot \vec{B} = 0 \quad (3.1.11)$$

However, reduction of Equations 1.1 - 1.4 to the sinusoidally time-varying magnetoquasi-static equations requires the following assumptions (2):

1. All fields vary sinusoidally with time.
2. Displacement currents and surface charges are neglected.
3. Free charges and surface currents are non-existent.

Assumption No. 1 was assumed by Schneider for power apparatus which operate at relatively low frequencies. The assumption made that all field quantities vary sinusoidally from D.C. to several hundred hertz is appropriate, since it is the eddy-current phenomena in the sinusoidal steady state which is to be modeled.

The second assumption on the displacement current where

$$\frac{\partial \vec{D}}{\partial t} = \varepsilon \frac{\partial}{\partial t} \vec{E} \tag{3.1.12}$$

is neglected is due to the relatively low permittivity (ε) of most material, and can be neglected in the presence of the conduction current J. Hence, the magnetic field and conduction current are assumed to be predominant in the operation of an eddy-current damper.

Maxwell's sinusoidally time-varying magnetoquasi-static field equations are:

$$\vec{\nabla} \times \vec{E} = -j\omega\vec{B} \tag{3.1.13}$$

$$\vec{\nabla} \times \vec{H} = \vec{J} \tag{3.1.14}$$

$$\vec{\nabla} \cdot \vec{B} = 0 \tag{3.1.15}$$

$$\vec{\nabla} \cdot \vec{J} = 0 \tag{3.1.16}$$

In addition to Maxwell's Equations are the constitutive relations:

$$\vec{B} = \mu\vec{H} \tag{3.1.17}$$

$$\vec{J} = \sigma\vec{E} \tag{3.1.18}$$

and the interface conditions

$$\vec{n} \cdot (\vec{B}_1 - \vec{B}_2) = 0 \tag{3.1.19}$$

$$\vec{n} \times (\vec{H}_1 - \vec{H}_2) = 0 \tag{3.1.20}$$

$$\vec{n} \times (\vec{E}_1 - \vec{E}_2) = 0 \tag{3.1.21}$$

The effective damping generated by eddy-currents in a conductor moving in a magnetic field is related to the power loss which is given by:

$$P = \int\int\int_v \frac{|\vec{J}|^2}{\sigma} dv \tag{3.1.22}$$

A quantity of use in the computation of inductance is the magnetic energy W_m. For nonlinear materials it is expressed by:

$$W_m = \tfrac{1}{2}\int\int\int_v \vec{B}\cdot\vec{H} dv \tag{3.1.23}$$

For linear-permeable materials, Equation 1.23 reduces to

$$W_m = \tfrac{1}{2}\iiint_v \frac{|B|^2}{\mu} dv \tag{3.1.24}$$

3.2 Magnetic Vector Potential Formulation

The Maxwell's equations cannot be utilized to solve the problem of eddy-current losses in a conducting sheet moving in a magnetic field. The use of vector potential functions has been employed by numerous authors to reduce the coupled first order partial differential equations into a single second order Helmholtz wave equation. The basic two approaches which Schneider presents in detail are called the magnetic vector potential (MVP) method and the electric vector potential (EVP) method.

The formulation of a two-dimensional eddy-current magnetic field problem requires the utilization of a vector potential function, rather than a scalar potential function. The reason for this is the inability of a scalar potential to adequately describe the vector properties of the eddy-current generated in a conducting sheet.

The magnetic vector potential method is based upon the use of a single component vector whose curl is the magnetic flux density given as follows:

$$\vec{\nabla} \times \vec{A} = \vec{B} \tag{3.2.1}$$

and

$$\vec{\nabla} \cdot \vec{A} = 0 \tag{3.2.2}$$

Using Maxwell's equations and the constitutive relationships and the vector identities

$$\vec{\nabla} \cdot (\vec{\nabla} \times \vec{V}) = 0 \tag{3.2.3}$$

$$\vec{\nabla} \times \vec{\nabla} U = 0 \tag{3.2.4}$$

where $\vec{\nabla}$ and U are arbitrary vector and scalar functions, respectively.

$$\vec{\nabla} \times (\vec{\nabla} \times \vec{E}) = -\nabla^2 \vec{E} + \vec{\nabla}(\vec{\nabla} \cdot \vec{E}) = -\nabla^2 \vec{E} \tag{3.2.5}$$

$$\text{if } \vec{\nabla} \cdot \vec{E} = 0$$

The following partial differential equation for the magnetic vector potential is developed

$$\frac{\partial}{\partial X}\left(\frac{1}{\mu}\frac{\partial A}{\partial X}\right) + \frac{\partial}{\partial Y}\left(\frac{1}{\mu}\frac{\partial A}{\partial Y}\right) - j\omega\sigma A = -J_o \tag{3.2.6}$$

where J_o is the applied current density in the Z direction, vector A is assumed acting in the Z direction.

The expression for the resultant current density vector J is composed of the applied current J_o and the eddy-current reaction $j\omega\sigma A$.

$$J = J_o - j\omega\sigma A \tag{3.2.7}$$

The expressions for the magnetic flux density components in the X and Y directions are given by

$$\vec{B} = \vec{\nabla} \times \vec{A} = \begin{vmatrix} i & j & h \\ \frac{\partial}{\partial X} & \frac{\partial}{\partial Y} & \frac{\partial}{\partial Z} \\ 0 & 0 & Az \end{vmatrix} \tag{3.2.8}$$

$$\vec{B} = \frac{\partial Az}{\partial Y} i - \frac{\partial Az}{\partial X} j \tag{3.2.9}$$

Hence, the magnetic flux density components are assumed to lie in the X-Y plane and are normal to the magnetic potential vector.

The power loss is given by

$$P = \iiint_v \frac{|J|^2}{\sigma} dv = \iiint_v \frac{|J_o - j\omega\sigma A|^2}{\sigma} dv \tag{3.2.10}$$

neglecting the applied current J_o and considering only the eddy-currents generated

$$Je = j\omega\sigma A \tag{3.2.11}$$

The eddy-current power dissipated is given by

$$P = \iiint_v \omega^2 \sigma \, (A \, A^*) \, dv \qquad (3.2.12)$$

For a two-dimensional conductor with an effective skin penetration depth of δe, the power loss is given by

$$P = \omega^2 \, \sigma \, \delta e \iint_a (A \, A^*) \, dX \, dY \qquad (3.2.13)$$

where A^* = complex conjugate magnetic potential vector function.

The MVP approach considers only one current component and two flux components. This approach is used for the computation of the magnetic field distribution, inductance and eddy-current losses in any power apparatus having one predominant current component. Inherent in the single component MVP approach is the existance of coupling between current carrying regions insulated from one another.

3.3 Electric Vector Potential Formulation

The general eddy-current problem to solve in its most general form is extremely difficult because it requires a three-dimensional analysis of the Helmholtz equation solution, if the conductor is saturated, then the problem is nonlinear as well. The problem of eddy-current generation is often reduced in complexity by considering simplified cases where the structure is either long or planar. In the first case, the electric field and current density possess only one component.

In the second case, the magnetic field is assumed to have only one component, while the current function may have two components.

The magnetic vector potential formulation is used in the first case, while the electric vector potential method is used for the planar representation. In both cases, the resulting partial differential equations are similar in nature to the general Helmholtz equation.

To employ the electric vector potential approach, Schneider assumes an electric potential function EVP(A) such that the curl of the EVP function is equal to the current density.

Thus,

$$\vec{\nabla} \times \vec{A} = \vec{J} \tag{3.3.1}$$

If $A = A(z)k$ only, then

$$\nabla \times A = \left(\frac{\partial Az}{\partial Y}\right) i - \left(\frac{\partial Az}{\partial X}\right) j \tag{3.3.2}$$

where

$$J_x = \left(\frac{\partial Az}{\partial Y}\right) \quad ; \quad J_y = -\frac{\partial Az}{\partial X} \tag{3.3.3}$$

From Maxwell's equation relating H and J

$$\vec{\nabla} \times \vec{H} = \vec{J}$$

Hence, the magnetic field strength vector H must be different from the EVP vector A by an arbitrary vector. Since the curl of this vector must vanish, the arbitrary vector must be equivalent to the gradient of a scalar function. Thus, we have

$$\vec{H} = \vec{A} - \vec{\nabla}\phi \tag{3.3.4}$$

If Ho is the excitation magnetic field intensity, then

$$\vec{H} = \vec{Ho} + \vec{A} - \vec{\nabla}\phi \tag{3.3.5}$$

Following the procedure of Carpenter and selecting the Coulomb gauge for $\vec{A}$ such that

$$\vec{\nabla} \cdot \vec{A} = 0$$

eliminates the sources of ϕ and removes the $\nabla\phi$ term from Equation 3.5

$$\vec{H} = \vec{Ho} + \vec{A} \tag{3.3.6}$$

Assuming that all field quantities are independent of the Z coordinate and that the permeability and conductivity are linear and isotropic, the following partial differential equation for A = A(Z) only is obtained

$$\frac{\partial^2 A}{\partial X^2} + \frac{\partial^2 A}{\partial Y^2} - \alpha^2 A = \alpha^2 Ho \tag{3.3.7}$$

where

$$\alpha^2 = j\omega\mu\sigma$$

The resultant magnetic field intensity H is composed of an excitation component Ho and an eddy-current component A with the corresponding current density components given by

$$J_X = \frac{\partial A}{\partial Y} \quad , \quad J_Y = -\frac{\partial A}{\partial X}$$

as stated in Equation 3.3.

In Maxwell's equations, across an interface, the condition

$$\vec{n} \times (\vec{H}_1 - \vec{H}_2) = 0 \qquad (3.3.8)$$

must be met.

This condition may be fulfilled by requiring the normal derivative of A to be discontinuous by the ratio of region conductivities

$$\frac{\partial A_1}{\partial n} = \frac{\sigma_1}{\sigma_2} \frac{\partial T_2}{\partial n}$$

where $\vec{n}$ is the unit vector normal to the interface.

The second or EVP approach allows for the generation of two-dimensional currents. In actuality, the eddy-current problem is three-dimensional, but the approximations of the two-dimensional solution is reasonable and is governed by the effective depth of penetration δ.

Inherent in the single-component EVP approach, as stated by Schneider, is the absence of coupling between conductive regions insulated from each other. The reasons for this is that the induced eddy-currents require a conductive path in order to flow from one region to another and also that only the excitation magnetic field incident to a particular conductive region is modified by the eddy-currents induced into that region. For the case of the eddy-current damper analysis, the EVP formulation will be utilized.

The solution to an EVP(A) problem can be represented graphically in the form of an equipotential plot. The difference of potential between two constant A lines equals the total per unit depth current flowing tangentially between them. Hence, A is a current describing function.

3.4 Galerkin Finite Element Formulation of the Electric Vector Potential Boundary Value Problem

The vector form of the Helmholtz equation may be solved by a finite element approximation. In the majority of finite element formulations, a variational principle must first be obtained. The governing partial differential equation is transformed into an equivalent integral or functional statement of the problem. Minimization of the functional yields the desired solution. Finlayson and Scriven state as early as 1967 that there is no practical need for variational formalism.. The Galerkin method or the method of weighted residuals is straight forward and avoids completely the effort and mathematical embellishment of a variational formulation, and that apart from self-adjoint linear systems, which are comparatively rare, there is no practical need for variational formalism.

Although the EVP partial differential equation is linear, self-adjoint and amenable to variational formalism, the Galerkin approximation is straight forward and is preferred. It is of interest to note that for any linear self-adjoint partial differential equation, the variational and Galerkin finite element approximations yield identical simultaneous equations.

Consider the general Helmholtz equation of the form

$$\frac{\partial}{\partial X}\left(\frac{1}{\mu}\frac{\partial A}{\partial X}\right) + \frac{\partial}{\partial Y}\left(\frac{1}{\mu}\frac{\partial A}{\partial Y}\right) - j\omega\sigma A = F \qquad (3.4.1)$$

where

- A = Unknown potential function varying sinusoidally in time with frequency.
- μ,σ = Material properties.
- F = Known excitation function.

Let $\bar{H}$ be an approximate solution to Equation 4.1 in a planar region. Since $\bar{A}$ will not in general satisfy Equation 4.1, a residual R will result.

$$R = \frac{\partial}{\partial X}\left(\frac{1}{\mu}\frac{\partial \bar{A}}{\partial X}\right) + \frac{\partial}{\partial Y}\left(\frac{1}{\mu}\frac{\partial \bar{A}}{\partial Y}\right) - j\omega\sigma A - F \tag{3.4.2}$$

In order to minimize the residual error R, it is multiplied by a weighting function W and the weighted integral over the region is set equal to zero.

$$\iiint_v WR \; dv = 0 \tag{3.4.3}$$

A major advantage of the Galerkin method is that it can be used to reduce the order of the derivations in the partial differential equation. This will have a considerable significance on the choice of the shape functions as to the permissible order of the polynomial functions used in the analysis.

The Galerkin weighted integral Equation (4.3) is first transformed by the Divergence theorem and Green's theorems which are obtained from the Divergence theorem.

For an arbitrary vector

$$\iiint_v \vec{\nabla}\cdot\vec{A}\,dv = \iint_s \vec{A}\cdot\vec{n}\,ds \tag{3.4.4}$$

In cartesian coordinates

$$\iiint_v \left(\frac{\partial Ax}{\partial x} + \frac{\partial Ay}{\partial y} + \frac{\partial Az}{\partial z}\right) dv = \iint_s [A_x\cos(x,n) + A_y\cos(y,n) + A_z\cos(z,n)]\,ds \tag{3.4.5}$$

Let $\vec{A} = u\vec{\nabla}v$

$$\iiint_v \vec{\nabla}\cdot(u\vec{\nabla}v)\,dv = \iint_s u\nabla v\cdot n\,ds \tag{3.4.6}$$

Expanding the volume integral and rearranging

$$\int_v u\nabla^2 V dv = -\int_v \vec{\nabla}u \cdot \vec{\nabla}V dv + \int_s u \frac{\partial V}{\partial n} dS \tag{3.4.7}$$

The above equation is known as Green's first identify.

Green's second identity is given by

$$\int_v (U\nabla^2 V - V\nabla^2 u)\, dv = \oint_c \left(u \frac{\partial V}{\partial n} - V \frac{\partial u}{\partial n}\right) dS \tag{3.4.8}$$

The expanded form of Equation (4.3) is

$$\iint_R W\left(\frac{\partial}{\partial X}\left(\frac{1}{\mu}\frac{\partial A}{\partial Y}\right) + \frac{\partial}{\partial Y}\left(\frac{1}{\mu}\frac{\partial A}{\partial Y}\right)\right) dR$$

$$- j\omega \iint_R W\sigma A\, dR - \iint_R WF\, dR = 0 \tag{3.4.9}$$

Applying Green's first identity

$$-\iint_R \frac{1}{\mu}\left(\frac{\partial W}{\partial X}\frac{\partial A}{\partial X} + \frac{\partial W}{\partial Y}\frac{\partial A}{\partial Y}\right) dR + \int_s \frac{W}{\mu}\frac{\partial A}{\partial n}\, ds$$

$$- j\omega \iint_R W\sigma A\, dR - \iint_R WF\, dR = 0 \tag{3.4.10}$$

The contribution due to the contour integral is assumed zero and thereby implicitly satisfying the homogenous Newman boundary conditions.

The second order partial differential equation is reduced to the following integral equation with first order derivations

$$\iint_R \frac{1}{\mu}\left(\frac{\partial W}{\partial X}\frac{\partial A}{\partial X} + \frac{\partial W}{\partial Y}\frac{\partial A}{\partial Y}\right) dR + j\omega \iint_R \sigma WA\, dR = -\iint_R WF\, dR \tag{3.4.11}$$

In the Galerkin method of weighted residuals, a set of shape functions may be chosen for the whole domain. These functions must also satisfy the boundary conditions.

In the first order finite element approximation of Equation (4.11), the region R is divided into a number of triangular elements over each of which A varies linearly and μ and σ are constant and the forcing function F is taken as its average value $\hat{F}$.

Applying these assumptions, Equation (4.11) becomes

$$\sum_{m=1}^{M}\left[\frac{1}{\mu_m}\iint_{R_m}\left(\frac{\partial W}{\partial X}\frac{\partial A}{\partial X} + \frac{\partial W}{\partial Y}\frac{\partial A}{\partial Y}\right) dR + j\omega\sigma_m \iint_{R_m} WA\, dR = -F_m \iint_{R_m} Wdr\right] \tag{3.4.12}$$

The summation extends over the μ elements into which region R is divided. In the first order finite element method, each subregion m is represented by a triangle having local nodes i, j, k, at its vertices. The values of the function A at the nodes

$$\{A\}_m = \begin{Bmatrix} A_i \\ A_j \\ A_k \end{Bmatrix}_m \tag{3.4.13}$$

For any point within the triangular region, the value of A is given by

$$A = [N_i \quad N_j \quad N_k] \begin{Bmatrix} A_i \\ A_j \\ A_k \end{Bmatrix} \tag{3.4.14}$$

The functions $N_i(X,Y)$ are called shape functions and have the property that

$$N_i(X_i, Y_i) = 1$$

$$N_i(X_j, Y_j) = N_i(X_k, Y_k) = 0$$

The value of A within the triangle is assumed to be linear of the form

$$A(X, Y)_m = a + bx + cy \tag{3.4.15}$$

Solving for A_i in terms of the coordinates X_i Y_i of the point

$$\begin{bmatrix} A_i = a + b\,x_i + cy_i \\ A_j = a + b\,x_j + cy_j \\ A_k = a + b\,x_k + cy_k \end{bmatrix}_{m \text{ element}} \tag{3.4.16}$$

Solving for the shape functions N_i, N_j, N_k we obtain

$$\begin{bmatrix} N_i = (a_i + b_j\,x + c_i y)/2\Delta m \\ N_j = (a_j + b_j\,x + c_j y)/2\Delta m \\ N_k = (a_k + b_k\,x + c_k y)/2\Delta m \end{bmatrix} \tag{3.4.17}$$

Where

$$a_i = X_j Y_k - Y_j X_k$$

$$a_j = X_k Y_i - Y_k X_i$$

$$a_k = X_i Y_j - Y_i X_j$$

$$b_i = Y_j - Y_k$$

$$b_j = Y_k - Y_i$$

$$b_k = Y_i - Y_j$$

$$c_i = X_k - X_j$$

$$c_j = X_i - X_k$$

$$c_k = X_j - X_i$$

Where Δm = area of triangle,

$$2\Delta m = (X_j - X_i)(Y_k - Y_i) - (X_k - X_i)(Y_j - Y_i)$$

$$= b_i c_j - b_y c_i = b_k c_j - b_j c_k$$

$$= b_k c_i - b_i c_k$$

The shape functions given by Equation (4.17) correspond to element m and only to points within the boundary region. The linear shape functions take on the value of unity at a node i and vary linearly to zero at the opposite nodes j and k. The value of A_i at the node i for element m is the same as the corresponding point j for element N. Although the function A is continuous in the first order finite element method, the first derivative is not continuous in passing from one element to an adjacent node.

The Galerkin finite element approximation is developed by choosing the shape functions as the weighting functions for element m.

$$W = \begin{bmatrix} N_i \\ N_j \\ N_k \end{bmatrix} \tag{3.4.18}$$

The partial derivatives are given by

$$\frac{\partial A_i}{\partial X} = b_i = \frac{1}{2\Delta m} \begin{bmatrix} b_i & b_j & b_k \end{bmatrix} \begin{bmatrix} A_i \\ A_j \\ A_k \end{bmatrix} \tag{3.4.19}$$

$$\frac{\partial A_i}{\partial Y} = c_i = \frac{1}{2\Delta m} \begin{bmatrix} c_i & c_j & c_k \end{bmatrix} \begin{bmatrix} A_i \\ A_j \\ A_k \end{bmatrix} \tag{3.4.20}$$

For the first order finite element approximation, the derivatives A_x and A_y are constant in the element m.

$$\frac{\partial W}{\partial X} = \frac{1}{2\Delta m} \begin{bmatrix} b_i \\ b_j \\ b_k \end{bmatrix} \tag{3.4.21}$$

$$\frac{\partial W}{\partial Y} = \frac{1}{2\Delta m} \begin{bmatrix} c_i \\ c_j \\ c_k \end{bmatrix} \tag{3.4.22}$$

The first integral

$$\frac{1}{\mu m}\int_{R_m}\left(\frac{\partial W}{\partial X}\frac{\partial A}{\partial X}+\frac{\partial W}{\partial Y}\frac{\partial A}{\partial Y}\right)dR$$

$$=\frac{1}{\mu m}\frac{1}{4\Delta^2 m}\int_m\left\{\begin{bmatrix}b_i\\b_j\\b_k\end{bmatrix}\begin{bmatrix}b_i & b_j & b_k\end{bmatrix}\right. \tag{3.4.23}$$

$$\left.+\begin{bmatrix}c_i\\c_j\\c_k\end{bmatrix}\begin{bmatrix}c_i & c_j & c_k\end{bmatrix}\right\}dR$$

Since the matrix coefficients are constant, the integral reduces to Δm. Expanding we obtain

$$\frac{1}{\Delta m 4\mu m}\begin{bmatrix} b_i^2+c_i^2 & b_ib_j+c_ic_j & b_ib_k+c_ic_k\\ b_ib_j+c_ic_j & b_j^2+c_j^2 & b_jb_k+c_jc_k\\ b_ib_k+c_ic_k & b_jb_k+c_jc_k & b_k^2+c_k^2\end{bmatrix} \tag{3.4.24}$$

The integral

$$j\omega\sigma\int_{R_m}WA\,dR$$

becomes

$$j\omega\sigma\int\begin{bmatrix}N_i\\N_j\\N_k\end{bmatrix}\begin{bmatrix}N_i & N_j & N_k\end{bmatrix}\begin{bmatrix}A_i\\A_j\\A_k\end{bmatrix}dR \tag{3.4.25}$$

$$= j\omega\sigma \int \begin{bmatrix} N_i^2 & N_i N_j & N_i N_k \\ N_i N_j & N_j^2 & N_j N_k \\ N_i N_k & N_j N_k & N_k^2 \end{bmatrix} dR \begin{bmatrix} A_i \\ A_j \\ A_k \end{bmatrix} \tag{3.4.25}$$

Carrying out the required integrations, we obtain

$$\frac{j\omega\sigma\Delta m}{12} \begin{bmatrix} 2 & 1 & 1 \\ 1 & 2 & 1 \\ 1 & 1 & 2 \end{bmatrix} \cdot \begin{bmatrix} A_i \\ A_j \\ A_k \end{bmatrix} \tag{3.4.26}$$

The following function integral is given by

$$- Fm \int_{R_m} W \, dR$$

$$= - Fm \int_{R_m} \begin{bmatrix} N_i \\ N_j \\ N_k \end{bmatrix} dR = - \frac{Fm}{3} \Delta m \begin{bmatrix} 1 \\ 1 \\ 1 \end{bmatrix} \tag{3.4.27}$$

Let $\psi m = \frac{\partial A}{\partial n}$ along a boundary element.

The contour integral is given by

$$- \oint \frac{1}{\mu m} W \psi m dc = - \frac{\psi m}{\mu m} \oint_c W dc \tag{3.4.28}$$

The normal derivative of A, ψm is assumed to be constant over each segment on c and is independent of A. Let it be a coordinate along c_m with its origin at node j and directed towards node k.

$$\text{Let } L = \sqrt{(X_k - X_j)^2 + (Y_k - Y_j)^2}$$

$$\oint_{wdc} = \int_{cm} \begin{bmatrix} N_i \\ N_j \\ N_k \end{bmatrix} dc = \int \begin{bmatrix} 0 \\ (L-t)/L \\ t/L \end{bmatrix} dt$$

$$\int_o^L \begin{bmatrix} 0 \\ (L-t)/L \\ t/L \end{bmatrix} dt = \begin{bmatrix} 0 \\ L/2 \\ L/2 \end{bmatrix}$$

Therefore the contour integral reduces to

$$= -\frac{\psi_m}{\mu_m} \begin{bmatrix} 0 \\ L/2 \\ L/2 \end{bmatrix} \qquad (3.4.29)$$

The single-component EVP partial differential equation for linear isotropic materials is

$$\frac{\partial^2 A}{\partial X^2} + \frac{\partial^2 A}{\partial Y^2} - \alpha^2 A = \alpha^2 Ho = F \qquad (3.4.30)$$

where

$\alpha^2 = j\omega\mu\sigma$

Ho = applied magnetic field intensity

The finite element equations for the m^{th} element is given by

$$\begin{bmatrix} S_{ii} & S_{ij} & S_{ik} \\ S_{ij} & S_{jj} & S_{jk} \\ S_{ik} & S_{jk} & S_{kk} \end{bmatrix}_m \begin{bmatrix} A_i \\ A_j \\ A_k \end{bmatrix} = \begin{bmatrix} F_i \\ F_j \\ F_k \end{bmatrix} \qquad (3.4.31)$$

where

$$S_{ij} = \frac{b_i b_j + c_i c_j}{4\Delta m} + \frac{\alpha m^2 \Delta}{12}$$

$$S_{ik} = \frac{b_i b_k + c_i c_k}{4\Delta m} + \frac{\alpha m^2 \Delta m}{12}$$

$$F_i = F_j = F_k = -\frac{\alpha m^2 \, Ho \, \Delta m}{3}$$

The addition of all of the elements leads to a set of simultaneous equations written in matrix form

$$[S]\ [A] = [F] \qquad (3.4.32)$$

where

S = N x N global EVP coefficient matrix

A = N x 1 nodal EVP vector

F = N x 1 nodal excitation vector

N = total No. of nodes in R and on C the boundary

The development of the EVP method implicity specifies homogeneous Newman boundary conditions on the contour C. It remains to explicity specify any known nodal values of A. This is performed for an arbitrary node i by entering zeros into the i^{th} row of S, except for one in the diagonal position and place the known nodal value of A in the i^{th} row of F.

After incorporating the boundary conditions, Equation (4.32) may be solved for by Gauss elimination or by an iteration scheme. The Gauss elimination method may be accomplished by an LU decomposition which also utilizes the symmetry of the banded S matrix.

After the EVP a vector is determined, then these nodal values may be used in the computation of the following quantities:

(a) H_m, the elemental magnetic field intensity which like A varies linearly over each element. The magnetic field intensity in each element may be approximated by

$$H_m = H_{mo} + \frac{A_i + A_j + A_k}{3} \quad . \tag{3.4.33}$$

(b) The element current density components in element m can be expressed as

$$J_x = (C_i A_i + C_j A_j + C_k A_k)/2\Delta m$$

$$J_y = -(b_i A_i + b_j A_j + b_k A_k)/2\Delta m$$

where Δm = elemental area

(c) The elemental eddy-current loss is

$$\Delta Pme = \left(\frac{J_x^2 + J_y^2}{\sigma}\right) \Delta m \quad , \text{ and}$$

the total eddy-current loss is given by

$$Pe = \sum_{m=1}^{M} \Delta Pme \quad .$$

IV. EDDY-CURRENT DAMPING OPTIMIZATION

INTRODUCTION

This presentation follows very closely the work of Mikulinsky and Shtrikman (1) and fills in some of the mathematical gaps between their equations. It essentially studies the optimization of [illegible]ddy-current damping device containing a metal disk moving in a magnetic field of cylindrical symmetry. Analytical equations for the damping which is produced by permanent magnets for a wide range of geometrical parameters of this device are presented. The geometry which produces the maximum damping under size constraints is also obtained.

Eddy-current dampers have numerous applications, e.g., in balances and in electrical supply meters. Eddy-current damping is obtained by the motion of a metallic body (which is to be damped) with velocity, $\vec{V}$, in a magnetic field. This motion creates electric current. Additionally, heat (Q) is produced which causes the decay of the electric current density, $\vec{J}$. The amount of heat produced is given by Joule's Law,

$$Q = \frac{1}{\sigma} \int \vec{J}^2 \, dV = f\vec{V}^2 \quad \text{Watts} \quad , \tag{4.1}$$

where σ is the conductivity of the body, V is the volume, and f is the viscous damping coefficient which we want to calculate. This coefficient was calculated for simple geometrical configurations by Davis and Reitz (2) and Schieber (3-5). A more realistic configuration, close to that used in some high speed levitated flywheels (6), will be studied in this paper.

The damper is constructed of a copper disk moving in a magnetic field. Each of the two permanent, identical cylindrical magnets, AA' and BB' (see Figure 1), consists of two magnetic cylindrical rings A and A' (B and

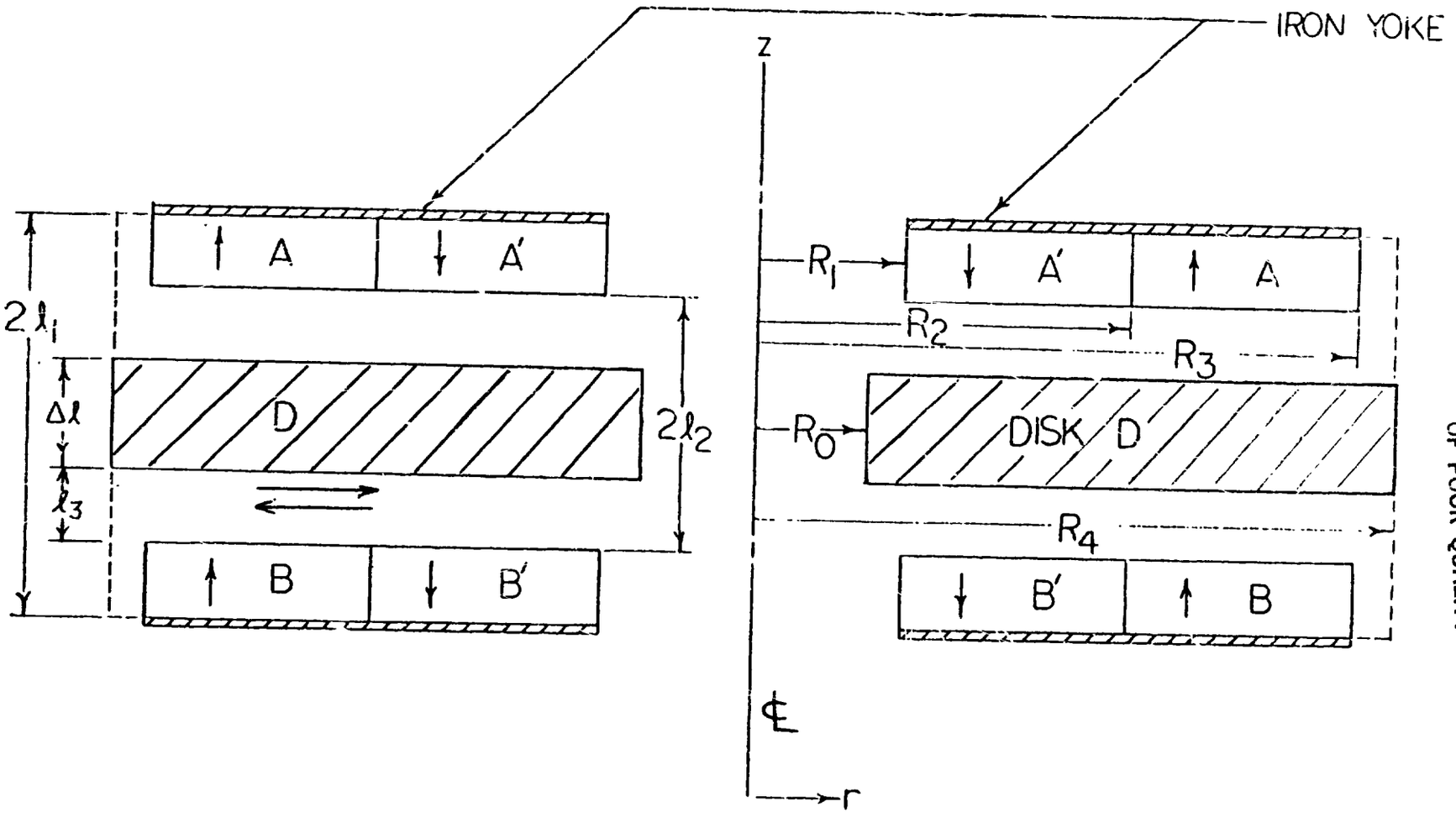

Figure 1. Cross section of eddy current damper

B'), with radii R_2 and R_3, magnetized in opposite directions. The copper disk, with internal radius R_0 and external radius R_4 can move in a direction perpendicular to the axis of cylindrical symmetry, C. This is the motion which will be damped.

For simplification of calculations, the hole of the disk will be neglected ($R_0 = 0$). This results in a small error which will be calculated by comparisons in two particular cases.

Case 1

The damping coefficient, f_1, for $R_3 = R_4$ will be compared with the damping coefficient, f_∞, for $R_4 \to \infty$ ($R_3/R_4 \to 0$). Both of the coefficients, f, and f_∞, are calculated for no holes in the disk or magnets ($R_0 = R_1 = 0$) and for thin systems ($\ell_1 << R_4$). For the value of R_2/R_3 which maximizes f, the difference between f_1 and f_∞ is approximately 10%-12%. Therefore, the portion of the disk outside of the magnetic field contributes no more than 12% of f. The part of the disk outside of the magnetic field where the radius of disk hole is not larger than the magnet's inner radius ($R_0 \leq R_1$) should contribute even less than 10%-12% to the damping coefficient, f.

Case 2

The system is thin ($\ell_1 << R_4$) and the magnet hole radius is large ($R_1 >> R_3-R_1$) in this case. Also, the two magnetic cylindrical rings, A and A' (B and B'), are equivalent in width ($R_2 = (R_1 + R_3)/2$). There is no difference between the value of f_∞, calculated with $R_0 = 0$ and $R_4 \to \infty$, and the value of f_1, calculated for $R \leq R_1$ and for $R_4 > R_3$. The hole in the disk still has no significant effect on the value of f. In further considerations, the hole in the disk will be neglected ($R_0 = 0$).

This analysis is based on thin systems only. However, the geometry of real systems approaches a thin system and these approximations should have a wide range of validity in practice.

A four-step procedure will be utilized to derive the damping coefficient. First, the magnetic field, $\vec{H}$, created by the permanent magnets A and B will be calculated. Using this field, the eddy-currents for small velocities, $\vec{V}$, will be calculated, neglecting the skin effect. Calculation of the heat production and the damping coefficient, according to Equation 1, is the third step. Finally, the geometry of the damper will be optimized to obtain maximum damping.

Reviewing some of the terms that will be used:

Symbol	Quantity	Unit
Q	Heat Production	Watts
$\vec{V}$	Velocity	Meter/Second
V	Volume	$Meter^3$
f	Viscous Damping Coefficient	Newton-Second/Meter
σ	Conductivity	$(Ohm\text{-}Meter)^{-1}$
$\vec{H}$	Magnetic Field Intensity	Ampere/Meter
$\vec{B}$	Magnetic Induction or Magnetic Flux Density	$Tesla = \frac{Newton\text{-}Second}{Coulomb\text{-}Meter}$
M	Magnetization	Tesla
ψ	Magnetic Potential	Ampere/Meter
$\vec{E}$	Electric Field Intensity	Volt/Meter
$\vec{J}$	Electric Current Density	$Ampere/Meter^2$
$\vec{D}$	Electric Flux Density	$Coulomb/Meter^2$
ρ	Electric Charge Density	$Coulomb/Meter^3$
ϕ	Electric Potential	Volt/Meter
μ	Permeability	Henry's/Meter
μo	Free Space Permeability = $4\pi \times 10^{-7}$	Henry's/Meter

Note:

1 Volt = 1 Joule/Coulomb

1 Ampere = 1 Coulomb/Second

1 Joule = 1 Newton-Meter

1 Ohm = 1 Volt/Ampere

1 Henry = 1 Volt-Second/Ampere

4.1 Magnetic Field

A magnetic field caused by static magnets is calculated by using 2 of Maxwell's equations.

$\vec{\Delta}\cdot\vec{B} = 0$, or, since $\vec{B} = \mu\vec{H}$ and $\vec{H} = -\vec{\nabla}\psi$, $\vec{\nabla}\cdot\vec{\nabla}\psi = \nabla^2\psi = \Delta\psi = 0$

$$\vec{\nabla} \times \vec{H} = \vec{J} + \frac{\partial \vec{D}}{\partial t} = 0 \qquad (4.1.1)$$

To facilitate calculations of the magnetic field, the cylindrical coordinate system will be used. The central axis C will be the z axis, r the distance from the z axis, and θ the angle measured from an arbitrary fixed direction in the plane perpendicular to the axis.

The boundary conditions are as follows:

On the iron yoke, $z = \pm \ell_1$, $\psi(r,\theta, \pm \ell_1) = 0$

Assume also that at $r = R_4$, $\psi(R_4, \theta, z) = 0$

The last boundary condition allows use of the same orthogonal system of functions for both magnetic potential, ψ, and electric potential, ϕ, arriving at a simple analytic solution for f. This last boundary condition will result in negligible error for a very thin system, $\ell_1 << R_3$. The error will be small for a disk with large radius, $R_4 >> R_3$. It will be assumed that in general this error will be negligible.

The other boundary conditions ensure that ψ and B_z are continuous on the surface at $z = \pm \ell_2$.

Due to the cylindrical symmetry of the system, the magnetic potential, ψ, is not dependent on the angle θ. Using the boundary conditions listed above, the solution of Equation (4.1.1) is the following:

$$\psi = -\frac{2M}{R_4^2} \sum_n \frac{C(n)}{\beta_n J_1^2(\beta_n R_4)} \frac{\sinh \beta_n(\ell_1-\ell_2)}{\sinh \beta_n \ell_1} J_0(\beta_n r)\sinh \beta_n z \qquad (4.1.2)$$

Where M is the absolute value of the magnetization,

$$C(n) = \beta_n^{-1} \left[2R_2 J_1 (\beta_n R_2) - R_1 J_1 (\beta_n R_1) - R_3 J_1 (\beta_n R_3)\right]. \quad (4.1.3)$$

The set β_n is given by the Bessel function $J_o (\beta_n R_4) = 0$ (4.1.4)

where $J_n(x) = \sum_{k=0}^{\infty} \frac{(-1)^k (x/2)^{n+2k}}{k!\Gamma (n+k+1)}$

or $J_o(x) = 1 - \frac{x^2}{2^2} + \frac{x^4}{2^2.4^2} - \frac{x^6}{2^2.4^2.6^2} + \ldots$

$J_1(x) = \frac{x}{2} - \frac{x^3}{2^2.4} + \frac{x^5}{2^2.4^2.6} - \frac{x^7}{2^2.4^2.6^2.8} + \ldots$

Solving for Equation (4.1.4), $\beta_n R_4 = 2.405$, 5.520, and 8.654 would be the first three solutions of this equation. Therefore, $\beta_1 = 2.405/R_4$, $\beta_2 = 5.520/R_4$, and $\beta_3 = 8.654/R_4$ would be the first three values of β_n. These values can be used in Equations (4.1.2) and (4.1.3) to find the potential, ψ, which defines the magnetic field inside the copper disk.

4.2 Eddy-Current

The electric current density, J, created by the motion of the disk in the magnetic field, H, is given by

$$\vec{J} = \sigma \left[\vec{E} + \mu_o \left(\vec{V} \times \vec{H}\right)\right] \tag{4.2.1}$$

with

$$\text{curl } \vec{E} = \vec{\nabla} \times \vec{E} = \partial \vec{B}/\partial t = 0, \text{ from Maxwell's equation when}$$

B is constant over time (therefore, $\vec{E} = -\vec{\nabla}\phi$), and div $\vec{J} = \vec{\nabla}\cdot\vec{J} = 0$, (4.2.2)

from the continuity equation when ρ is constant over time

Taking the divergence of Equation (4.2.1),

$$\vec{\nabla}\cdot\vec{J} = \vec{\nabla}\cdot\sigma\left[\vec{E} + \mu_o \left(\vec{V} \times \vec{H}\right)\right] = 0$$

$$= \sigma \left[\vec{\nabla}\cdot\vec{E} + \mu_o \left[\vec{\nabla}\cdot\left(\vec{V} \times \vec{H}\right)\right]\right] = 0$$

$$= \sigma \left[\vec{\nabla}\cdot\left(-\vec{\nabla}\phi\right) + \mu_o \left[\vec{\nabla}\cdot\left(\vec{V} \times \vec{H}\right)\right]\right] = 0$$

$$\Delta\phi = \nabla^2\phi = \mu_o \left[\vec{\nabla}\cdot\left(\vec{V} \times \vec{H}\right)\right]$$

$$= \mu_o \left[\vec{H}\cdot\left(\vec{\nabla} \times \vec{V}\right) - \vec{\nabla}\cdot\left(\vec{V} \times \vec{H}\right)\right]$$

$$= -\mu_o \vec{\nabla}\cdot\left(\vec{V} \times \vec{H}\right) \tag{4.2.3}$$

for small velocities that are approximately constant.

Using Maxwell's equation with electric fields varying slowly over time, $\vec{\nabla} \times \vec{H} = \vec{J}$ and multiplying both sides by $-\mu_o\vec{V}$, $-\mu_o\vec{V}\cdot\left(\vec{\nabla} \times \vec{H}\right) = \mu_o\vec{V}\cdot\vec{J}$.

Equations (4.2.1) and (4.2.3) are substituted into this equation obtaining

$$\begin{aligned}\Delta\phi &= -\mu_o\vec{V}\cdot(\sigma[\vec{E} + \mu_o(\vec{V} \times \vec{H})]) \\ &= \mu_o\sigma\vec{V}\cdot[-(-\vec{V}\phi)-\mu_o(\vec{V} \times \vec{H})] \\ &= \mu_o\sigma[\vec{V}\cdot\vec{V}\phi - \vec{V}\cdot\ \mu_o(\vec{V} \times \vec{H})] \\ &= \mu_o\sigma[\vec{V}\cdot\vec{V}\phi - \mu_o\vec{H}\cdot\ (\vec{V} \times \vec{V})] \\ &= \mu_o\sigma\ \vec{V}\cdot\vec{V}\phi \qquad (4.2.4)\end{aligned}$$

For very small velocities, $\Delta\phi = 0$. (4.2.5)

Velocity is estimated as $V\alpha\ell\omega$, where ℓ is the characteristic size of the disk and $\omega\sim1/\tau$ is the inverse characteristic time, τ. Equation (2.5) can be used if $\ell<<(\mu_o\sigma\omega)^{-\frac{1}{2}}\sim\ell_{sk}$, skin length, or $V<<(\mu_o\sigma\ell)^{-1}$. When $\sigma = 10^8$ (Ohm-M)$^{-1}$ and $\ell\sim(10^{-2} - 10^{-1})$m, a velocity, V, $<<(0.1 - 1)$m/sec, allows use of Equation (4.2.5).

At the disk surface, the boundary condition is

$$j_n = 0 \qquad (4.2.6)$$

where j_n is normal to the surface component of current density, $\vec{j}$.

The solution of Equation 4.2.5, using the boundary condition given in Equation 4.2.6 is

$$\phi = -4MV\frac{\sin\phi}{R_4}\sum_{h=0}^{\infty}\frac{\beta_{1n}}{\sinh\beta_{1n}\frac{\Delta\ell}{2}\,(R_4{}^2\beta_{1n}^2-1)}\frac{J_1(\beta_{1n}v)}{J_1(\beta_{1n}R_4)}\cosh\beta_{in}z$$
$$\sum_{m=0}^{\infty}\frac{c(m)}{J_1{}^2(\beta_mR_4)}\frac{\sinh\beta_m(\ell_1-\ell_2)}{\sinh\beta_m\ell_1}\frac{\sinh\beta_n\frac{\Delta\ell}{2}}{\beta_{1n}{}^2-\beta_m{}^2}J_1'(\beta_mR_4) \qquad (4.2.7)$$

The set β_{1n} is given by

$$J_1'(\beta_{1n}R_4) = 0 \qquad (4.2.8)$$

Where the Bessel function

$$J_1'(\beta_{1n}R_4) = \tfrac{1}{2}\,[J_0(\beta_{1n}R_4) - J_2(\beta_{1n}R_4)] = 0$$

4.3 Damping Coefficients

The damping coefficient, f, is found using Equations 4.1, 4.1.2, 4.2.1 and 4.2.7.

From Equation (4.1),

$$Q = f\vec{V}^2 = \frac{1}{\sigma} \int \vec{J}^2 dV \tag{4.1}$$

but using Equation (4.2.1),

$$\vec{J} = \sigma[\vec{E} + \mu_o(\vec{V} \times \vec{H})] \tag{4.2.1}$$

therefore,

$$Q = f\vec{V}^2 = \frac{1}{\sigma} \int \sigma^2[\vec{E} + \mu_o(\vec{V} \times \vec{H})]^2 dV$$

Equation (4.2.2) gives

$$\vec{V} \times \vec{E} = 0, \quad \vec{E} = -\vec{\nabla}\phi \tag{4.2.2}$$

This results in

$$\begin{aligned} Q = f\vec{V}^2 &= \sigma\int[-\nabla\phi + \mu_o(\vec{V} \times \vec{H})]^2 dV \\ &= \sigma\int[(\nabla\phi)^2 - 2\mu_o\vec{\nabla}\phi(\vec{V} \times \vec{H}) + \mu_o^2(\vec{V} \times \vec{H})^2] d\bar{v} \end{aligned} \tag{4.3.1}$$

Solving for f,

$$f = \pi M^2 \sigma R_4^3 \left\{ \left[\sum_n \bar{c}(n) \frac{\sinh x_n L}{\sinh x_n L_1} \right]^2 \frac{3 \sinh x_n \Delta L + x_n \Delta L}{x_n^3 J_1^2(x_n)} \right. \tag{4.3.2}$$

$$\left. -16 \sum_n \frac{x_{1n} \coth(x_{1n}\Delta L/2)}{x_{1n}^2 - 1} \left[\sum_m \bar{c}(m) \frac{\sinh x_m L}{\sinh x_m L_1} \frac{\sinh(x_m L/2)}{x_{1n}^2 - x_m^2} \frac{J_1'(x_m)}{J_1^2(x_m)} \right]^2 \right\}$$

where x_n and x_{1n} are the roots of the following 2 equations:

$$J_0(x_n) = 0, \quad J_1'(x_{1n}) = J_0(x_{1n}) - J_2(x_{1n}) = 0 \tag{4.3.3}$$

Using

$$\bar{c}(n) = 2\lambda_2 J_1(x_n\lambda_2) - \lambda_1 J_1(x_n\lambda_1) - \lambda_3 J_1(x_n\lambda_3)$$

$$L = (\ell_1 - \ell_2)/R_4$$

$$L_1 = \ell_1/R_4 \qquad (4.3.4)$$

$$\Delta L = \Delta\ell/R_4$$

$$\lambda_i = R_i/R_4$$

Three particular cases will now be investigated.

(1) For a very thin system, $L_1 = \ell_1/R_4 \ll 1$, Equation (4.3.2) results in

$$f = 4\pi M^2 \sigma R_4^3 \left(\frac{L}{L_1}\right)^2 \Delta L \left[\sum_n \frac{\bar{c}(n)^2}{x_n^2 J_1^2(x_n)} - 2\sum_n \frac{1}{x_{1n}^2 - 1}\left[\sum_m \bar{c}(m) \frac{x_m}{x_{1n}^2 - x_m^2} \frac{J_1^1(x_m)}{J_2^2(x_m)}\right]^2\right] \qquad (4.3.5)$$

(2) If the radius of the disk is approaching infinity, $R_4 \to \infty$, the parameters

$$\Delta\beta_n = \frac{x_n + 1 - x_n}{R_4} \quad \text{and} \quad \Delta\beta_{1n} = \frac{x_{1n} + 1 - x_{1n}}{R_4}$$

are small, allowing replacement of the sums in Equation (4.3.5) with integrals. Assume that the major contribution to f arises from x_n, $x_{1n} \gg 1$, which will be verfied below.

For the Bessel functions, use the asymptotic form

$$J_m(z) = \sqrt{\frac{2}{\pi z}} \cos\left(z - \frac{\pi m}{2} - \frac{\pi}{4}\right) \qquad (4.3.6)$$

resulting in

$$x_n = x_{1n} = \frac{3}{4}\pi + \pi n$$

$$J_1'(x_m) \alpha \sin\pi m = 0 \qquad (4.3.7)$$

The only nonzero term in the second half of Equation 4.3.5 is the term with $x_{1n} = x_m$ because

$$\lim_{x_m \to x_{1n}} \frac{J_1'(x_m)}{x_{1n}^2 - x_m^2} = -\frac{1}{2x_{1n}} J_1'(x_n) = \sqrt{\frac{1}{2\pi x_{1n}^3}} (-1)^n$$

is finite. Substituting this result into Equation 4.3.5 and replacing the sum with the integral, Equation 4.3.5 becomes

$$f = \frac{\pi M^2 \sigma}{2} \int_0^\infty d\beta \left[C(\beta) \frac{\sinh\beta(\ell_1 - \ell_2)}{\sinh\beta\ell_1} \right]^2 (\sinh\beta\Delta\ell + \beta\Delta\ell) \qquad (4.3.8)$$

where $C(\beta)$ is given in Equation 4.1.3. Therefore, as β goes to zero, the integrand in Equation 4.3.8 also goes to zero and the primary contribution to the integral is from the finite β. This results in our earlier assumption, $x_n \sim \beta R_4 >> 1$.

(3) The final case to be considered is for a very thin system, $\ell_1/R_4 << 1$, with a disk of infinite radius, $R_4 \to \infty$. Substituting into Equation 4.3.8,

$$f = \pi M^2 \sigma \frac{(\ell_1 - \ell_2)^2}{\ell_1^2} \Delta\ell \int_0^\infty d\beta\, C(\beta)^2 \qquad (4.3.9)$$

Using the normalization equation,

$$\int_0^\infty J_m(\beta r)\, J_m(\beta r')\, \beta d\beta = \frac{1}{r} \sigma(r - r'),$$

and Equation 4.1.3, the integral in Equation 4.3.9 can be calculated, arriving at the final analytic result

$$f = \frac{\pi M^2 \sigma}{2} \frac{(\ell_1 - \ell_2)^2}{\ell_1^2} \Delta\ell\, (R_3^2 - R_1^2) \qquad (4.3.10)$$

4.4 Optimization of Damping Coefficient

The results of the numerical calculations and optimization of the damping coefficient, f, will be presented in this section. The case that will be studied is one in which the magnets lie in a thin system, $L_1 << 1$, contain no hole, $R_0 = R_1 = 0$, and are uniformly magnetized in one direction, $R_2 = 0$. The reduced damping coefficient

$$\phi = \frac{f}{4\pi} M^2 \sigma \left(\frac{\ell_1 - \ell_2}{\ell_1} \right)^2 \Delta\ell \quad [m^2] \tag{4.4.1}$$

is calculated as a function of R_3/R_4, magnet radius/metal disk radius, with $R_3 = 8 \times 10^{-2}$, according to Equation 4.3.5. The summation indexes n and m were varied from one to 10, giving a 10 x 10 matrix, resulting in a maximum at $R_3/R_4 = 0.3$. For $R_3/R_4 < 0.3$, the calculations are incorrect due to large values of n and m contributing to f when R_4 is large. For $R_3/R_4 > 0.3$, the accuracy of this calculation is reasonably good with the 10 x 10 matrix. As R_3/R_4 decreases in this region, ϕ increases. For $R_3 \geq R_4$, f = 0, since the magnetic field in the disk is uniform and the magnetic flux in the disk does not change during its motion for a thin system. Therefore, it would be expected that $f \to 0$ for $R_3/R_4 = 1$. It is found, from numerical calculations, that the function ϕ is sensitive to the order of matrix m x n at $R_3/R_4 = 1$. The order of matrix was varied from 1 x 1 to 12 x 12. The magnitude of ϕ monotonically decreases 6 times in this interval when the order of the matrix increases. Extrapolating for a large order matrix results in $\phi \to 0$, which agrees with the prediction made above.

As a numerical example, the damping coefficient, f, will be calculated for a copper disk moving between two barium ferrite magnets with $\sigma = 0.6 \times 10^{-8}$ (Ohm-M)$^{-1}$, M = 0.35 tesla, $(\ell_1 - \ell_2)/\ell_1 = 0.66$,

$\Delta\ell = 0.8 \times 10^{-2}$m, and $R_3 = 8 \times 10^{-2}$m. For $R_3/R_4 = 0.3$, f = 250 Newton-sec/meter. If $R_4 \to \infty$, f = 250 Newton-sec/meter, according to Equation 4.3.10.

Calculations of ϕ as a function of $(R_3/R_4)^2$, with $R_1 = 0$, $L_1 \ll 1$, $R_3 = 8 \times 10^{-2}$m, and three values of R_3/R_4 (1, 0.8, 0.66), demonstrate that the maximum value of the damping coefficient, f = 220 Newton-sec/meter, is obtained when $(R_2/R_3)^2 = 0.5$. This implies that for optimal results, the area of the oppositely magnetized rings should be the same. The magnitude of ϕ, 220 Newton-sec/meter, for the case in which $R_3 = R_4$ is only 10-12% less than the value of ϕ for the case of $R_3/R_4 \to 0$, with all other parameters unchanged. Therefore, increasing the disk/magnet radius ratio (R_3/R_4) is of little value. It can also be verified that the assumption made earlier, that the results obtained with the disk hole radius $(R_0) \leq$ magnet radius (R_1) are not considerably different from those results where $R_0 = 0$. Actually, if the disk volume contained between R_3 and R_4 changes the value of f less than 10-12%, for $R_4 \to \infty$, it is natural that the volume of the disk with radius less than R_1 would change the value of f even less than 10%.

The optimal width of the copper disk, $\Delta\ell_m$, can be found from Equation 3.5 for thin systems. For fixed total width, ℓ_1, of the system, the given gap between magnet and disk, $\ell_3 = \ell_2 - \Delta\ell/2$, and for real systems $\ell_3 = 0.1$ cm and $\Delta\ell_m = (\ell_1 - \ell_2)_m = \frac{2}{3}(\ell_1 - \ell_3)$. The maximum value of the damping coefficient, f_m, with respect to $\Delta\ell$ is

$$f_m = \frac{32}{27}\pi M^2 \sigma R_4^2 \frac{(\ell_1-\ell_3)^3}{\ell_1^2}\left[\sum_n \frac{\bar{c}(n)^2}{x_n^2 J_1^2(x_n)} - 2\sum_n \frac{1}{x_{1n}^2-1}\left[\sum_m \bar{c}(m)\frac{x_m}{x_{1n}^2-x_m^2}\frac{J'(x_m)}{J_1^2(x_m)}\right]^2\right] \quad (4.4.2)$$

Comparing the calculations of ϕ using the exact Equation 4.3.2 with the approximate Equation 4.3.5, it is observed that the error is less than 10% for values of $\ell_1/R_4 < 0.1$. When $\ell_1/R_4 > 0.1$, the error increases. Therefore, when $\ell_1/R_4 < 0.1$, the approximate Equation 4.3.5 can be used. As the value of ℓ_1/R_4 increases, the magnitude of ϕ decreases. The reason for this decrease is that the z component of the magnetic field is the primary contributor to the damping coefficient, f. This component of the magnetic field causes the current in the plane perpendicular to the z direction, which is the most important factor for damping. As the value of ℓ_1/R_4 increases, the z component of the magnetic field decreases.

4.5 Conclusions

In summary, the most general equation for the damping coefficient, f, is Equation 4.3.2. Calculation of Equations 4.3.3 and 4.3.5 is necessary for solving Equation 4.3.2. In the case where $L_1 = \ell_1/R_4 << 1$, the simplified Equation 4.3.5 may be used. To obtain the maximum damping coefficient, f, the following parameters should be used:

$$(R_2/R_3)^2 = 0.5 \quad ; \quad \Delta\ell = \ell_1 - \ell_2 = \frac{2}{3} \ (\ell_1 - \ell_3) \tag{4.5.1}$$

The first of these two parameters allows for the areas of the oppositely magnetized rings to be equal. The second parameter relates the thickness of the disk, $\Delta\ell$, to the magnet thickness, $\ell_1 - \ell_2$, and to the total thickness of the system, ℓ_1, minus the thickness of the gap between the magnet and the disk, ℓ_3. Using the optimal parameters, Equation 4.5.1, the damping coefficient, f. can be calculated from Equation 4.3.10,

$$f = \frac{4\pi M^2 \sigma}{27} \ \frac{(\ell_1 - \ell_3)^3}{\ell_1^2} \ (R_3^2 - R_1^2) \tag{4.5.2.}$$

in all practically important cases with reasonable accuracy.

References

1. Mikulinsky, M. and Shtrikman, S.; Optimization of an Eddy Current Damper, EEIS (1979).

2. Davis, L. E. and Reitz, J. R.; Eddy Currents in Finite Conducting Sheets, J. Appl. Phys., 42, 4119 (1971).

3. Schieber, D.; Force on a Moving Conductor Due to a Magnetic Pole Array, Proc. IEE 120, 1519 (1973).

4. Schieber, D.; Braking Torque on Rotating Sheet in Stationary Magnetic Field, Proc. IEE 121, 117 (1974).

5. Schieber, D.; Optimal Dimensions of Retangular Electromagnet for Braking Purposes, IEEE Mag.-11, 948 (1975).

6. Penticki, C. J. and Ponbeau, P.; Progress in Astronautics and Aeronautics, 55, 35 (1977).

7. Hornreich, R. M. and Shtrikman, S.; Optimal Design of Synchronous Torque Couplers, IEE Mag.-14, No. 5 (1978).

8. Hornreich, R. M. and Shtrikman, S.; An Application of Brown-Morrish Theorem to Force Transmitting Devices, IEEE Mag. (in press).

9. Christy, R. W., Milford, F. J., and Reitz, J. R.; Foundations of Electromagnetic Theory; Addison-Wesley Publishing Company, Third Edition, 1980.

V. PROPERTIES RELATING TO EDDY-CURRENT DAMPERS OPERATING IN CRYOGENIC ENVIRONMENTS

5.1 Resistivity Values of Damper Materials

From the simplified basic equation for the damping coefficient

$$C_d = \frac{B^2 l A}{\rho} ,$$

it is obvious that C_d is maximized by a minimum in the resistivity, ρ. Thus, it is imperative that the damper material have the lowest possible resistivity, along with the required mechanical properties for operation at 27°K.

The electrical resistivity of most pure metallic elements at ordinary and moderately low temperatures is approximately proportional to the absolute temperature. It is postulated that the microscopic mechanism responsible for the temperature dependence is the interference to the flow of electrons caused by the thermal agitation of the crystal lattice. At very low temperatures, however, the resistivity approaches a residual value almost independent of temperature. This residual resistance is attributed to lattice imperfections and impurities. A small impurity has the effect of adding a temperature-independent increment to the resistivity.

Alloys, as a rule, have resistivities much higher than those of their constituent elements and resistance-temperature coefficients that are quite low. For example, the alloy, 60 parts copper, 40 nickel (constantan), has a room-temperature resistivity of about 44 micro-ohm cm while copper and nickel separately have resistivities of 1.7

and 6 micro-ohm respectively. Also, while the residual resistances of the pure metallic elements at very low temperatures are very small, that of constantan is about 95 percent of the room-temperature value.

Table 5.1 shows the temperature dependence of resistance of several possible candidate elements for use as an eddy-current damper.

TABLE 5.1

Effect of Temperature on the Electrical Resistance of Several Pure Elements [1]

(Values are given as R/R_0, where R is the resistance of a specimen at the indicated temperature and R_0 is its resistance at 0°C or 273°K)

Temp. °K	Temp. °C	R/R_0 Al	Cu	Mg	Ni	Pb	Zn
193	-80	0.641	0.649	0.674	0.605	0.683	0.678
173	-100	.552	.557	.590	.518	.606	.597
153	-120	.464	.465	.505	.437	.530	.516
133	-140	.377	.373	.419	.361	.455	.435
113	-160	.289	.286	.332	.287	.380	.353
93	-180	.202	.201	.244	.217	.306	.271
73	-200	.120	.117		.156	.232	.188
53	-220	.071	.047		.112	.157	.108
33	-240	.049	.012		.089	.075	.041
20	-253	.0427	.00629		.085	.0303	.014

Silver has a resistivity-ratio at 27°K of only about twice that of copper, but pure silver has very poor mechanical and machining properties. Copper has the lowest resistivity at the required working temperature and its mechanical characteristics are satisfactory, although it's machineability is poor.

A literature search for values of resistivity, ρ, for a "pure" copper at low temperatures has indicated the values as shown in Table 5.2.

TABLE 5.2

Resistivity of "Pure" Copper

Source	T_{rm} 20°C = 293°K 67°F = 527°R	T_{LN_2} -197°C = 76°K -323°F = 137°R	Tssme -247°C = 27°K -411°F = 49°R
A-	---	~2×10^{-9} Ω-m	~3×10^{-11} Ω-m
B	---	---	~3×10^{-11} Ω-m
C	1.553×10^{-8} Ω-m (±.005) (273°K)	1.86×10^{-9} Ω-m (±.02)	~4×10^{-11} Ω-m
D	1.7×10^{-8} Ω-m	~3×10^{-9} Ω-m	< 1×10^{-9} Ω-m
E	1.55×10^{-8} Ω-m	~2×10^{-9} Ω-m	~1.6×10^{-10} Ω-m
F	~1.6×10^{-8} Ω-m	~2×10^{-9} Ω-m	~1.4×10^{-10} Ω-m

(A) L. A. Hall. "Survey of Electrical Resistivity Measurements on 16 Pure Metals, in the Temperature Range 0 to 273°K", N.S.B. Technical Note 365, Washington, D.C.

(B) P. K. Moussouros and J. F. Kos. "Temperature Dependence of the Electrical Resistivity of Copper at Low Temperatures", Can. J. Phys., Vol. 55, No. 23, 1977, pp 2071-2079.

(C) F. R. Fickett. "A Preliminary Investigation of the Behavior of High Purity Copper in High Magnetic Fields", N.B.S., Cryogenics Division, U-235, June 1972.

(D) "Handbook of Thermophysical Properties of Solid Materials", Vol. I, 1961.

(E) D. L. Grigsby. "Electrical Properties of Copper, Manganin, Evanohm, Cupron and Constantan at Cryogenic Temperatures", Hughes Aircraft Co., October 1966, Electronic Properties Information Center, I.R. No. 40.

(F) R. Barron. "Cryogenic Systems", McGraw-Hill, 1966.

5.2 Behavior of High Purity Copper in High Magnetic Fields[1]

At low temperatures, the resistivity of copper increases almost linearly with increasing magnetic field. This is true for a range of purity of 200 < RRR < 7000 and for a temperature range of 4K < T < 35K. RRR stands for the Residual Resistance Ratio which is equal to R(273K)/R(4K) and is a sensitive indicator of purity, i.e., increasing ratio represents an increasing purity. Increases in the resistivity by a factor of 120 have been observed for a very high purity copper sample at 4K in a field of ~100K gauss or 10 tesla.

However, for any magnetic field and temperature, the value of the resistivity can be accurately predicted by Kohler's rule which is

$$\frac{\Delta R}{R_o} = f\left(\frac{B}{R_o}\right)$$

where B is the magnetic field (flux density), R_o is the resistance at zero field and $\Delta R = R(B)-R_o$. For pure metals, f is a single-valued and monotonically increasing function of B/R_o.

A Kohler diagram for copper is shown in Figure 1, which is a plot of $\Delta R/R_o$ versus B·RR(T), where RR(T) is the resistance ratio, R(273K)/R(T), and $R(T) = R_o$.

---

1. F. R. Fickett. "A Preliminary Investigation of the Behavior of High Purity Copper in High Magnetic Fields", N.B.S., Cryogenics Division, U-235, June 1972.

Consider now an example for a practical damper design with a copper disk. Using a realistic magnetic flux density for a permanent magnet of one tesla or 10^4 gauss, an extremely low value of resistivity at 27K = 4×10^{-11} Ω-m and a resistivity at 273K = 1.55×10^{-8} Ω-m, then B·R(273K)/R(T) = 3.9×10^3 kilogauss and from Figure 1, we see that the resistance due to the magnetic field has increased by 100 percent or a factor of 2. However, if a more conservative value of resistivity at 27K of 5×10^{-10} Ω-m is used, then the resistance increase is only about 3 to 4 percent.

FIGURE 1

Kohler Diagram for Copper

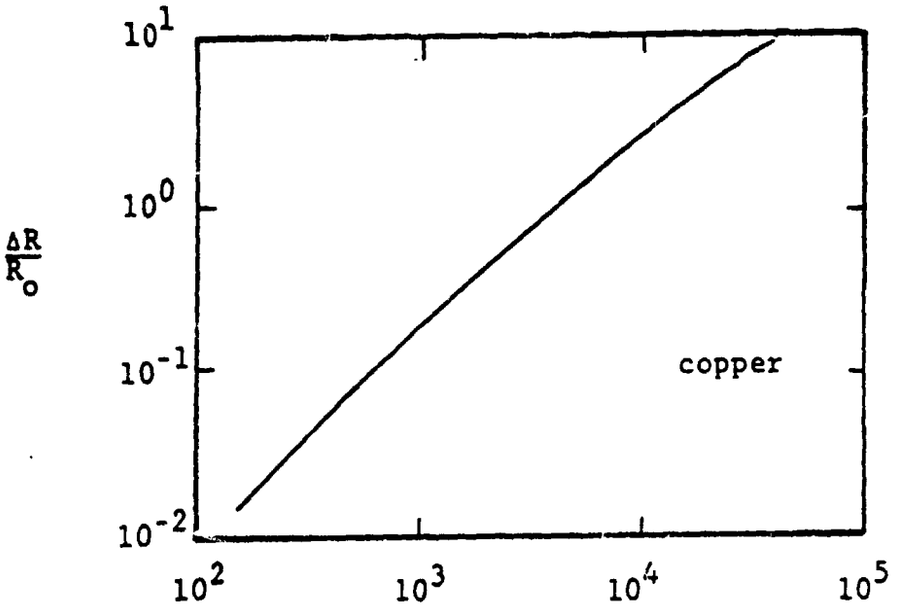

Thus, it would appear that the dominating factor in the increase of resistivity due to the magnetic field would be the purity (RRR) of the copper. A practical value of resistivity at 27K would probably lie somewhere between the two examples above and thus the problem of an increase in resistivity due to a magnetic field and hence a decrease in the damping coefficient should not be a severe or overriding concern.

5.3 Eddy-Current Depth of Penetration[1,2]

The solution of Maxwell's equation, when a sinusoidal magnemotive force is applied on a nonferrous conducting plate, gives a wave of flux density B_o that enters the plate from the outside surface at the start of each half-cycle, and penetrates to a depth δ, called the depth of penetration. If δ is less than d, the half thickness of the plate, the magnetic flux as well as the eddy-currents generated are essentially restricted to a layer of depth δ on each surface of the plate. If the δ is larger than d, the flux-density waves from each side meet in the center of the plate before the end of the half-cycle of the sinusoidal magnemotive force and eddy-currents flow throughout the full width of the plate.

The equations listed below,

$$\nabla^2\vec{H} = j\omega\sigma\mu H$$

$$\nabla^2\vec{E} = j\omega\sigma\mu E$$

$$\nabla^2\vec{J} = j\omega\sigma\mu I,$$

give the basic relation between time and space derivatives of the magnetic field, electric field, or current density for any point located in a conductor.

Solving for the current distribution equation, for the case of a plate conductor with current flow parallel to the surface, the depth of penetration is

$$\delta = \left(\frac{2}{\omega\sigma\, B_o/H_m}\right)^{1/2} = \frac{1}{\sqrt{\pi\, f\, \sigma\, \mu}} \quad \text{meters.}$$

---

1. P.D. Agarwal. "Eddy-Current Losses in Solid and Laminated Iron", AIEE Trans., 1959, 78, Pt. (1), pp 169-181.

2. S. Ramo and J. Whinnery. "Fields and Waves in Modern Radio", John Wiley & Sons, Inc., NY, 1953.

The complete solution indicates that the current magnitude decreases exponentially as it penetrates into the conductor. Thus, δ is the depth for which the current density has decreased to 1/e (~36.9) of its value at the surface.

From the standpoint of an eddy-current damper, it is apparent that there would be an optimum range of thickness for the conducting plate, i.e., too thin a plate for the frequencies expected and the full damping potential is not utilized, and with too thick a plate, there is excess plate material and weight, etc., which is serving no useful purpose. Using a conservative value of $\rho = 0.5 \times 10^{-9} \Omega$-m for copper at 27°K and $\mu = 4\pi \times 10^{-7}$ Henrys/meter, a plot of the depth of penetration versus frequency is shown in Figure 1.

This figure shows that for the range of frequencies of interest for the SSME, namely, ~36,000 RPM or 600 Hz, the depth of penetration is only on the order of 5×10^{-2} cm. Even at 1000 RPM or 16 Hz, the penetration depth is quite small, $\delta = 0.15$ cm. Thus, at operating speeds of ~36,000 RPM, with an 0.25 inch (0.635 cm) copper disk as the damping conductor, most of the eddy-currents would reside very the surface and little use would be made of the bulk of the material. It would seem that, at first glance, perhaps a much more efficient design would consist of a layered or laminated type of disk construction, such as shown in Figure 2.

FIGURE 2

Laminated Damper Disk for Improved Efficiency

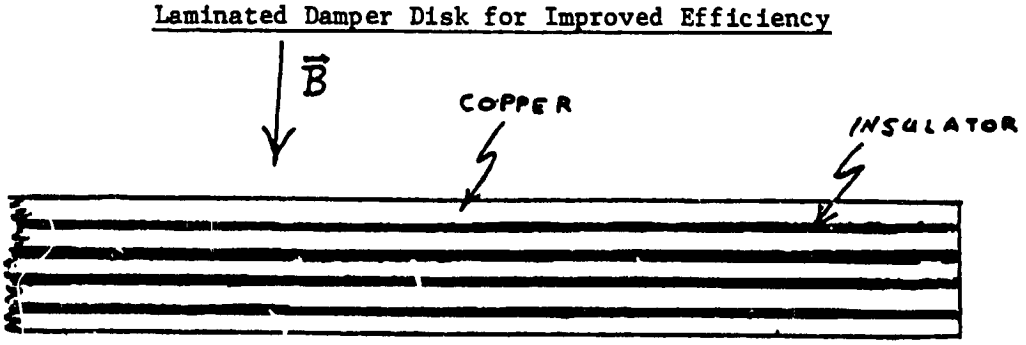

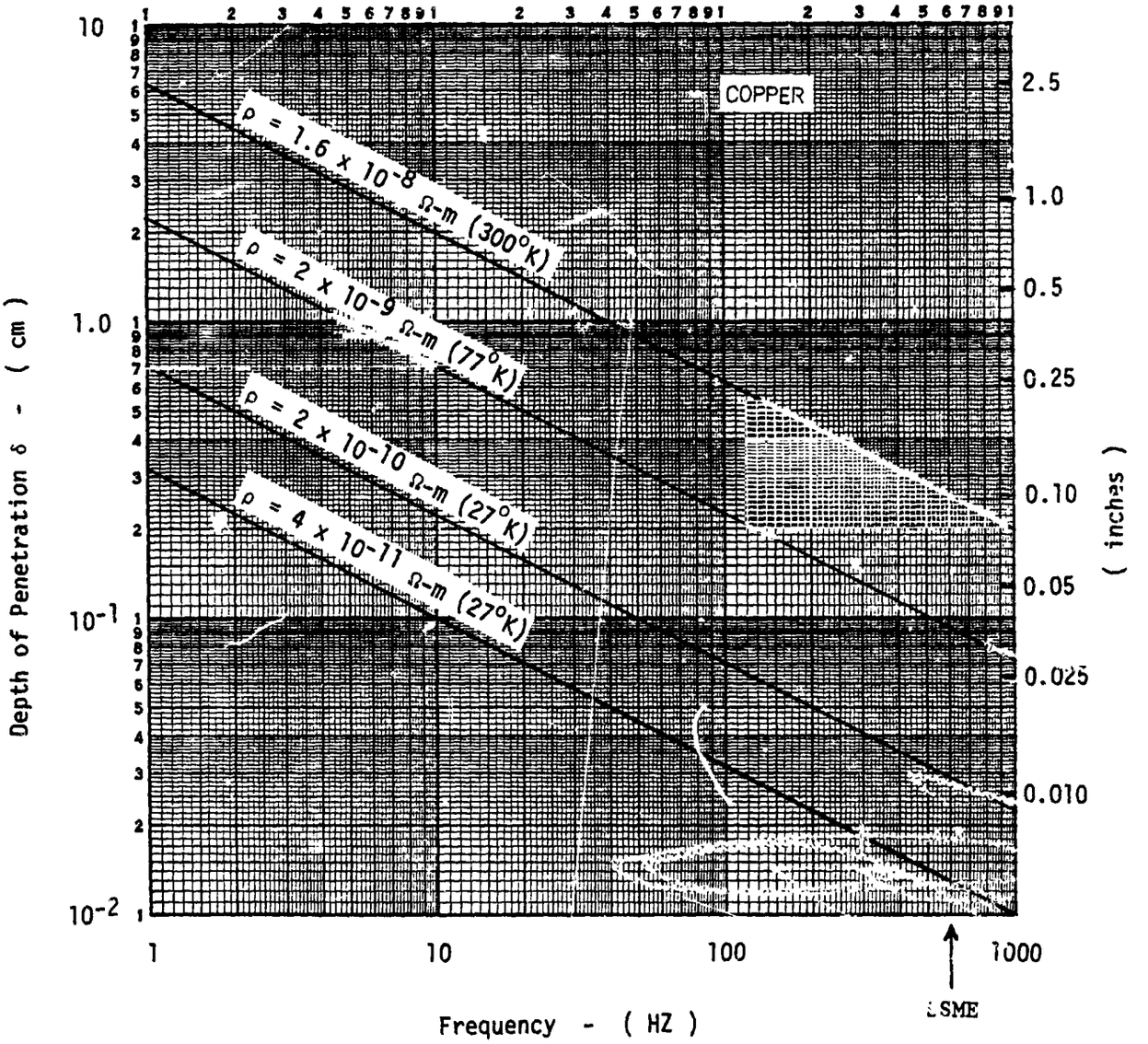

Figure 1. DEPTH OF PENETRATION VS FREQUENCY

Several thin copper sheets, with insulated layers between, could make up the total disk thickness, with the thickness of one copper sheet still much greater than the depth of penetration, but now the total magnitude of eddy-currents has increased by a factor equal to the number of laminations of sheets. This, in turn, would mean that the damping effect has also increased by the same factor.

This design is exactly opposite to the design of transformer cores, etc., where the laminations are made parallel to the changing magnetic field in an effort to eliminate or drastically reduce the eddy-current and hysteresis losses.

5.4 Magnetic Induction Variation With Temperature

The remanance, or magnetic induction which remains in a magnetic circuit after an applied magnetomotive force is removed, is temperature dependent. Generally, it will decrease as the temperature increases and will become zero at the Curie point, at which all ferromagnetic properties vanish. This, then, implies that the remanance would conversely increase as the temperature decreases, and indeed this effect is observed in some cases. There are both non-reversible variations and reversible variations as a function of temperature.

The non-reversible effect results in a change in the remanance of a magnetized magnet and it's circuit which has been temperature cycled. This non-reversible change on stabilizing processes is associated with a loss in the remanant induction. But the initial value of remanance may be restored by remagnetizing the stabilized magnet, so long as the temperature variation did not result in an irreversible metallurgical change of the magnet material.

After stabilization over a given temperature range, any further changes of remanance within this temperature range are reversible. This relative reversible variation in percent is calculated by measuring the remanance $B_d(t)$ at the temperature to within the stabilized range and then comparing this with the room temperature remanance $B_d(20)$ by the expression

$$\frac{B_d(t) - B_d(20)}{B_d(20)} \times 100\% \quad .$$

Thus, a temperature coefficient over a given range can be determined. Both the non-reversible and reversible variations are dependent upon

a shape factor or L/D ratio (length of magnet to the equivalent diameter of magnet) and to the magnetic material type. For instance, for a temperature range from -60°C to +80°C, the net coefficient is negative and may be as large as several tenths of a % per °C. Alinco V, for example, has a temperature coefficient of -0.024 %/°C for L/D = 8 over a temperature range of 0 to 80°C.

Mr. Shuk Rashidi of Hitachi Magnetics Corporation indicated that they test magnets down to -100°C and he estimated that the temperature coefficient may be as large as 0.04 %/°C at very low temperatures. Their catalog gives a value of 0.033 %/°C for HICOREX, a rare-earth cobalt permanent magnet, from 20°C to -100°C.

Thus, while hard data on magnet properties at low temperatures is apparently not presently available, it appears as though a beneficial increase of magnetic induction and hence the damping coefficient may be experienced. For example, with a cobalt magnet and increase in induction of approximately 10% or more should occur at 27°K. Since the damping coefficient varies as the square of the magnetic induction, the net result should be at least a 20% increase in damping. Laboratory testing of this phenomena should be carried out to establish more accurate data on the temperature coefficient and the effect of temperature recycling on the magnetic properties.

VI. EXPERIMENTAL TESTS

A series of tests, using a simple vibrating rod, was conducted to observe the phenomena of eddy-current damping and the effect of damper material thickness, layers and temperature.

6.1 Vibrating Rod Set-Up

The basic apparatus consisted of a 1/2" thick aluminum plate, which was securely attached to a rigid upright stand [see Fig. 6.1]. The rod length was adjustable. A half-flat on the end of the rod allowed for the attachment of the damper. The damper was always 2" wide x 3 1/2" high and the thickness was varied from 0.031" to 0.275".

A rather ancient magnetron Alnico V magnet provided the magnetic flux. It had a 1.25" diameter pole face with a gap of 0.82" and produced an average field of approximately 1200 gauss (0.12 tesla). The magnet was mounted on a small laboratory jack and could be raised so that it was centered on the damper, or it could be lowered about 6" to make tests without the magnetic field acting on the damper.

The relative amplitude of vibration of the rod was measured by a proximity probe mounted so as to detect motion about 2" above the damper. The output of the proximitor was connected to one input of an HP-5420A Digital Signal Analyzer. The rod was struck to induce vibrations by an impact hammer with an attached accelerometer. The accelerometer output was connected to the second input and this permitted a variety of information to be obtained directly from the HP-5420A, such as frequency spectrum, transfer function--both real and imaginery, time average for observing the signal decay and the damping.

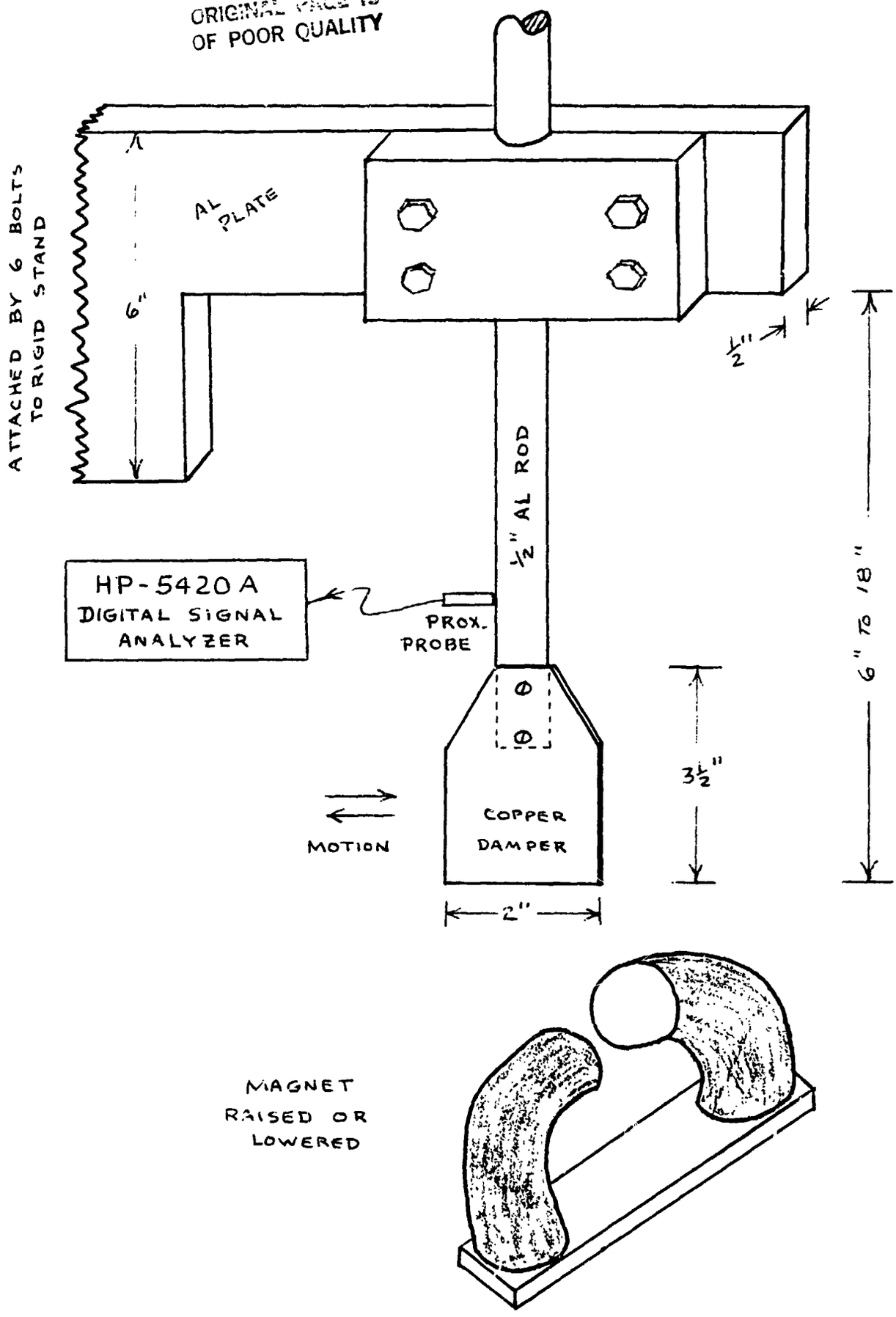

Figure 6.1 VIBRATING ROD SET-UP

A styrofoam container, with and without the magnet centered on the bottom, was filled with liquid nitrogen, placed on the jack and raised and lowered for observing vibration data for low temperature (77°K) damper tests.

It was found that, within experimental error, the observed damping effect did not change for tests, without the magnet, conducted at room temperature or at LN_2 temperature.

6.2 Damping Calculations

The damping coefficients for the vibrating rod were calculated from the rod and damper mass, the resonant frequency and the log decrement of the rod motion wave-form after being struck. The critical damping of a one-dimensional system is related to the stiffness, mass, and natural frequency by

$$C_c = 2\sqrt{km} = 2m\omega_n. \tag{6.1}$$

The actual or measured damping coefficient, C_m, is related to the critical damping by the damping ratio or factor,

$$\zeta = \frac{C_m}{C_c}, \tag{6.2}$$

and for small values of this damping ratio,

$$\zeta = \frac{\delta}{2\pi}, \tag{6.3}$$

where δ = log decrement = $\ln \frac{x_1}{x_2} = \frac{1}{n} \ln \frac{x_0}{x_n}$,

x = amplitude of vibration,

n = number of cycles.

Thus, the measured damping coefficient can be determined from

$$C_m = \zeta C_c = \frac{\delta}{2\pi} \, 2m(2\pi f_n)$$

$$\boxed{C_m = 2m\delta f_n} \quad \frac{\text{lb-sec}}{\text{in}} \text{ or } \frac{\text{N-sec}}{\text{m}}. \tag{6.4}$$

The theoretical damping coefficient, as derived earlier in this report, may be calculated from

$$\boxed{C_t = \frac{B^2 V}{\rho}} \quad , \tag{6.5}$$

where B = magnetic flux density,

V = volume of damper material in magnetic field,

ρ = resistivity of damper material.

The theory thus indicates that the damping effect should vary linearly with damper thickness, at least for thickness less than the penetration depth. Also, the damping should increase by a factor of about 8 when the damper material is at liquid nitrogen temperature, since $\rho T_{Rn} \approx 1.6 \times 10^{-8} \Omega$-m and $\rho T_{LN_2} \approx 2 \times 10^{-9} \Omega$-m.

6.3 Practical Observations

The exact nature and paths of the eddy-currents are extremely difficult to examine analytically, as several of the texts on motors and E & M have acknowledged.

For the case of a solenoid or iron-core transformer, the eddy-current picture is fairly clear. The changing magnetic field and the volume of material in which the eddy-currents are induced are both well defined and thus the theoretical damping coefficient relation, Eq. 6.5, should yield accurate information.

However, for the proposed SSME eddy-current damper configuration, the picture is considerably different and unclear. The EMF which produces the eddy-currents is induced solely by a changing magnetic field, according to Faraday's Law:

$$EMF = -\frac{\partial \phi}{\partial t} = -\frac{\partial (BA)}{\partial t} . \qquad (6.6)$$

Thus, for the case, where the damper material extends in all directions well beyond the area of the magnet pole faces, it is obvious that the magnetic field is not going to be changing in the moving material over most of the internal area of the pole faces, since the field is assumed uniform here. The magnetic field will be changing in the moving damper material near the edges and fringe regions outside the pole face area where the stationary magnetic field exhibits a gradient or non-uniformity. More simply expressed, if there was no fringing and the magnetic field was uniform exactly over the entire pole face area, then EMFs (hence eddy-currents) would be produced in the moving material only at the edges of the pole face area where change of flux is occurring, and no

EMFs would be generated in the material interior area of the pole face, since there is no $\frac{\partial \phi}{\partial t}$ in this region. The implications of this indicate that it would be extremely difficult to calculate a theoretical damping coefficient from Eq. 6.5 for this practical situation because, due to fringing, neither the magnetic field B nor the exact damper material volume (area x thickness) is known for the regions of interest.

To check the validity of the concept that no eddy-currents would be produced in the moving damper material in the interior area of the magnet pole face, a simple qualitative type experiment was performed. A one foot long insulated pendulum, with a circular 1/32 inch thick copper disc of diameter 5/8 inch attached at the bottom, was rigged so that it would swing for 65 to 70 cycles in air when started with an initial deflection of 1/4 inch (see Fig. 6.2).

Next, a magnet with a 1 7/16 inch diameter pole face was placed so that the copper disc on the pendulum was halfway into the pole face area and would swing in the center of the gap separation perpendicular to the magnetic field. Thus, a portion of the disc would be cutting magnetic lines as it travelled from a low to high magnetic field and vice-versa, and an eddy-current damping effect should be present. Indeed, this was observed as the pendulum would now swing for only 35 to 40 cycles with an initial deflection of 1/4 inch from a rest position.

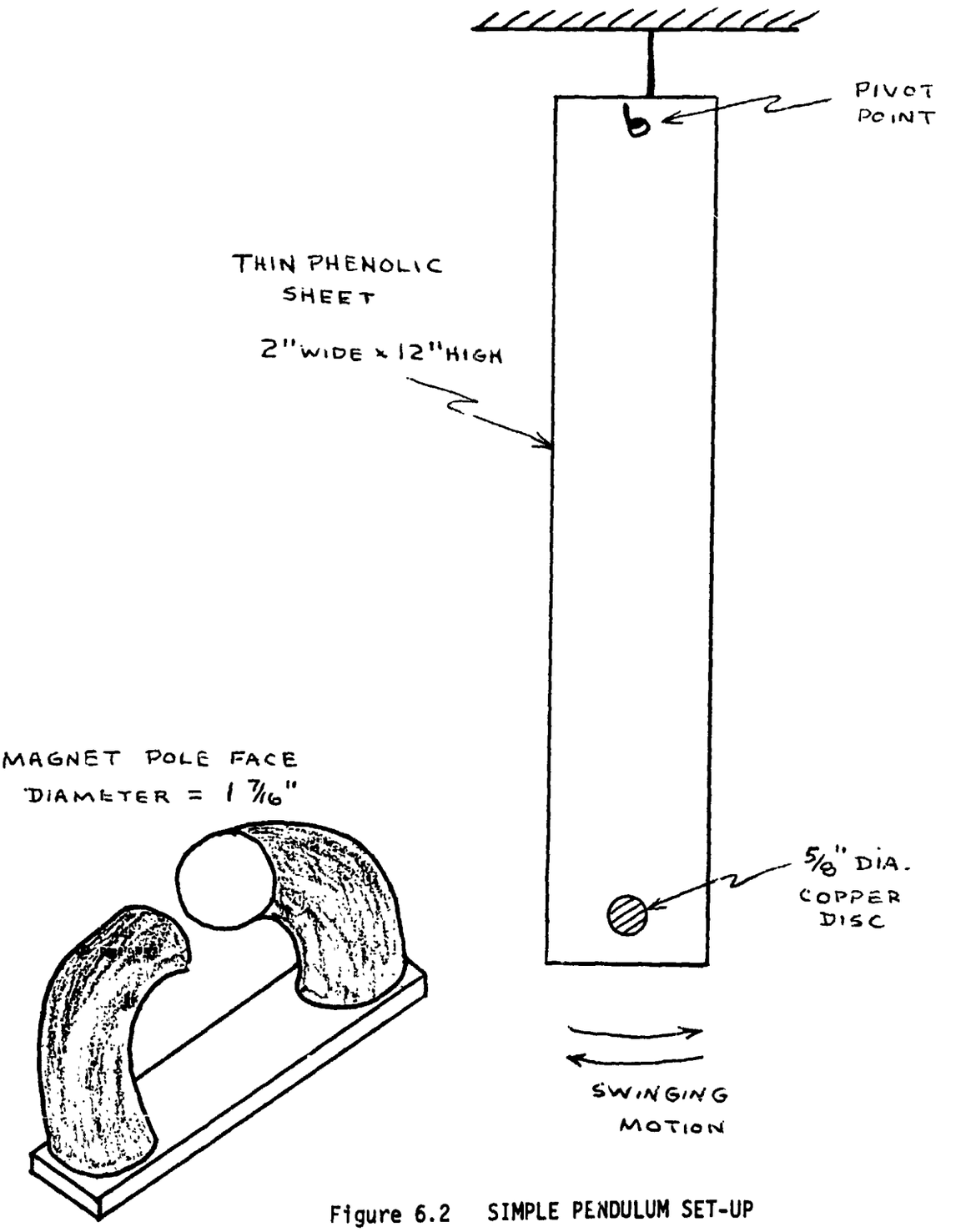

Figure 6.2 SIMPLE PENDULUM SET-UP

Finally, the magnet was again moved such that the disc was now in the center of the magnetic field. The swing test was then found to again produce 65 to 70 cycles for the 1/4 inch initial deflection. These 3 cases were each repeated for about 10 trials. The results are shown in the table below.

TABLE 6.1

Pendulum Swing Test Results

Initial Conditions	No. of Cycles of Swing for 1/4" Initial Deflection
No Magnet - Free Swing	65 to 70
Copper disc on pendulum half into magnet gap - large gradient present	35 to 40
Copper disc on pendulum located at center of magnetic field (i.e., gap) - uniform magnetic field	65 to 70

This brief experiment clearly demonstrated that the area or volume of damper material in the interior uniform magnetic field region does not contribute to eddy-current damping, since there is no variation of magnetic flux within the damper material to induce the EMF's needed for eddy-current generation. Thus, to optimize the damping effects for this configuration, which is similar to that proposed for the SSME, the regions of largest magnetic field gradients should be maximized, along with the volume of damper material in this region. The magnetic shape could have a strong influence on the fringing or gradient

picture, i.e., a square cornered magnet should produce more fringing as compared to a round magnet. Also, it would appear that several long rectangular magnets would be more effective as compared to a circular magnet of equal pole-face area, since the area of uniform magnetic field is greatly reduced, whereas the magnet edge area, at which the large gradients occur, is greatly increased.

An idea for possible exploration would be to insert small segments or pieces of a ferrous material into the copper damper in the inner pole-face region where the flux density, B, is generally very uniform, and hence produces no induced emf's for eddy-current damping when the damper is moving. WIth a ferrous insert, the magnetic field would now have a gradient, thus inducing emfs which produce the desired damping effect. The inserts should not penetrate the total damper thickness, so that some low resistivity copper is present to maximize the eddy-current damping.

Again, this is an extremely difficult problem, to calculate the damping from theory. Probably the most feasible path would be for a series of experimental tests to be conducted with various empherical relations resulting.

6.4 Results of Variation of Volume and Temperature of Damper Material

Using the vibrating rod set-up as described in Section 6.1, a number of tests were conducted to observe the effect of eddy-current damping with variation of thickness and temperature of the damper material. The measured damping coefficient, C_m (Eqn. 6.4), was determined from the calculated mass and the log decrement and vibrating frequency as observed on the time-record plot from the HP-5420A. Typical plots of the time-record taken without and with the magnet are shown in Figs. 6.3 and 6.4.

The increase in damping due solely to the effects of eddy-currents could thus be determined by noting the difference in the measured damping coefficients, C_m, from the "without" magnet to the "with" magnet case. This increase in damping, expressed as a percent, is plotted in Fig. 6.5 as a function of damper thickness for both the room temperature and liquid nitrogen tests. The increase in damping, ΔC_m in lb-sec/in, versus damper thickness is shown in Fig. 6.6.

If the thecretical damping coefficient, $C_T = \frac{B^2\ LA}{\rho}$, is compared to the measured increase in damping, $\Delta C_m = C_m(\text{magnet}) - C_m\ (\text{no magnet})$, by a factor K, such that

$$K = \frac{C_T}{\Delta C_m}$$

then the plot of K versus damper thickness as shown in Fig. 6.7 gives an indication of how accurately this relationship represents the response of the set-up configuration, compared to an ideal one, where K should equal unity.

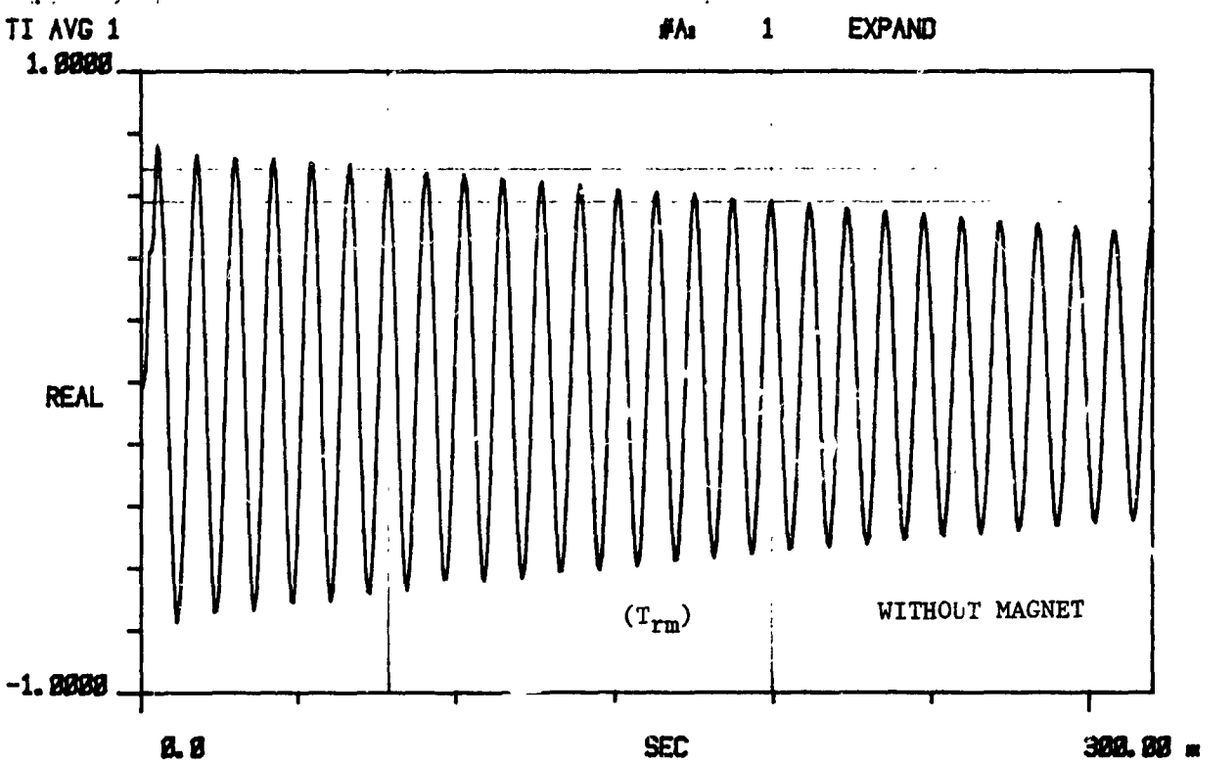

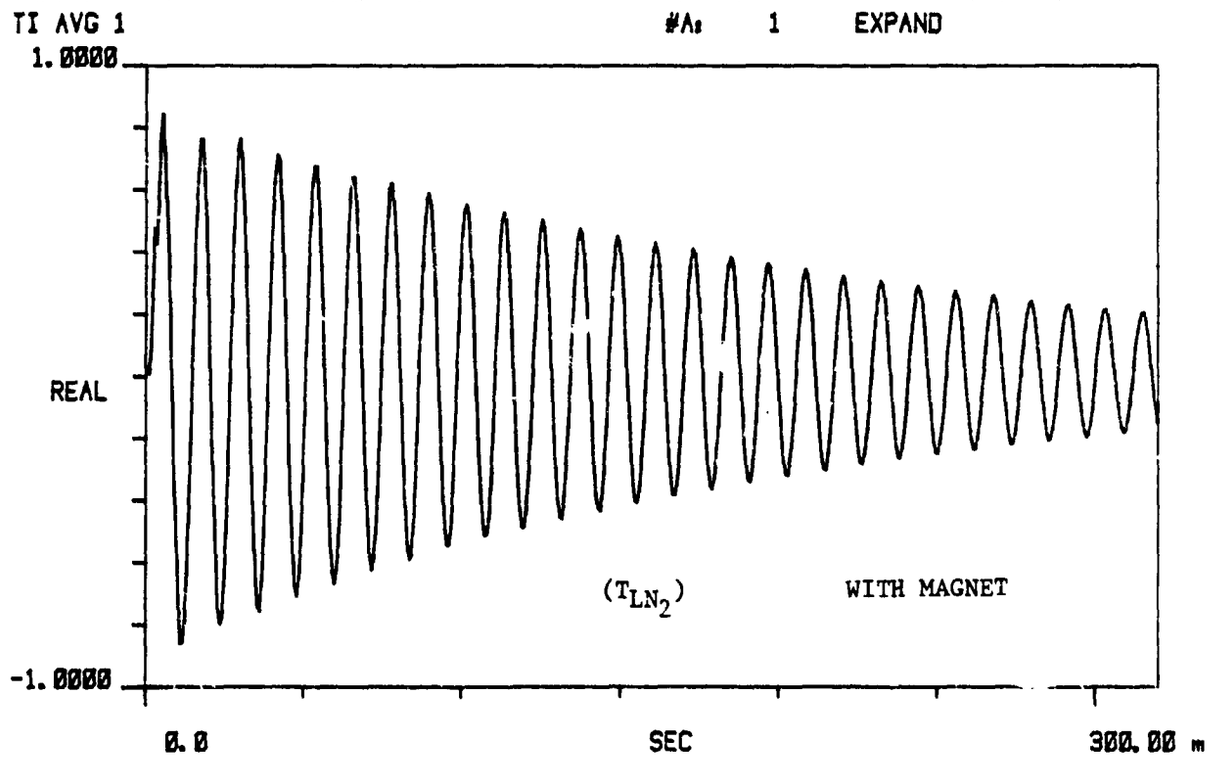

Figure 6.3. Typical Time Records of Probe Output for Determining Frequency and Log Decrement

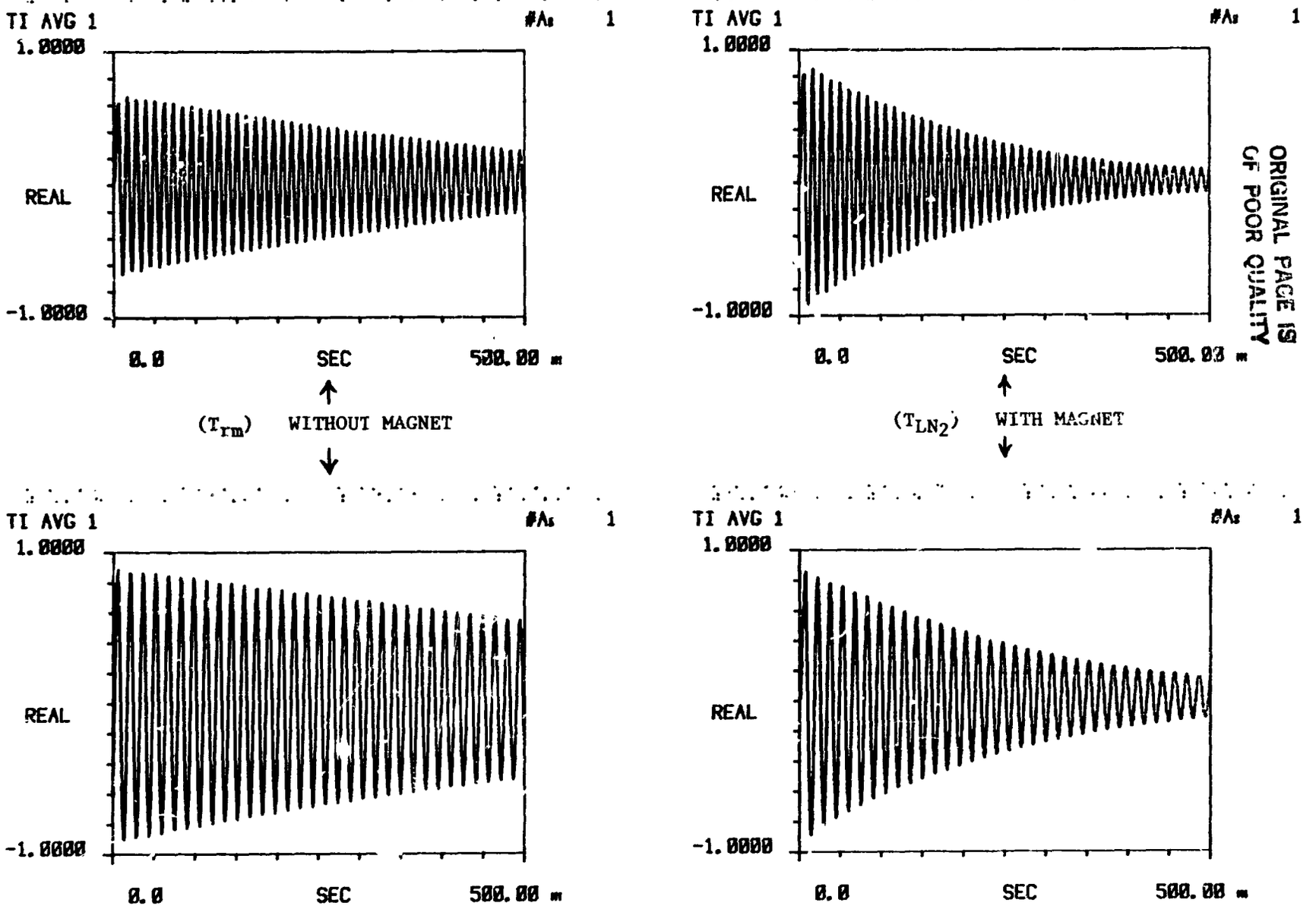

Figure 6.4 Typical Time Records of Probe Output for Determining Frequency and Log Decrement

% INCREASE IN DAMPING (with and w/o magnet)

vs

DAMPER THICKNESS

B_{avg} = 1200 Gauss

Copper

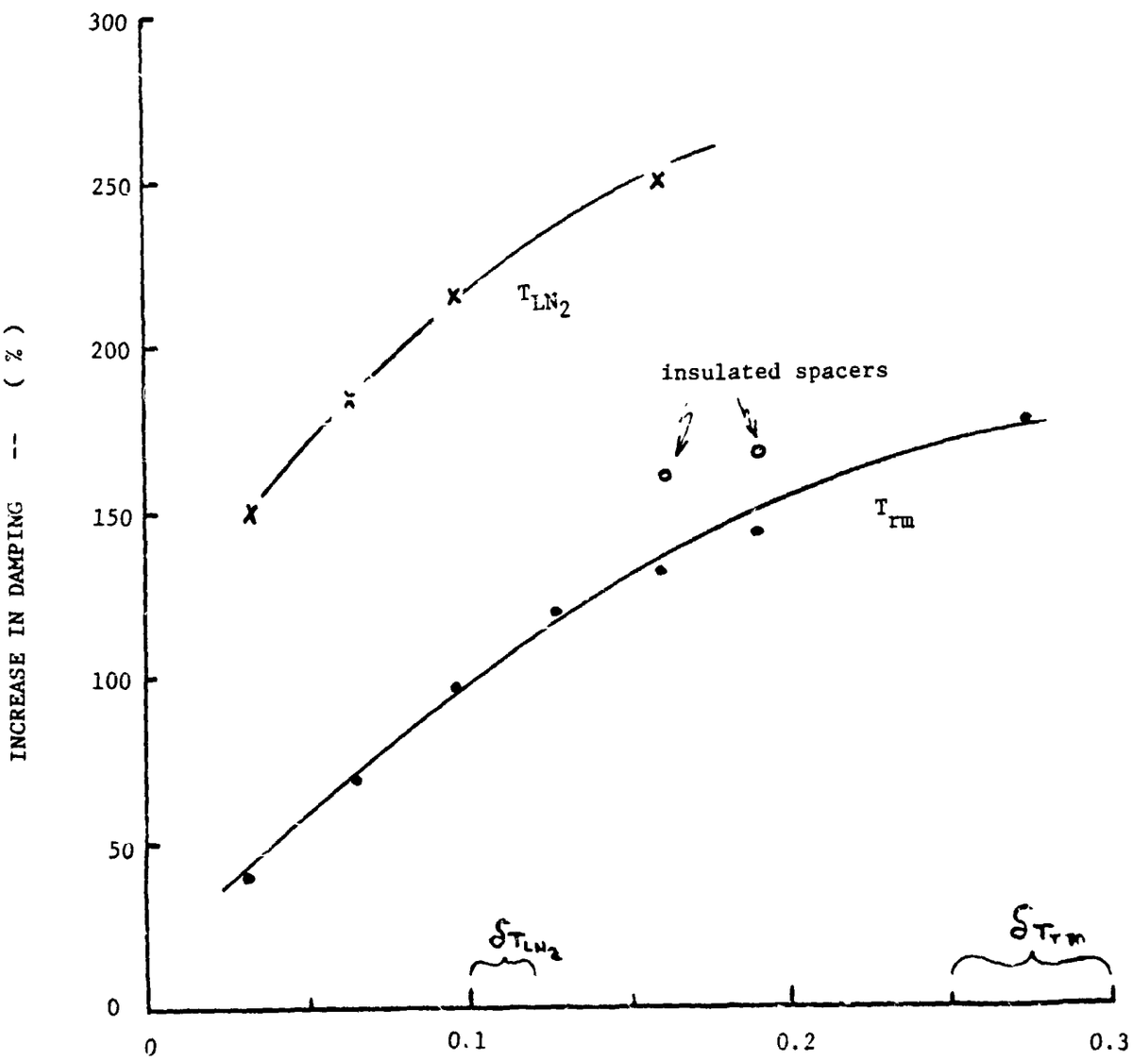

DAMPER THICKNESS - (inches)

Figure 6.5

$\Delta C_M = C_{M(magnet)} - C_M(no\ magnet)$

vs

DAMPER THICKNESS

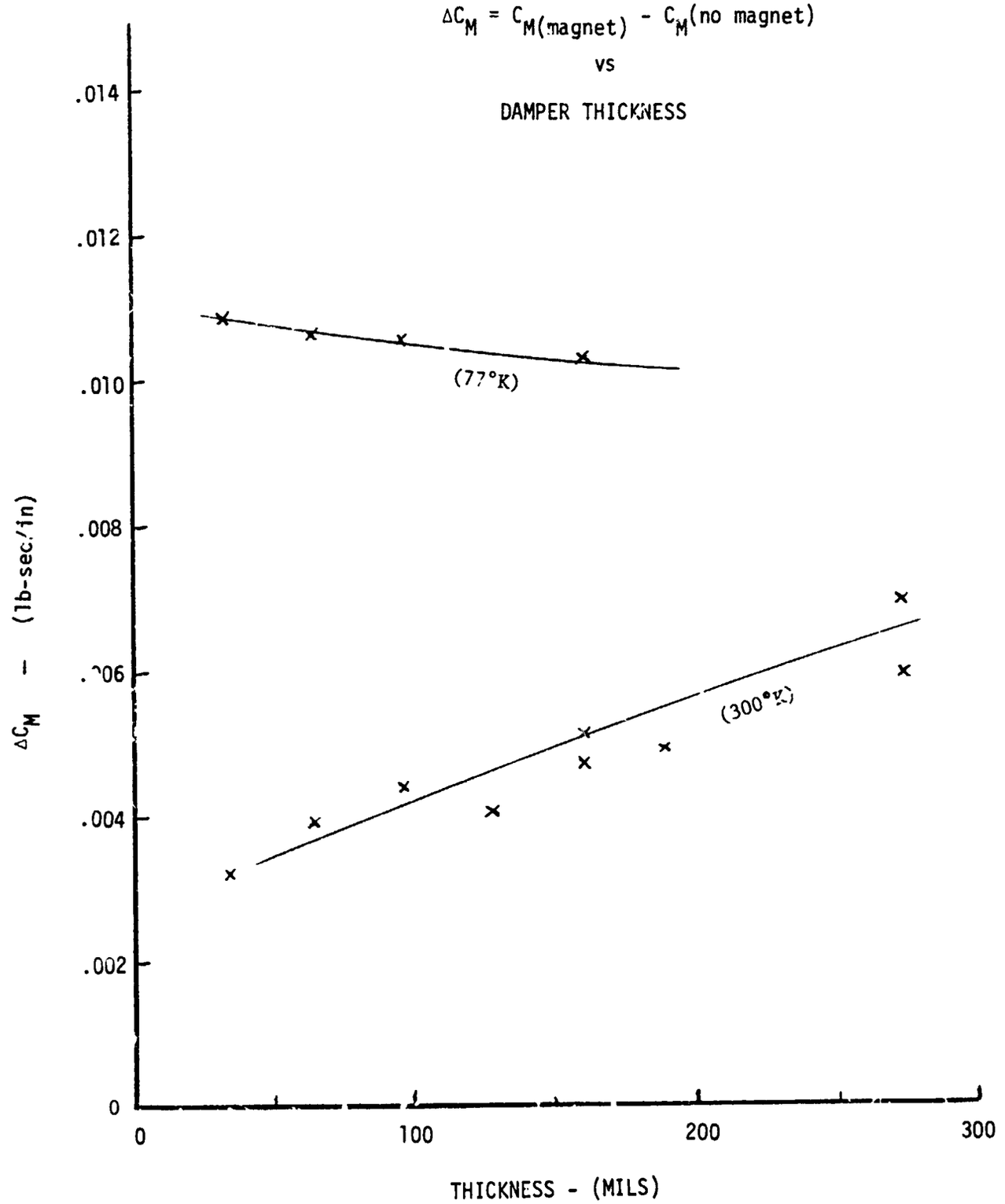

Figure 6.6

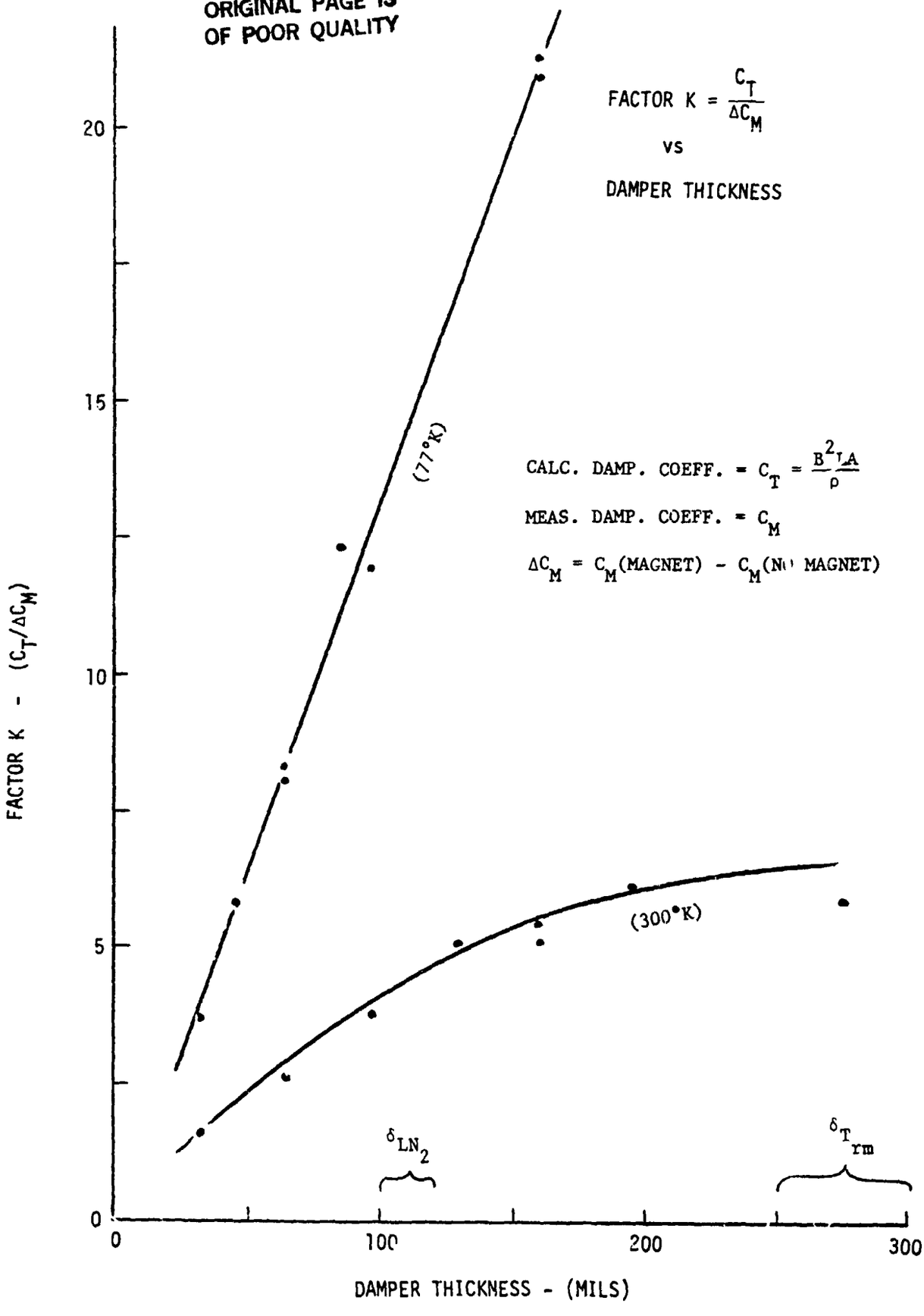

Figure 6.7

From an inspection of these three figures, several immediate observations can be made.

1. The eddy-current damping does increase with increasing damper thickness, although not linearly as the theory predicts.
2. There is a large increase in the eddy-current damping as the temperature is lowered from room temperature to liquid nitrogen temperature, 76°K. However, for the smallest thickness, the magnitude of the increase was only about one-half the expected value of δ, and as the damper thickness increased, this value decreased even more.
3. The large values of the factor K indicate that the measured eddy-current damping is considerably less than the theory predicts and that this discrepancy increases with damper thickness.
4. The two data points using a laminated damper, made of individual 0.032 inch thick copper damper sections with a thin paper sheet between sections, perhaps suggest that there may be an additional increase in damping achieved by taking into account the eddy-current depth of penetration as explained earlier. However, more experimental data is necessary to further explore this concept.

6.6 Discussion

The results of this rather crude test show that the measured eddy-current damping does not compare favorably with the expected theoretical damping values for the various tests. There are several obvious reasons relating to the causes for this discrepancy and they are as follows:

A. The proper value of the magnetic flux density, B, to be used in the theoretical damping coefficient is very difficult to determine. For this experimental set-up, a profile of the flux density at the mid-span between the two pole faces showed that at the center, B ≈ 1700 gauss, while around the mid-span circumference, B ≈ 1000 gauss. A value of 1200 gauss was used in the calculations. However, as noted in Section 6.3, Practical Observations, the eddy currents necessary for the desired damping are induced by the moving damper only in the presence of a magnetic field gradient, i.e., in the near-regions to the edges of the magnet pole faces. Eddy currents are not induced in a constant field. Thus, with the fringing effects being an unknown for this set-up, it would be very difficult to assign a number for the flux density, B. With the proper equipment, a complete profile of the flux density at the plane of the damper could be obtained over an area considerably greater than just the pole face area, and perhaps an average or effective value of B could be determined.

B. the proper value of damper area to be used in the theoretical damping coefficient is also difficult to determine. The same reasoning as discussed in A above applies to the area parallel to the plane of the pole-face. The correct value of area should be that over which there is a magnetic field gradient occuring. Some effective value of area should be used, but the magnet pole face area was used for these tests.

C. For the low-temperature tests conducted with liquid nitrogen, it is possible that the damper did not come to an equilibrium temperature, since no temperature measurement of the copper material was made. Within about five minutes after insertion into the liquid nitrogen, the violent boil-off from the nitrogen vaporization had almost ceased and then data-taking began, but the actual temperature of the damper may have been higher than the LN_2 temperature used in the calculations, due to insufficient time for thermal equilibrium, and thus the damper resistivity would be greater than value used for the calculations.

Also, the calibration of the displacement probe is somewhat suspect at the low temperatures. This type of probe is temperature sensitive and the gap or D.C. voltage was noted to change from 8.2 volts at room temperature to over 11.2 volts at LN_2 temperature. The probe was approximately 1 to 1 1/2 inches above the liquid nitrogen level and it definitely was

much colder than the room temperature. However, no attempt was made to determine its temperature or to calibrate the probe at low temperatures. The change in calibration for a 70°F to 100°F change is given as about 1% by the manufacturer, but no data was available for the lower temperatures.

CRITICAL SPEED ANALYSIS OF NASA EDDY-CURRENT DAMPER TEST APPARATUS

ackground and Introduction

igure 1 represents the schematic diagram of the NASA eddy-
it damper test apparatus. The rotor configuration is designed
erate in liquid nitrogen. The object of the eddy-current
test apparatus is to examine the damping characteristics
assive eddy-current damper operating in cryogenic conditions.
je t of this research program is to determine the feasibility
e application of such a device for cryogenic turbomachinery,
s the liquid oxygen and hydrogen pumps used on the SSME.
n the development of high speed high performance turbopumps
ing with cryogenic liquids such as oxygen or hydrogen, it is
ely difficult to incorporate damping into the bearings or
For example, modern aircraft engines mounted on ball bearing
ts must incorporate squeeze film oil dampers in order to control
orations caused by unbalance response, or the nonsynchronous
caused by aerodynamic cross coupling effects. Under cryogenic
ons, it is impossible to incorporate the conventional squeeze
mper design. High performance turbopumps that run through
it frequencies must have additional external damping incorpor-
to the bearings or structural system in order to adequately
the vibrations. This is necessary if high bearing life of
ling elements is to be assured.

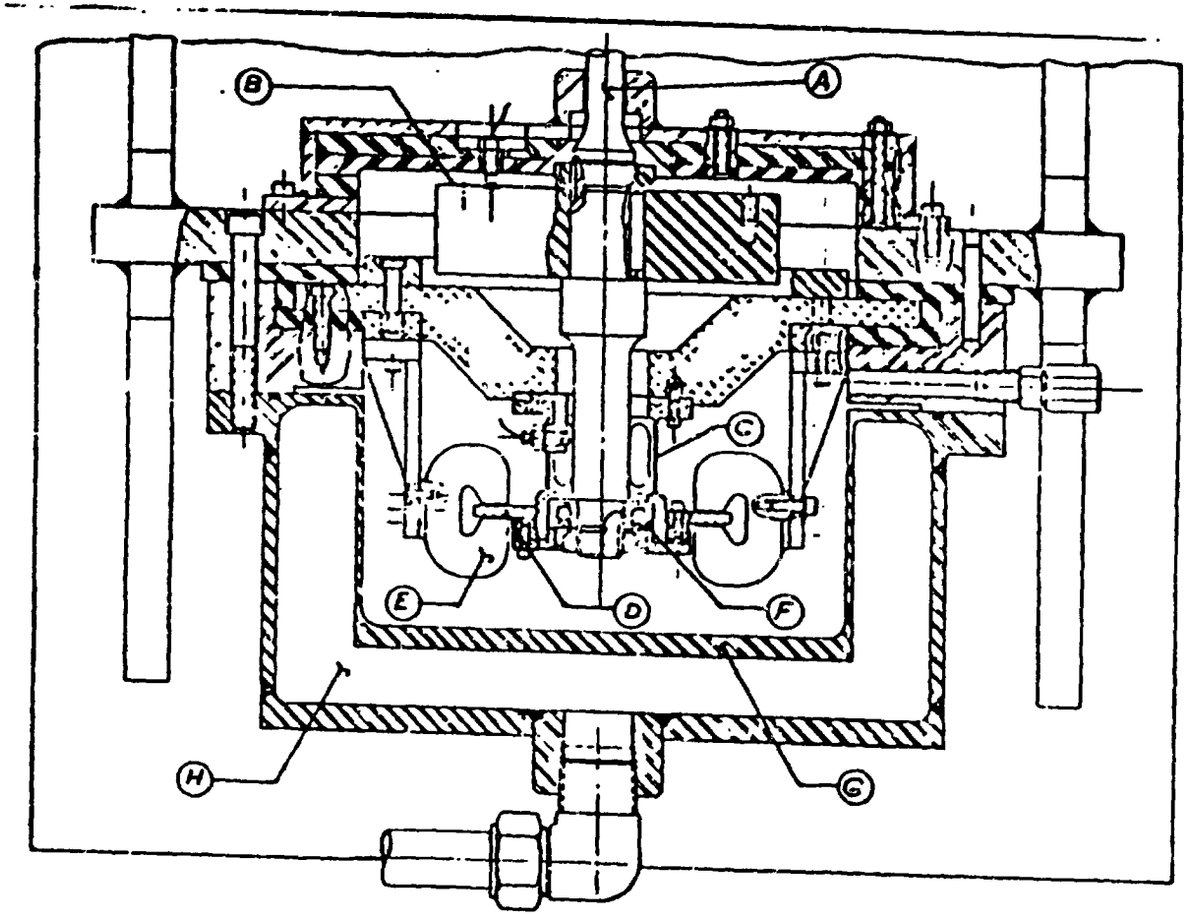

A TEST SHAFT
B INERTIA MASS LOCATION OF UNBALANCE
C SQUIRREL CAGE SPRING
D PURE COPPER CONDUCTOR
E PERMANENT MAGNETS
F DEEP GROOVE BALL BEARING
G CRYOGENIC CONTAINMENT VESSEL
H VACUUM

FIGURE 1 - EDDY-CURRENT DAMPER TEST APPARATUS

In this phase of the investigation, the critical speeds of the NASA eddy-current test apparatus are examined to determine the mode shapes and percent of strain energy distribution between the shaft and the bearing supports. The eddy-current damper will be mounted at the No. 2 bearing location (see Fig. 2). The eddy-current damper will be most effective if a high percentage of the system strain energy is associated with the No. 2 bearing support.

7.2 Critical Speed Analysis of Original Design

The NASA eddy-current test apparatus was analyzed, using the computer program CRTSPD developed by the University of Virginia to operate on the HP-9845B computer system. Incorporated with the computer program is the graphics procedure to illustrate the mode shapes. Figure 2 represents the rotor model of the NASA eddy-current test apparatus. For the first design, the system was considered as a two-bearing system in which the first bearing is a self-aligning ball bearing with an estimated stiffness of 85,000 lb/in. The eddy-current damper will be located at bearing 2 and its stiffness will be determined by the combination of the retainer spring rate stiffness plus the additional stiffness generated by the magnetic field. For this bearing, a value of 10,000 lb/in was chosen.

The first model has 14 stations and the characteristics of this model are given in Table 1. The total weight of the test rotor is approximately 16.6 pounds. The system was examined for a speed range of 200 to 20,000 RPM. There is predicted to be only one critical speed in the operating speed range and this value is 3,656, as noted in Table 2. This table represents the first mode shape and also gives the distribution of strain energy in the shaft and bearings and the distribution of rotor kinetic energy. It is of interest to note that in the original design, 73% of the total strain energy is in the strain energy of bending and only 27% is in the bearings. This distribution of strain energy is not particularly desirable and it is perferable to have a higher percentage of strain energy in the damper bearing location. It is also of interest to note that sections 4 through 6 contain over 67% of the strain energy of

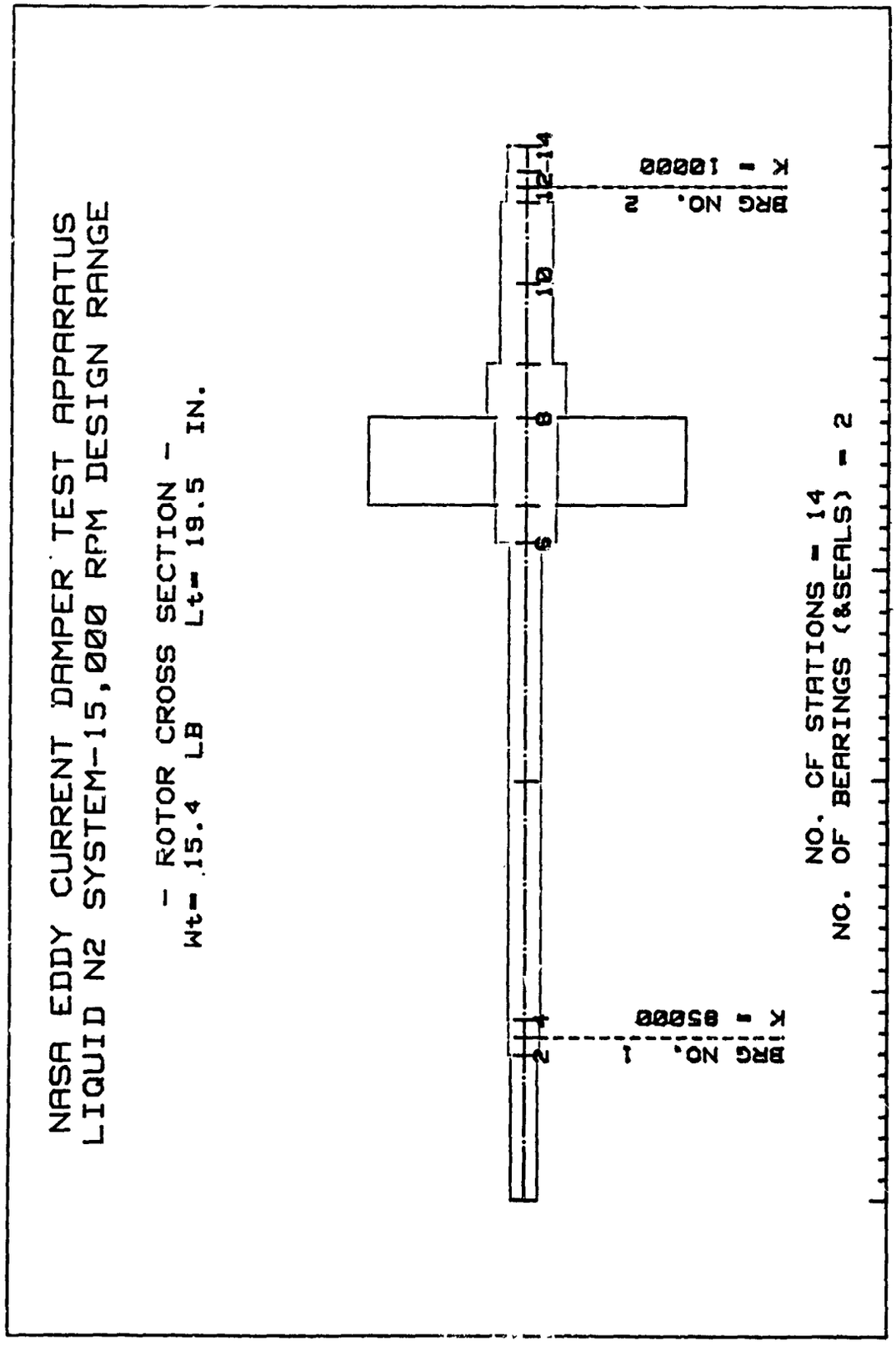

FIGURE 2

TABLE 1

NASA EDDY CURRENT DAMPER TEST APPARATUS
LIQUID N2 SYSTEM-15,000 RPM DESIGN ,STIFF SHAFT

N= 14 NBRG= 2 NCASE= 1 NMODES= 3 Eps= .000010

I	W(LBS)	L(I)	D(I)	EI	IP	IT
1	.1	2.70	.50	9.204E+04	23.442E-04	46.74E-03
2	.1	.33	.59	1.784E+05	28.997E-04	47.14E-03
3	.0	.33	.59	1.784E+05	11.110E-04	78.72E-05
4	.5	4.42	1.00	1.473E+06	61.957E-03	83.08E-02
5	1.0	4.42	1.00	1.473E+06	12.280E-02	16.61E-01
6	.6	.68	1.15	2.576E+06	77.923E-03	84.25E-02
7	6.6	1.62	1.19	2.953E+06	58.303E+00	40.10E+00
8	6.7	1.00	1.50	7.455E+06	11.546E-02	13.43E-02
9	.4	1.49	1.00	1.473E+06	90.956E-03	96.64E-03
10	.3	1.49	1.00	1.473E+06	41.258E-03	81.29E-03
11	.2	.28	.79	5.736E+05	22.144E-03	41.53E-03
12	.0	.28	.79	5.736E+05	30.301E-04	17.69E 04
13	.0	.47	.75	4.659E+05	35.677E-04	24.41E-04
14	.0	0.00	.75	4.659E+05	20.527E-04	15.57E-04

ROTOR WEIGHT= 16.6 LB, LENGTH= 19.5 IN., C.G.= 13.0 IN. FROM LEFT

Ipt=5.89E+01 LB-IN^2, Itcg=8.32E+02 Davg= .9 IN., EIavg=1.53E+06

BEARING STATION LOCATIONS :

BRG. NO. 1 = 3 BRG. NO. 2 = 12

BRG. STIFFNESS VALUES :

BRG. NO. 1 ST. 3 K= 85000 LB/IN
BRG. NO. 2 ST. 12 K= 10000 LB/IN

ROTOR BOUNDARY CONDITIONS ARE FREE-FREE
WHIRL MOTION IS S
Irpm= 500 Drpm= 1000 Frpm= 30000

L1AVG= 3.383E-06 L2AVG= 4.304E-06 L3AVG= 4.333E-06 EIAVG= 1.529E+06

TABLE 2

NASA EDDY CURRENT DAMPER TEST APPARATUS
LIQUID N2 SYSTEM-15,000 RPM DESIGN RANGE

UNDAMPED ROTOR MODE SHAPES AND ENERGY DISTRIBUTION
WITH TRANSVERSE SHEAR DEFORMATION
SYNCHRONOUS FORWARD MODE SHAPE

NO. 1 CRITICAL SPEED = 3656 ITER= 6 DELTA=-.000001993

ST	X	THETA	M	V	USHAFT (DIM STRAIN ENERGY)	UBEARING (DIM STRAIN ENERGY)	Kbrg	Ket (DIM KINETIC)	Ker (DIM KINETIC)
1	-.609	.311	0.0000	0.0000				0	0
2	-.050	.310	-.0005	-.0002				0	0
3	.018	.310	-.0006	-.0002	0	1	85,000	0	-0
4	.086	.309	-.0058	-.0200				0	0
5	.870	.188	-.0751	-.0199	10			3	0
6	1.000	-.133	-.1388	-.0163	57			3	0
7	.939	-.138	-.1476	-.0169	1			54	-1
8	.783	-.150	-.1368	.0136	3			38	0
9	.68[illegible]	-.152	-.1058	.0396				2	0
10	.5[illegible]	-.164	-.0580	.0410	2			1	0
11	.3[illegible]	-.169	-.0092	.0419				0	0
12	.326	-.170	.0000	.0422	0	26	10,000	0	-0
13	.294	-.170	.0000	-.0001				0	-0
14	.241	-.170	.0000	-.0000				0	-0
					73	27		101	-1

Utotal=20.30E+02; Ke total=20.36E+02; % ERROR ENERGY BALANCE= -.3

CRITICAL SPEED SUMMARY

NASA EDDY CURRENT DAMPER TEST APPARATUS
LIQUID N2 SYSTEM-15,000 RPM DESIGN RANGE
WITH TRANSVERSE SHEAR DEFORMATION

SYNCHRONOUS CRITICAL SPEED ANALYSIS

Brg. NO. 1 ST. 3 K= 85000 Lb/In
Brg. NO. 2 ST. 12 K= 10000 Lb/In

NO.	CRITICAL SPEED RPM	(HZ)	Wmode LB	Imode LB-IN^2 (It-w*Ip)	WTmode LB	Kmode LB/IN	Ushaft (DIM. STRAIN) (ENERGY)	Ubrg (DIM. STRAIN) (ENERGY)	KEt (DIM.KIN)	KEr (DIM.KIN)
1	3,656	(61)	10.8	-.1	10.7	4,072	73	27	101	-1

bending. This indicates that there is considerable bending at this location for the first mode. The strain energy at the damper bearing may be increased by increasing the effective shaft diameter at locations 4 through 6.

Examining the kinetic energy distribution, it is seen that only one percent of the energy is associated with gyroscopic effects. The rotor total kinetic energy may be viewed mainly as translatory motion, rather than gyroscopic motion. This implies that a simplified rotor modal may be used to represent the dynamic characteristics of the experimental test apparatus for future analysis and calculations. This feature is highly desirable when running the experimental facility in order to experimentally determine the effective damper stiffness and damping coefficients.

It is also of interest to note that 92% of the kinetic energy is associated with stations 7 to 8, the large disk on the rotor. Therefore, this rotor may be successfully balanced for the first mode by only a single plane at the major disk location. In addition to the rotor kinetic energy, the effective rotor modal weight and modal stiffness is given in Table 2.

Figure 3 represents the rotor first mode. From Table 2 and also Figure 3, it is noted that the maximum amplitude occurs at station 6. Figure 4 is similar to Figure 3 in that it represents an animated mode shape for the first mode. Note that the amplitude of motion at the ball bearing support is almost a node point. It is also of interest to observe that the bearing amplitude at the damper is only 33% of the maximum rotor amplitude. This is an indication that the original shaft design may be too flexible.

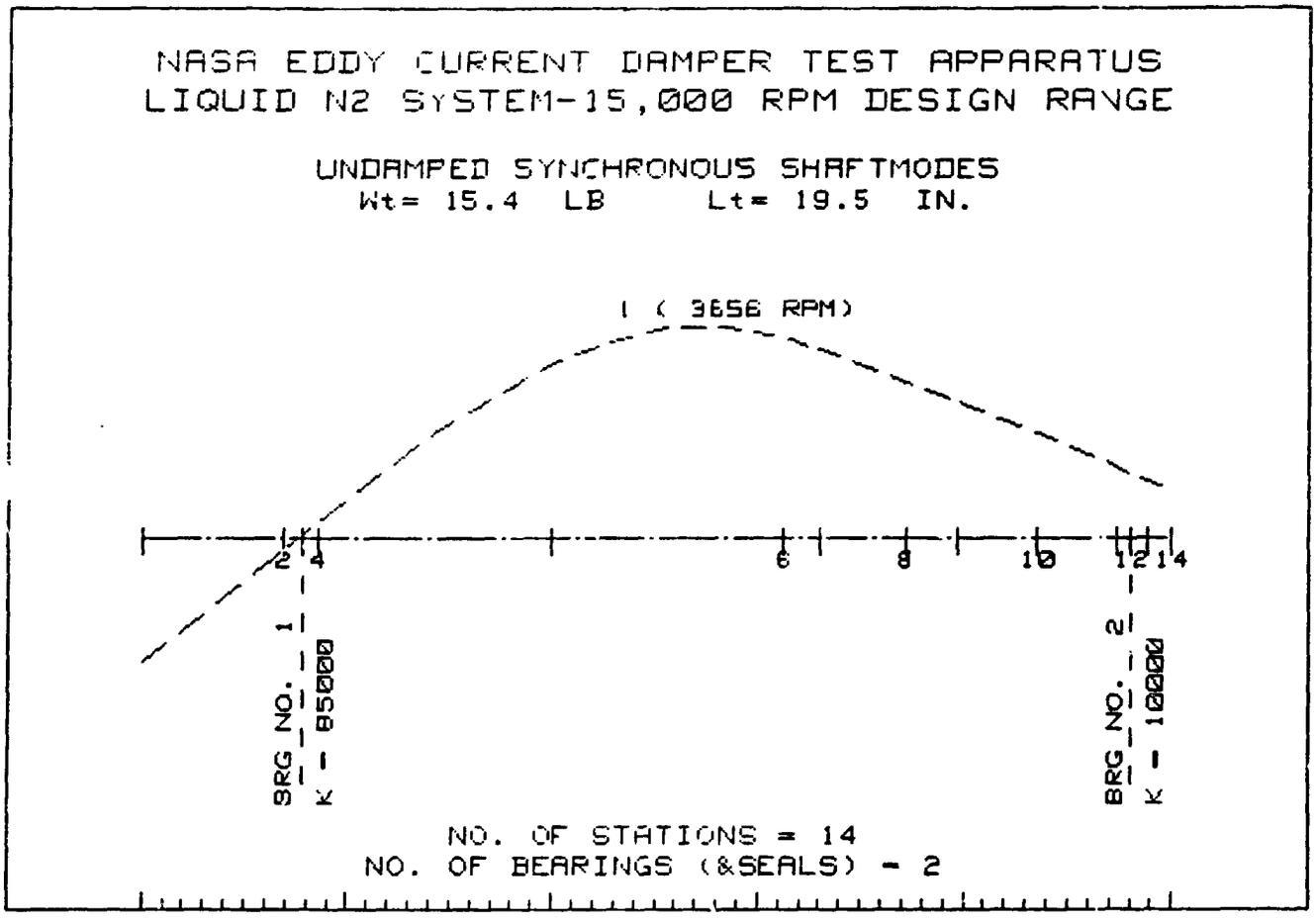

FIGURE 3

C-2

ORIGINAL PAGE IS
OF POOR QUALITY

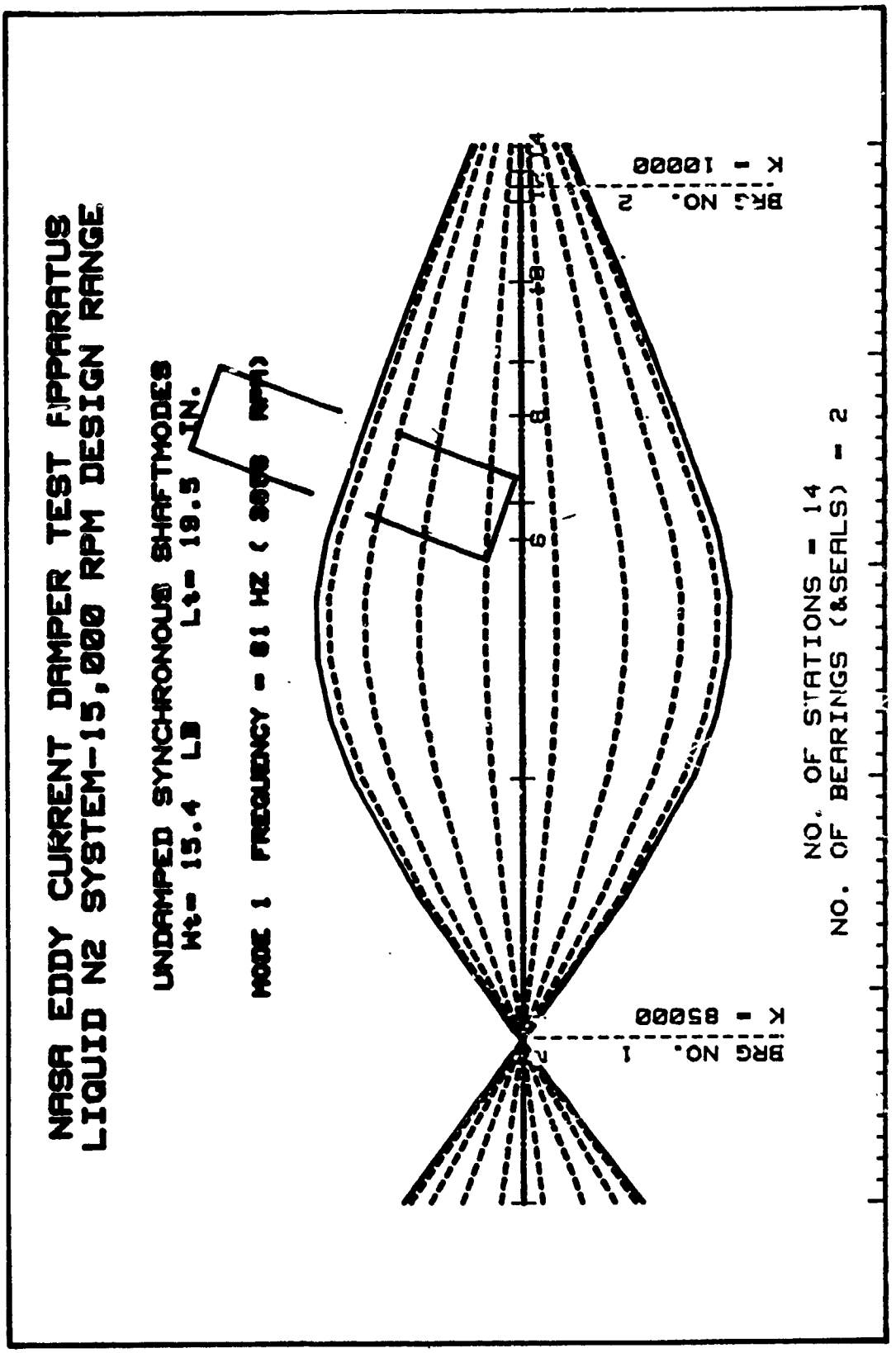

FIGURE 4

7.3 Stiffened Rotor Design

A design rotor for the eddy-current damper apparatus was considered in which the shaft section between 4 and 6 was increased from 0.62 to 1.0 inches. Figure 5 represents the stiffened rotor design. Table 3 gives the critical speed mode shape for the rotor with the stiffened design. The critical speed has been increased to 5,441 RPM. Note that the strain energy at the damper support has increased from 27 to 60%. The performance of this model would be much more satisfactory in the test apparatus. The stiffened rotor was analyzed to 30,000 RPM. Only one critical speed was determined to be in the operating speed range. The mode shape and animated mode shape are shown in Figures 6 and 7, respectively.

A third model was run in which a coupling weighing approximately one pound was placed at the shaft end. A timer-pulley arrangement will be used to drive the rotor system. The rotor model with the pulley arrangement is shown in Figure 8. The analysis of the rotor critical speed with the pulley indicates that the overhung pulley will have very little effect on the rotor first critical speed. The balancing should be done primarily at the major disk location.

The influence of the pulley is to cause a second critical speed to occur, just outside the operating speed range at approximately 21,000 RPM. This frequency may be changed somewhat depending upon the exact weight of the pulley. The shaft modes and animated modes are given in Figures 9, 10 and 11, respectively.

ORIGINAL PAGE IS
OF POOR QUALITY

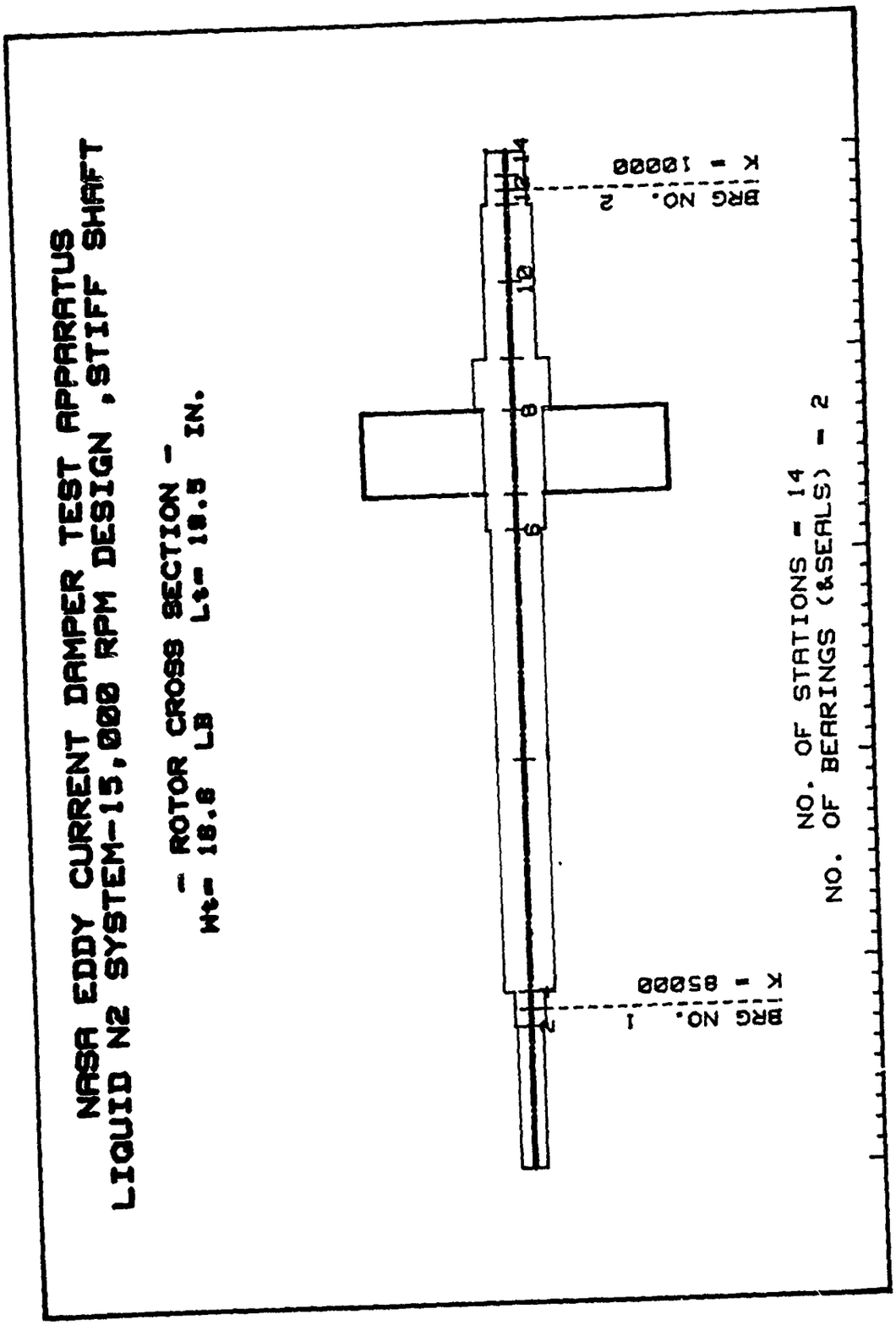

FIGURE 5

TABLE 3

NASA EDDY CURRENT DAMPER TEST APPARATUS
LIQUID N2 SYSTEM-15,000 RPM DESIGN ,STIFF SHAFT

UNDAMPED ROTOR MODE SHAPES AND ENERGY DISTRIBUTION
WITH TRANSVERSE SHEAR DEFORMATION
SYNCHRONOUS FORWARD MODE SHAPE

NO. 1 CRITICAL SPEED = 5441 ITER= 4 DELTA= .00000460752

ST	X	THETA	M	V	USHAFT (DIM STRAIN ENERGY)	UBEARING (DIM STRAIN ENERGY)	Kbrg	Ket (DIM KINETIC)	Ke^ot (DIM KINETIC)
1	-.387	.217	0.0000	0.0000				0	3
2	.003	.215	-.0003	-.0001				0	3
3	.051	.215	-.0004	-.0001	0	2	85,000	0	-3
4	.098	.213	-.0065	-.0187				0	3
5	.676	.163	-.0883	-.0185	4			3	3
6	.986	.033	-.1596	-.0161	20			4	3
7	.998	.018	-.1691	-.0140	3			43	-3
8	1.000	-.013	-.1524	.0099	6			44	3
9	.989	-.019	-.1181	.0345	1			3	3
10	.951	-.051	-.0651	.0360	4			2	3
11	.891	-.064	-.0104	.0371	1			1	3
12	.879	-.065	.0001	.0377	0	60	10,000	0	-3
13	.866	-.065	.0000	-.0002				0	-3
14	.846	-.065	.0000	-.0001				0	-3
					38	62		100	3

Utotal=64.02E+02; Ke total=64.30E+02; % ERROR ENERGY BALANCE= -.4

CRITICAL SPEED SUMMARY

NASA EDDY CURRENT DAMPER TEST APPARATUS
LIQUID N2 SYSTEM-15,000 RPM DESIGN ,STIFF SHAFT
WITH TRANSVERSE SHEAR DEFORMATION

SYNCHRONOUS CRITICAL SPEED ANALYSIS

Brg. NO. 1 ST. 3 K= 85000 Lb/In
Brg. NO. 2 ST. 12 K= 10000 Lb/In

NO.	CRITICAL SPEED RPM	(HZ)	Wmode LB	Imode LB-IN^2 (It-v/w*Ip)	WTmode LB	Kmode LB/IN	Ushaft (DIM. STRAIN) (ENERGY)	Ubrg (DIM. STRAIN) (ENERGY)	KEt (DIM.KIN)	KEr (DIM.KIN)
1	5,441	(91)	15.3	.0	15.3	12,860	38	62	100	0

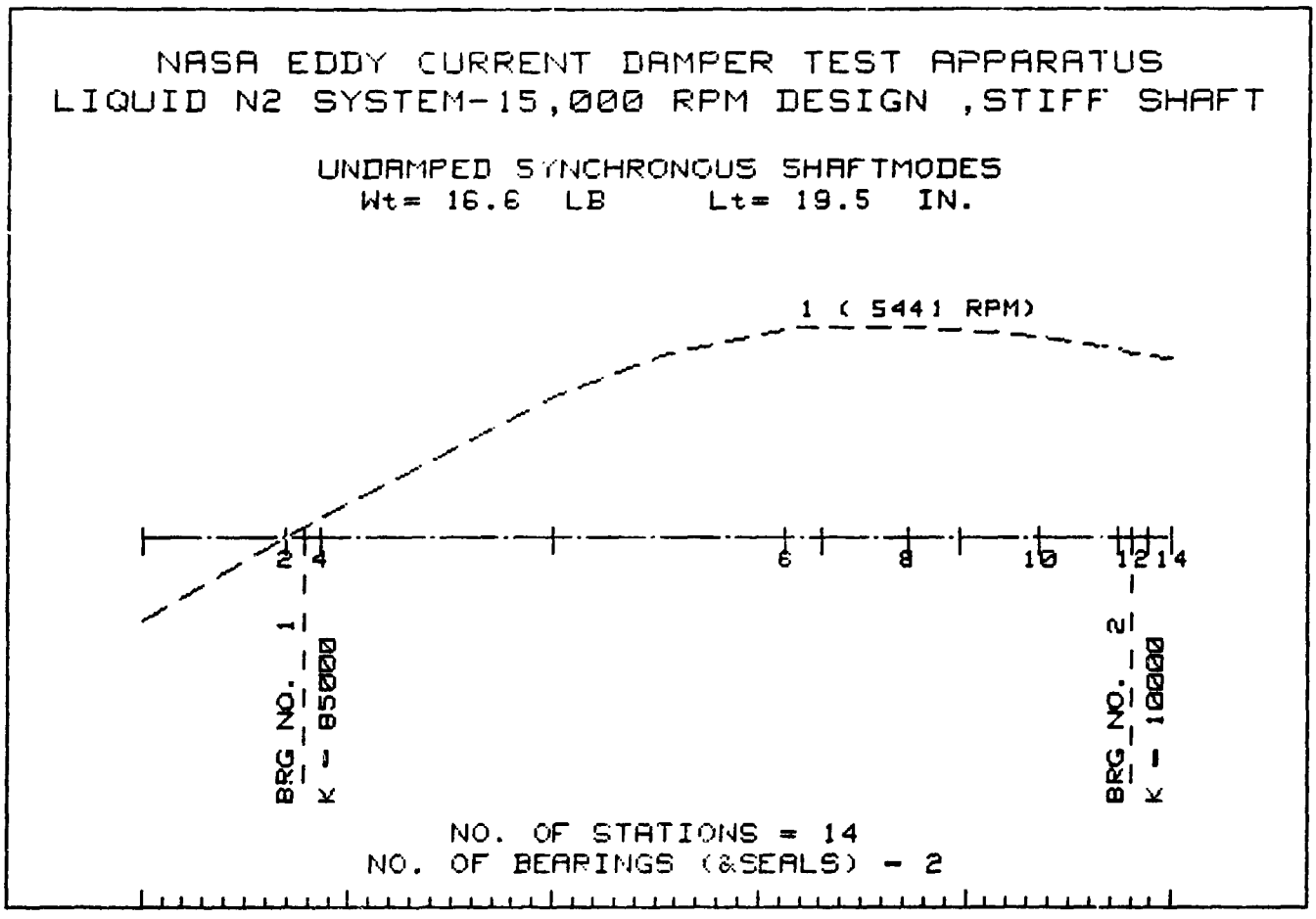

FIGURE 6

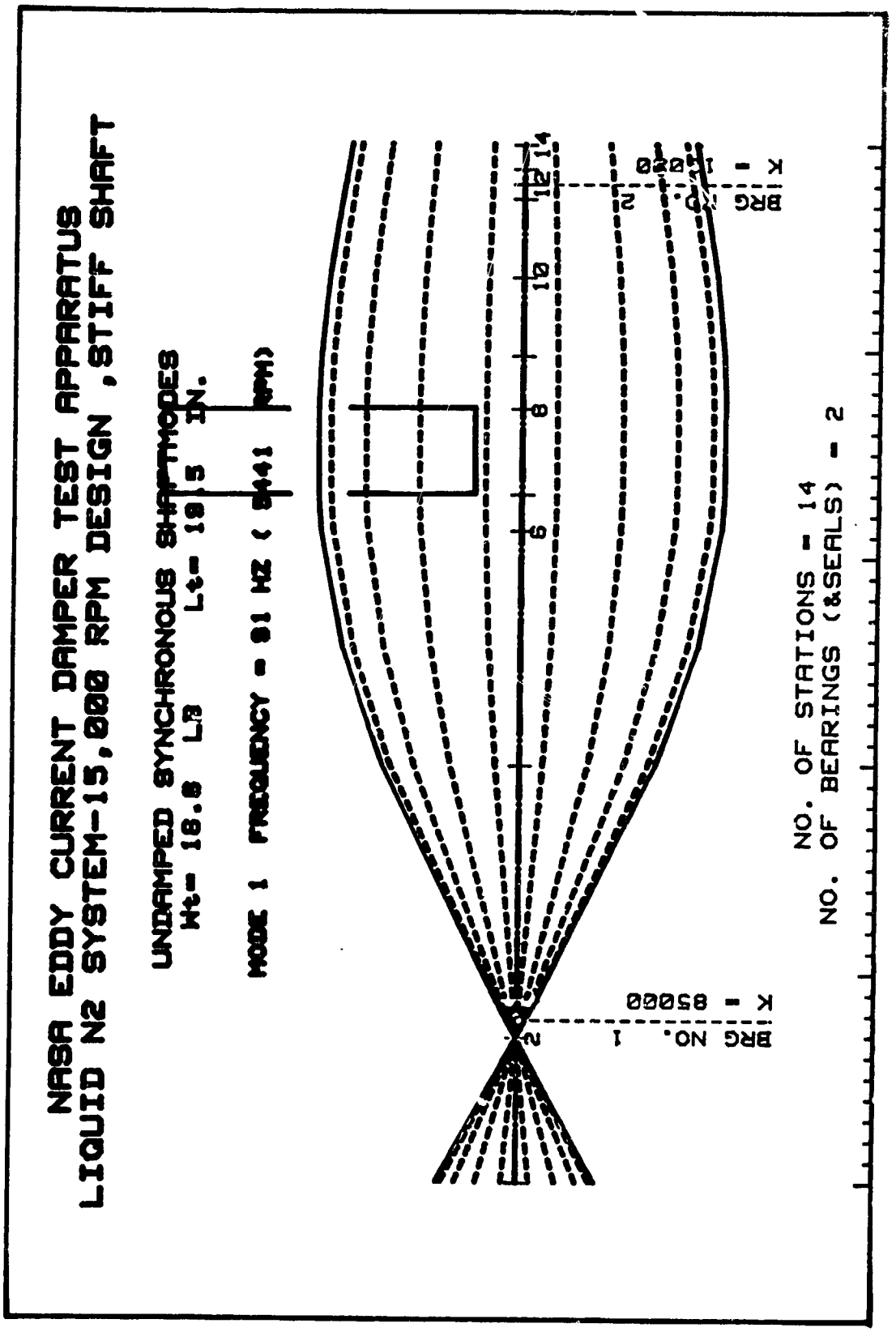

FIGURE 7

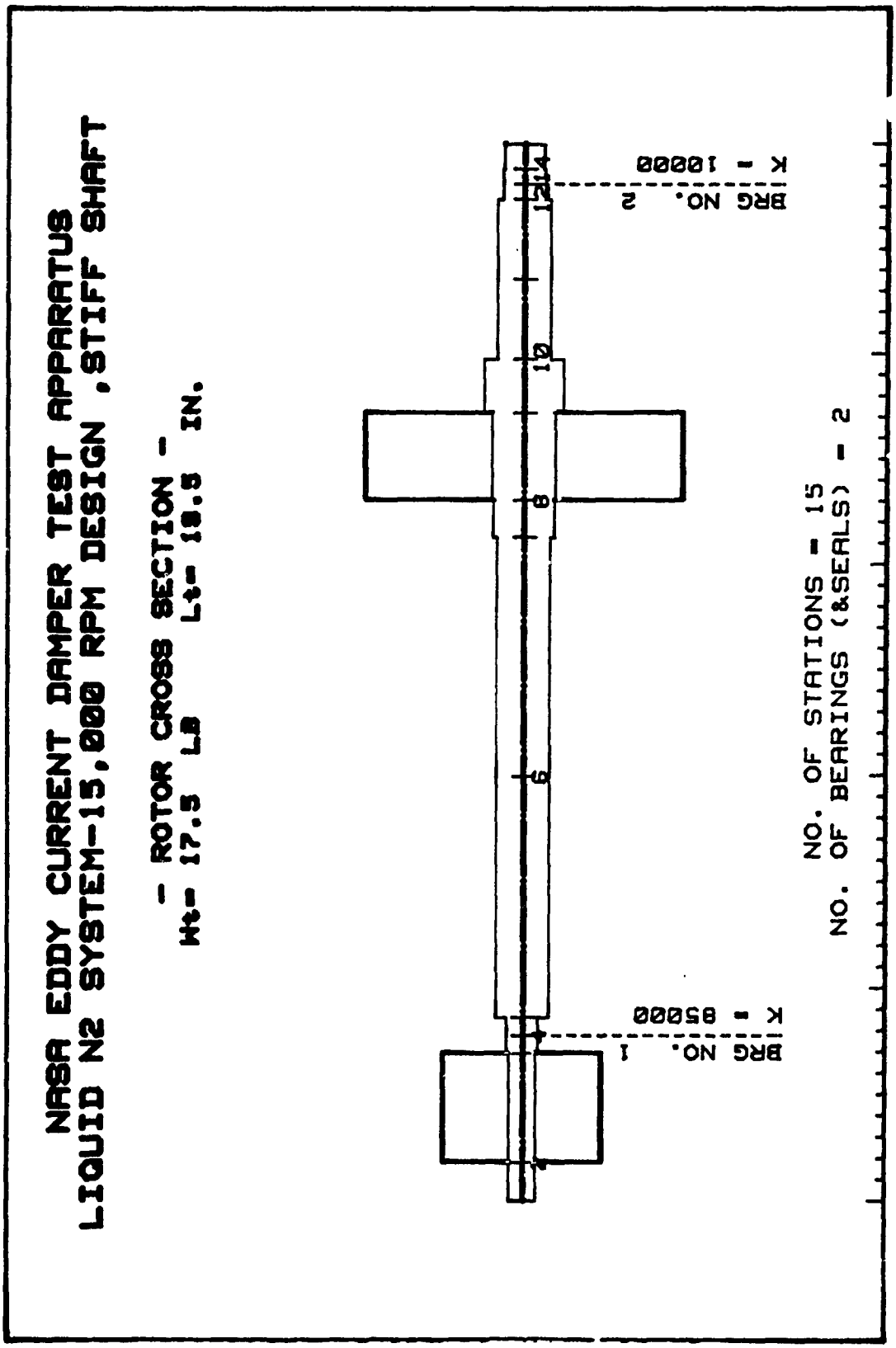

FIGURE 8

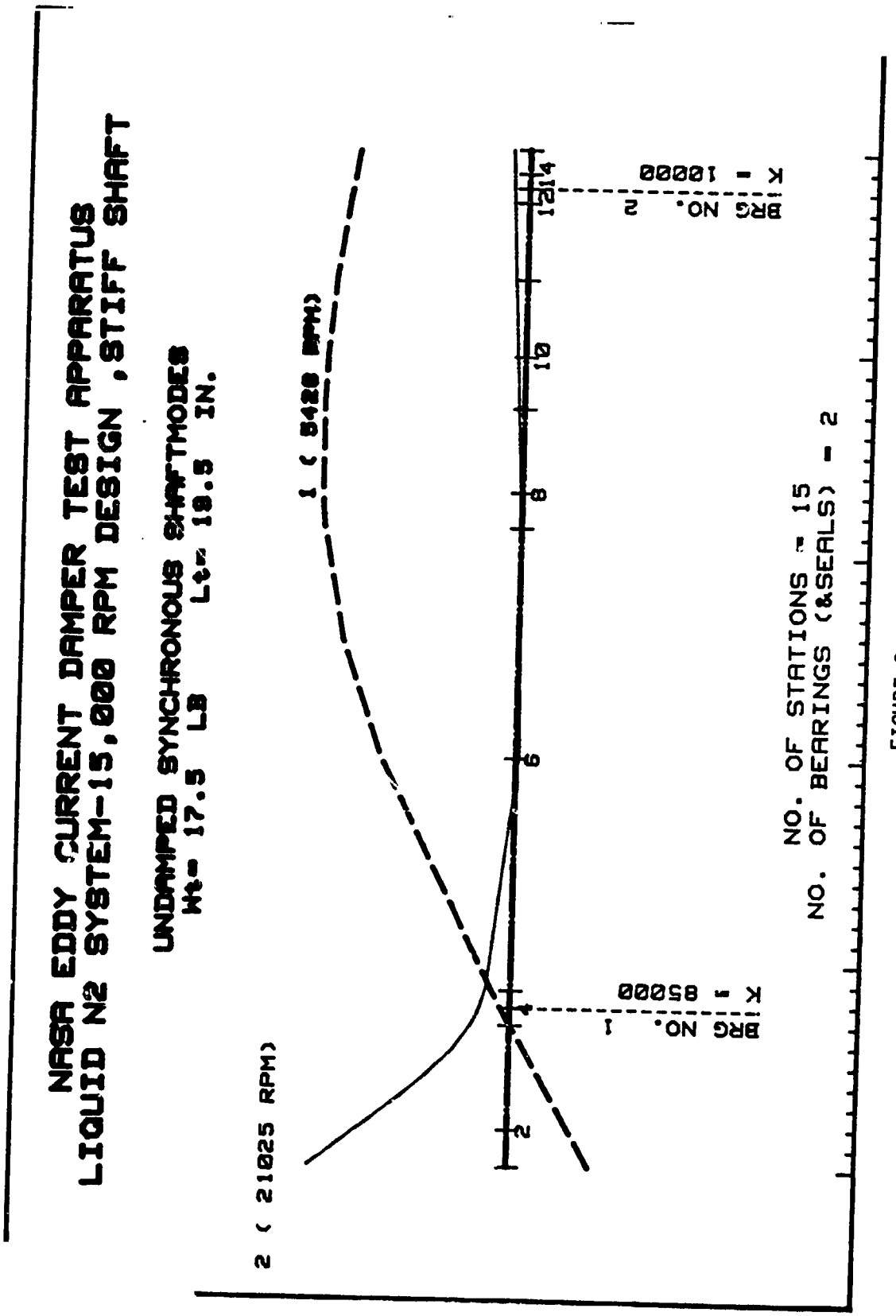

FIGURE 9

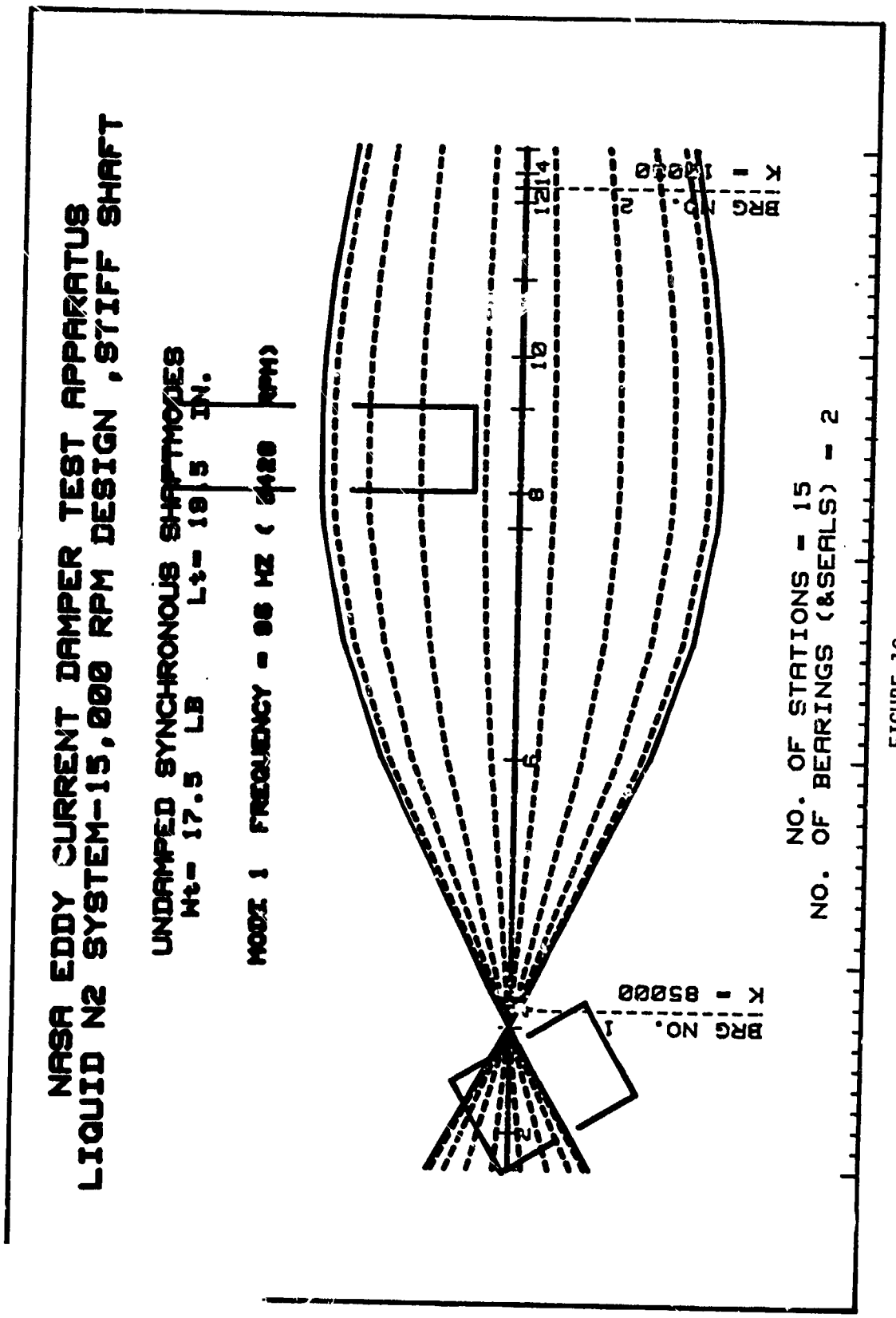

FIGURE 10

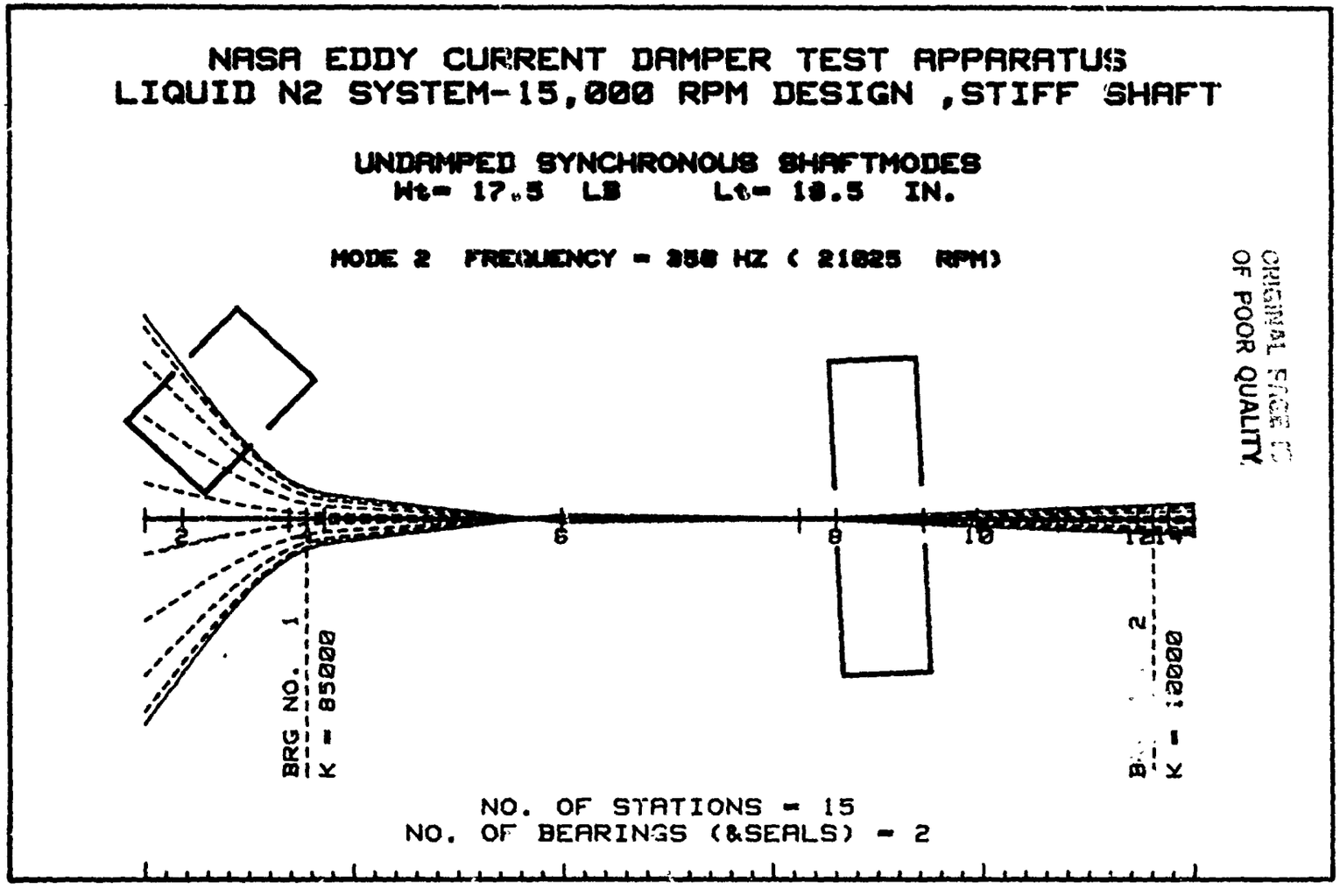
NASA EDDY CURRENT DAMPER TEST APPARATUS
LIQUID N2 SYSTEM-15,000 RPM DESIGN ,STIFF SHAFT
UNDAMPED SYNCHRONOUS SHAFTMODES
Wt= 17.5 LB Lt= 18.5 IN.
MODE 2 FREQUENCY = 358 HZ (21825 RPM)
ORIGINAL PAGE IS
OF POOR QUALITY
2
6
8
10
12
BRG NO. 1
K = 85000
2
00001 = K
NO. OF STATIONS = 15
NO. OF BEARINGS (&SEALS) = 2

FIGURE 11

7.4 Summary and Conclusions

The critical speeds of the NASA eddy-current damper test rig were calculated. It was determined that there would be only one critical speed present in the operating speed range of 15,000 RPM. However, in the analysis of the original rotor design, it was determined that the eddy-current damper bearing would contain only 27% of the strain energy of the total system for the first mode. This low percentage of strain energy would make the eddy-current damper extremely inefficient, due to the high shaft flexibility.

A new rotor was analyzed in which the shaft stiffness between sections 4 and 6 was increased from 0.62 to 1.0 inch. This stiffening of the shaft increased the strain energy distribution from 27% to 60%. An analysis was also performed with the pulley mass attached to the shaft. There will only be one critical speed present even with the pulley mass included. It was also determined that the pulley mass and self-aligning ball bearing will have little effect on the dynamic characteristics of the eddy-current test rotor.

From an examination of the rotor mode shape, it is seen that the rotor system may be approximated by a single mass Jeffcott rotor using the rotor modal characteristics. The rotor may be balanced by single plane corrections at section B, the inertia mass location. The damper may be therefore examined under a large range of unbalances and rotor eccentricities to examine nonlinear effects in the eddy-current damper.

In the determination of the damper characteristics, it is desirable to have noncontacting inductance probes to monitor the shaft

motion and also strain gauges mounted on the retainer squirrel cage spring to determine forces transmitted to the eddy-current damper. By means of the shaft displacements and direct determination of forces transmitted to the eddy-current damper, the damping and stiffness characteristics of the system may be determined for a range of speeds and unbalances.

VIII. DISCUSSION AND CONCLUSIONS

The object of this investigation was to study the feasibility and characteristics of a passive eddy-current damper for application in a cryogenic pump. In the design of the cryogenic pump with duplex ball bearings, it is extremely difficult to incorporate sufficient damping into the system to control the critical speeds or the occurence of self excited whirl instability. Flexible supports with coolant friction damping have not proven to be successful in cryogenic pumps.

The concept of the passive eddy-current damper is that the outer nonrotating brace of the rolling element be supported by a nonferrous disk which moves in a permanent magnet field. The eddy-current damper has been used for commercial applications such as meters and instruments in which a small amount of damping is required.

The theoretical predictions for the amount of damping generated is proportional to the power loss generated by the induced eddy-currents created in the damper material. In a simplified eddy-current damper analysis, the damping coefficient is proportional to the magnetic flux density squared, the damper volume and conductivity. With the new rare earth magnetic materials available, a substantially larger field can be achieved than with the conventional Alinco magnets. The operation at cryogenic temperatures should cause a substantial improvement over ambient conditions due to the increase in conductivity of the material. There is possibly an off setting factor in that the full damping effectiveness is not achieved due to the skin penetration effect of AC currents, the higher the frequency of oscillation, the less the penetration

depth of the eddy-currents into the conductor. This means that the full volumn of the conductor is not available as a damper material. This effect needs more experimental testing to be verified.

Preliminary tests conducted at NASA and at the University of Virginia showed a substantial increase in damping characteristics under cryogenic temperatures. However the elementary tests conducted at the University of Virginia did not simulate the high frequency operation that would be encountered with a cryogenic pump operating in a 30,000 rpm speed range.

The characteristics of an eddy-current damper were analysed from several elementary standpoints and also by means of a finite element two dimensional analysis program using the electric potential vector approach. By means of this finite element analysis, a very complex geometry may be computed. However one difficulty in the theoretical calculation of the eddy-current damping is the realistic determination of the effective magnetic flux density, effective material volume and possibly the effect of the depth of penetration. An experimental program is necessary to arrive at empherical relationships. Because of these problem areas, it was difficult to assign an exact computation of the damping generated by the finite element program.

In general it is felt that the concept of the passive eddy-current damper is feasible in a cryogenic pump and further experimental testing on this system should be conducted on a high speed simulation model. The passive eddy-current damper has the distinct advantage in that it has no moving parts and hence is not subjected to fatigue or wear. It may also be possible to incorporate into the eddy-current damper design a squeeze film damper to generate initial damping characteristics based on shear of the fluid film.

REFERENCES*

1. Ek, M. C., "Solution of the Subsynchronous Whirl Problem in the High Pressure Hydrogen Turbomachinery of the Space Shuttle Main Engine," AIAA/SAE 14th Joint Propulsion Conference, July 25-27, 1978, Las Vegas, NV.

2. Childs, D. W., "The Space Shuttle Main Engine High-Pressure Fuel Turbopump Rotor-Dynamic Instability Problem," Journal of Engineering for Power, Vol. 100 (January 1978).

3. Vance, J. M., and Rogel, A. C., "High Speed Rotor Dynamics - An Assessment of Current Technology for Small Turboshaft Engines," Journal of Aircraft, Vol. 102, No. 4 (April 1975), pp. 295-304.

4. Gunter, E. J., Jr., "The Influence of Internal Friction on the Stability of High Speed Rotors," ASME Transactions, Journal of Engineering for Industry, Vol. 89, Series B (November 1967), pp. 683-688.

5. Gunter, E. J., Jr., and Kirk, R. G., "Aerodynamic Instability in Turbomachinery," presented at the International Rotor Dynamics Conference, August 1974, Denmark.

6. Gunter, E. J., Jr., "Rotor-Bearing Stability," Proceedings of First Turbomachinery Symposium, Gas Turbine Laboratories, Texas A & M University, Texas A & M University Press (October 1972), pp. 119-141.

7. Gunter, E. J., Jr., Barrett, L. E., Palazzolo, A. B., and Allaire, P. E., "Final Report - The Dynamic Analysis of the Space Shuttle Main Engine - High Pressure Fuel Turbopump, Part III - Linearized Stability Analysis," Research Laboratories for the Engineering Sciences, University of Virginia, Report No. UVA/528140/ME76/104, September 1976.

8. Branagan, L., Kirkpatrick, W. M., and Gunter, E. J., Jr., "Stability Analysis of the Oxygen Pump for the Space Shuttle Main Engine," Research Laboratories for the Engineering Sciences, University of Virginia, Report No. UVA/528140/MAE80/118, October 1980.

9. Gunter, E. J., Jr., and Flack, R. D., "Experimental Measurements of the Space Shuttle Main Engine Fuel and Oxygen Turbopump Vibration Characteristics," Proceedings of the 27th International Instrumentation Symposium, Indianapolis, IN, Instrumentation in the Aerospace Industry - Advances in Test Measurement, Vol. 18, Part 2 (April 1981), pp. 393-397.

10. Gunter, E. J., Jr., Springer, H., and Humphris, R. R., "Dynamic Unbalance Response and Stability Characteristics of a Vertical Three-Mass Rotor-Bearing System," Rotor Dynamics Laboratory, Department of Mechanical and Aerospace Engineering, University of Virginia, Report No. UVA/643078/MAE81/106 November 1981.

11. Magge, N., "Philosophy, Design and Evaluation of Soft-Mounted Engine Rotor Systems," Journal of Aircraft, Vol. 12, No. 4 (April 1975), pp. 318-324.

12. Cunningham, R. E., Gunter, E. J., Jr., and Fleming, D. P., "Design of an Oil Squeeze Film Damper Bearing for a Multimass Flexible Rotor-Bearing System," NASA TN D7892, February 1975.

13. Cunningham, R. E., "Steady-State Unbalance Response of a Three Disk Rotor on Flexible Damped Supports," Journal of Mechanical Design, Vol. 100, No. 3 (July 1978), pp. 563-573.

14. Bansal, P. N., and Hibner, D. H., "Experimental and Analytical Investigation of Squeeze Film Bearing Damper Forces Induced by Offset Circular Whirl Orbits," Journal of Mechanical Design, Vol. 100, No. 3 (July 1978), pp. 549-557.

15. Gunter, E. J., Jr., "Influence of Flexibly Mounted Rolling Element Bearings on Rotor Response, Part 1 - Linear Analysis," ASME Transactions, Journal of Lubrication Technology, Vol. 29, Series F, No. 1 (January 1970), pp. 59-75.

16. Barrett, L. E., and Gunter, E. J., Jr., "Steady-State and Transient Analysis of a Squeeze Film Damper Bearing for Rotor Stability," NASA Contract Report, Federal Scientific and Technical Information, Springfield, VA, NASA CR-2548, May 1975.

17. Gunter, E. J., Jr., Barrett, L. E., and Allaire, P. E., "Design and Application of Squeeze Film Dampers for Turbomachinery Stabilization," Proceedings of the Fourth Turbomachinery Symposium, Gas Turbine Laboratories, Texas A & M University, Texas A & M University Press (October 1975), pp. 127-141.

18. Gunter, E. J., Jr., Barrett, L. W., and Allaire, P. E., "Stabilization of Turbomachinery with Squeeze Film Dampers - Theory and Application," Proceedings of the Conference on Vibrations in Rotating Machinery, Cambridge University, September 1976.

19. Gunter, E. J., Jr., Barrett, L. E., and Allaire, P. E., "Design of Nonlinear Squeeze Film Dampers for Aircraft Engines," ASME Transactions, Journal of Lubrication Technology, Vol. 99, Series F, No. 1 (January 1977), pp. 57-64.

20. Gunter, E. J., Jr., Li, D. F., and Barrett, L. E., "Dynamic Characteristics of a Two-Spool Gas Turbine Helicopter Engine," Proceedings of the Conference on the Stability and Dynamic Response of Rotors with Squeeze Film Bearings, U.S. Army Research Office, Triangle Park, NC (May 8-10, 1979), pp. 24-52.

21. Barrett, L. E., and Gunter, E. J., Jr., "Stabilization of Aerodynamically Excited Turbomachinery with Hydrodynamic Journal Bearings and Supports," Symposium on Rotordynamic Instability Problems in High Performance Turbomachinery, NASA Conference Publication 2133 (1980).

22. Crede, Charles E., "Application and Design of Isolators," Shock and Vibration Handbook, Vol. 2, Chapter 32, pp. 32-33.

23. Roters, H. C., "Electromagnetic Devices," John Wiley & Sons, Inc., New York, 1941.

24. Siskind, C. S., "Electrical Machines," 2nd Edition, McGraw-Hill Book Co., Inc., New York, 1959.

25. Dawes, C. L., "Electrical Engineering - Vol. I - Direct Currents," 4th Edition, McGraw-Hill Book Co., Inc., New York, 1952.

26. Underhill, E. M., "Permanent Magnet Handbook," Crucible Steel Co. of America, 1957.

27. Golding, E. W., "Electrical Measurements and Measuring Instruments," 4th Edition, Sir Isaac Pitman & Sons., Ltd., London, 1955.

28. Parker, R. J. and Studders, R. J., "Permanent Magnets and Their Application," John Wiley & Sons, Inc., New York, 1962.

29. Whitmer, R. M., "Electromagnetics," Prentice-Hall, Inc., New York, 1954.

30. Matsch, L. W., "Electromagnetic and Electromechanical Machines," 2nd Edition, Thomas Y. Crowell, New York, 1972.

31. Halliday, D. and Resnick, R., "Physics," Combined Edition, John Wiley & Sons, Inc., New York, 1965.

32. Thomson, W. T., "Theory of Vibration with Applications," Prentice-Hall, Inc., New Jersey, 1972.

33. Cullity, B. D., "Introduction to Magnetic Materials," Addison-Wesley Publishing Co., Massachusetts, 1972.

*Other References are given throughout the text of this report.

Appendix I - Literature Search

Print 5/5/1-66
DIALOG File8: COMPENDEX - 70-82/JUN (Copr. Engineering Informat

1233325 ID NO.- EIA202013325
MAGNETIC DAMPING OF ELECTRODYNAMIC LEVITATION SYSTEMS FOR HIGH SPEED TRAINS.
Okuma, Shigeru; Amemiya, Yoshifumi
Nagoya Univ, Jpn
Proc - Int Conf on Electr Mach, Pt 1, Athens, Greece, Sep 15-17 1980 Organ by Natl Tech Univ of Athens, Chair for Electr Mach, Greece, 1980 p 248-255
The magnetic damping of electrodynamic levitation systems for high speed trains is studied. The magnetic damping is shown to be negative at high speeds, by analysis using transient theory. A physical explanation of negative magnetic damping is given. A new method to improve magnetic damping for vertical motion is proposed, which is realized by the train coils for levitation with homopolarity instead of conventional alternating polarity. Another method is proposed to improve the stability for both vertical and horizontal motions of the combined system of propulsion and guidance. 6 refs.
DESCRIPTORS: *MAGNETIC LEVITATION, (ELECTRIC RAILROADS, Magnetic Levitation).
IDENTIFIERS: HIGH-SPEED TRAINS
CARD ALERT: 704, 681

1105053 ID NO.- EI810105053
DAMPING CHARACTERISTICS OF THE REPULSIVE MAGNETIC LEVITATION VEHICLE.
Fujiwara, Shunsuke
Jpn Natl Railw
Q Rep Railw Tech Res Inst (Tokyo) v 21 n 1 Mar 1980 p 49-52
CODEN: QRTIA8
ISSN 0033-9008
Fourier transform analyses for magnetic damping force of passive damping and of biased field damping have been done using a simple model. Also their experimental results which use rotary test setup are presented. Experimental proofs for damping characteristics have been reported, and experimental results for passive damping and biased field damping methods, their analytical methods are shown.
DESCRIPTORS: (*MAGNETIC LEVITATION, *Mathematical Models), RAILROAD ROLLING STOCK, (RAILROADS, Japan).
IDENTIFIERS: RAILROAD TRANSPORTATION, DAMPING, MAGNETIC LEVITATION VEHICLES
CARD ALERT: 704, 682, 681, 433, 921

1162071 ID NO.- EI810762071
UNTERSUCHUNGEN AN EINEM ELEKTRODYNAMISCHEN SCHWINGUNGSERREGER. $left brackets$ Studies of an Electrodynamic Vibration Generator $right brackets$.
Kiekbusch, A.
Feingeraetetechnik v 29 n 11 1980 P 490-493 CODEN: FGRTA3
ISSN 0014-9683
This paper deals mainly with the damping improvement or quality minimization of electrodynamic vibration generators. The measurement results of experiments and the results of modifications of the generator are presented without comment. In addition to eddy current damping, electrodynamic dampers and damping techniques using magnetic fluids are considered. 11 refs. In German.
DESCRIPTORS: *VIBRATORS, (VIBRATIONS, Damping), ELECTRODYNAMICS.
CARD ALERT: 422, 601, 931, 701

1112806 ID NO.- EI810212806
OPTIMIZATION OF AN EDDY CURRENT DAMPER.
Mikulinsky, M.; Shtrikman, S.
Weizmann Inst of Sci, Rehovot, Isr
Electr Mach Electromech v 5 n 5 Sep-Oct 1980 p 417-432
CODEN: EMELDG
ISSN 0361-6967
An eddy current damping device containing a metal disk moving in a magnetic field of cylindrical symmetry is studied. Analytic equations are presented for the damping which is produced by permanent magnets for a wide range of geometrical parameters of the device. The geometry leading to the maximal damping under size constraints is obtained. 6 refs.
DESCRIPTORS: *EDDY CURRENTS.
CARD ALERT: 701

1102818 ID NO.- EI810102818
OPTIMIZATION OF AN EDDY CURRENT DAMPER.
Mikulinsky, M.; Shtrikman, S.
Weizmann Inst of Sci, Rehovot, Isr
Conv of Electr and Electron Eng in Isr, 11th, IEEE Proc, Tel-Aviv, Oct 23-25 1979 Publ by IEEE (Cat n 79Ch1566-9), Piscataway, NJ, 1980 Pap D1.3, 5 p
The eddy current damping device containing a metal disk moving in magnetic field of cylindrical symmetry is studied. Analytical equations for the damping which is produced by permanent magnets for a wide range of geometrical parameters of the device are presented. The geometry leading to the maximal damping under size constraints is obtained. 6 refs.
DESCRIPTORS: *ELECTRODYNAMICS.
IDENTIFIERS: EDDY CURRENTS
CARD ALERT: 701

1056704 ID NO.- EIB00756704
MAGNETIC DAMPING CHARACTERISTICS OF MAGNETICALLY SUSPENDED ULTRAHIGH-SPEED VEHICLES.
Takano, Ichiro; Ogiwara, Hiroyasu
Toshiba Corp, Jpn
Electr Eng Jpn v 98 n 5 Sep-Oct 1978 p 14-23 CODEN: EENJAU
ISSN 0424-7760
The induction repulsion-type superconducting levitation system is being studied intensively. This paper discusses the effects of various damping methods on the induction repulsion-type coil track system using a superconducting magnet. In analyzing the characteristics of active damping, the authors consider two cases: where one of four superconducting coils on one side loses its superconducting state; and where the exciting current of one normal-conducting ground coil is interrupted. 9 refs.
DESCRIPTORS: (*VEHICLES, *Magnetic Levitation), SUPERCONDUCTING MAGNETS.
CARD ALERT: 432, 704

1089535 ID NO.- EIB01289535
EQUIVALENT CIRCUIT FOR AN EDDY-CURRENT SCREENED AIR-CORED MACHINE.
Prior, D. L.; Anyaeji, C. A.
Univ of Liverpool, Engl
Proc - Int Conf on Electr Mach, v 1, Brussels, Belg, Sep 11-13 1978 Organ by Kathol Univ Louvain, Lab for Electr Mach, Belg, 1978 p SP3. 8. 1-SP3. 8. 10
An equivalent circuit has been derived for the direct-axis of an air-cored machine having two eddy-current screens or dampers. The circuit parameters are shown to be products of the armature inductance, the coupling coefficients and the time-constants of the windings and screens. Methods of determining the time-constants are considered and the results are compared with those measured on an experimental model. Although developed for mains or negative sequence frequencies, the technique could be extended to hunting frequency operation and a second, q-axis, circuit developed. 8 refs.
DESCRIPTORS: *ELECTRIC MACHINERY, SYNCHRONOUS, SUPERCONDUCTING MAGNETS, ELECTRIC GENERATORS, SYNCHRONOUS, (ELECTRIC NETWORKS, Equivalent Circuits).
CARD ALERT: 705, 704, 703

1017961 ID NO.- EIB00317961
PERFORMANCE TESTS OF SERVO VIBRATION DAMPER TO STABILIZE MACHINING ALUMINUM ALLOYS.
Okada, Yoji; Shibata, Takao; Iwasa, Mutsumi
Ibaraki Univ, Hitachi, Jpn
J Jpn Inst Light Metals v 29 n 8 Aug 1979 p 340-346 CODEN: JILJAZ
An electro magnetic servo damper has been developed to overcome chatter in machining. This paper introduces it and describes applications to machining aluminum alloys, carbon steel and superplastic materials. 9 refs. In Japanese with English abstract.
DESCRIPTORS: (*ALUMINUM AND ALLOYS, *Machining), (CARBON STEEL, Machining).
CARD ALERT: 541, 604, 545

1006862 ID NO.- EIB01006862
NICHTLINEARE SCHWINGUNGEN SCHWERER ROTOREN MIT VETIKALER WELLE UND KIPPSEGMENTRADIALLAGERN. $left bracket$ Nonlinear Vibrations of Large Rotors with Vertical Shaft Guided in Radial Tilting-Pad Bearings $right bracket$.
Springer, Helmut
Tech Univ Vienna, Austria
Forsch Ingenieurwes v 45 n 4 1979 p 119-132 CODEN: FIGWA5
ISSN 0015-7899
An approximation method is presented making it possible to calculate the pressure in hydrodynamic bearings in a very economic way. The method is used to investigate non-linear transient vibrations of a vertically suspended rotor system in the presence of large amplitudes of vibrations in the guide bearing of the shaft. The rotor system is modeled using finite beam elements. Static and dynamic unbalances as well as gyroscopic forces caused by rotating disc-shaped masses, magnetic pull, external damping forces etc. can be calculated applying the theory. Solving the non-steady-state Reynolds equation for each slider of the radial guide bearings, one can calculate the resulting forces exerted by the oil film of the bearings. The inertia forces of the sliders and the flexibility of the bearing construction supporting the sliders are taken into account. As an example a simple vertical rotor-bearing-system with 28 degrees of freedom is investigated using numerical methods. The response of the system to impact forces and to unbalance is discussed. The dynamic stiffness (mechanical impedance for harmonic excitation) of a guide bearing with twelve tilting-pads is computed as a function of the vibration amplitude of the shaft. 12 refs. In German.
DESCRIPTORS: (*ROTORS, *Vibrations), (BEARINGS, Thrust), (SHAFTS AND SHAFTING, Vibrations).
CARD ALERT: 601, 931, 602

994217 ID NO.- EI791294217
EFFECT OF ROTOR EDDY-CURRENT DISTRIBUTION ON DAMPING AND SHIELDING IN A $UPERCONDUCTING GENERATOR.
Ula, A. H. M. S.
MIT, Cambridge, Mass
IEEE Power Eng Soc, Prepr, Summer Meet, Vancouver, BC, Jul 15-20 1979 Publ by IEEE, New York, NY, 1979 Pa A 79 422-7, 8 p
The eddy-current distribution in the conducting rotor shields of a superconducting generator is a complex phenomenon which may have significant effects on the transient performance of the machine. In this paper this frequency-dependent eddy-current distribution in the $left double quote$ thick $right double quote$ conducting shield is represented in the extended two-axis circuit model of the machine by multiple circuits, each having its own parameters. The effects of the eddy-current distributions on the damping of the rotor torque angle oscillations and the shielding of the field winding in a superconducting generator following a power system fault is investigated using this model, and quantitative values are presented. The effect of the number of circuits representing the eddy-current distribution of the accuracy of the results is also presented along with its effect on the computational efficiency. 15 refs.
DESCRIPTORS: (*ELECTRIC GENERATORS, AC, *Stability), (SUPERCONDUCTING DEVICES, Applications),
IDENTIFIERS: SUPERCONDUCTING GENERATORS, EDDY CURRENTS, ROTOR SHIELDS, ELECTROMAGNETIC SHIELDING
CARD ALERT: 705, 731, 704

989919 ID NO.- EI791189919
ASYMPTOTIC THEORY OF A MAGNETIC DAMPER.
Novoselov, V. S
Mech Solids v 13 n 5 1978 p 20-23 CODEN: MESOBN
The theory of solutions of singularly perturbed ordinary differential equations is employed to make an asymptotic description of the motion of the core of a magnetic damper of an artificial Earth satellite. An asymptotic 2 pi -periodic solution is set up. The zero terms of this solution correspond to ideal motion such that the damper axis precisely tracks a line of force of the geomagnetic field. It is shown that the first-order terms cause the damper axis to lag behind the magnetic line of force. Estimates are also made for the boundary functions that appear in the solution for the $left double quote$ boundary layer $right double quote$ when the initial data are perturbed.
DESCRIPTORS: (*SATELLITES, *Stability),
CARD ALERT: 655

953623 ID NO.- EI790753623
END EFFECT ON MAGNETIC DAMPING FORCE OF SUPERCONDUCTING INDUCTIVE MAGNETIC LEVITATION SYSTEM.
Amemiya, Yoshifumi; Ohkuma, Shigeru
Nagoya Univ, Jpn
Electr Eng Jpn v 97 n 6 Nov-Dec 1977 p 67-73 CODEN: EENJAU
ISSN 0424-7760
In the inductive magnetic levitation system, the superconducting vehicular coil induces a short-circuit current in the ground coil and the magnetic fluxes of the two coils produce a repulsive force to levitate the vehicle. This paper studies the end effect of magnetic flux distribution on the magnetic damping force and also the transient phenomena occurring in the ground coils. It is assumed that the space distribution of magnetic flux produced by vehicular coils is not known a priori. The calculation assumes that only the configuration of vehicular and ground coils is known. The end effect discussed is the vehicular end effect, not the coil end effect. The vehicular end effect, which occurs at the front end of the vehicle, is of transient nature and attenuates as the vehicles move away. The magnetic damping force can be analyzed by comparing the damping force exerted on the front end of the vehicle with that exerted on the rear end. 8 refs.
DESCRIPTORS: *MAGNETIC LEVITATION, MAGNETIC FIELD EFFECTS, SUPERCONDUCTING MAGNETS,
IDENTIFIERS: MAGNETIC DAMPING FORCE
CARD ALERT: 704, 701, 943

937754 ID NO.- EI790537754
ON THE EFFECT OF A VARIABLE STIFFNESS-TYPE DYNAMIC ABSORBER WITH EDDY-CURRENT DAMPING.
Seto, Kazuto; Yamanouch, Mitsuo
Natl Def Acad, Yokosuka, Kanagawa, Jpn
Bull JSME v 21 n 160 Oct 1978 p 1482-1489 CODEN: BJSEA8
ISSN 0021-3764
A dynamic absorber is presented which consis of a variable stiffness-type spring, a mass, and a magnetic damper using the damping effect of eddy-currents. It has advantages that the absorber is able to use for improving the damping property of a main vibration system where changes of the natural frequency take place, and it is stable in damping characteristics under varying environment. To examine its practical applications, the damping performance of the absorber is studied in both experimental and theoretical aspects with a specific view to improving the dynamic stiffness of the ram' structure. Further, the relation between viscous damping coefficient and intermediate factors of the magnetic damper is deduced in order to realize the best damping optionally. 9 refs.
DESCRIPTORS: (*SHOCK ABSORBERS, *Mathematical Models),
CARD ALERT: 413, 601, 921

928286 ID NO.- E1795428286
RAPID ROTATION OF A SATELLITE WITH A MAGNETIC DAMPER $EM DASH$ 3. ALLOWANCE FOR CHANGES OF THE DAMPER STATE.
Sadov, Yu. A.
Cosmic Res v 16 n 3 May-Jun 1978 p 278-283 CODEN: CSCRA7 ISSN 0010-9525
It is shown that the trajectories of the end of the kinetic momentum vector for a time interval $similar$ 1/ $epsilon$ consist of alternating arcs of two conservative motions which correspond to the two possible deployment positions of the magnetic damper. The dissipative processes which occur upon a change of the damper state lead to the $left double quote$ ejection $right double quote$ of the trajectories of the end of the kinetic momentum vector from the changeover line. 2 refs.
DESCRIPTORS: *SATELLITES.
CARD ALERT: 655

814622 ID NO.- E1780214622
ANALYSIS AND EXPERIMENTS OF THE ELECTRO-MAGNETIC SERVO VIBRATION DAMPER.
Okada, Yoji
Ibaraki Univ, Hitachi, Jpn
Bull JSME v 20 n 144 Jul 1977 p 696-702 CODEN: BJSEA8
To improve the modal damping of a structure, some types of active dampers such as an electro-dynamic or an electro-hydraulic servo damper were investigated and reported. However, they have a few defects such as the large size of force generator and their expensiveness. A simple servo damper which has a couple of electro-magnets in push-pull operation is introduced, and three types of servo damper constructions are tested to decrease the peak resonances of the ram system such as a planer machine tool and with good results. 5 refs.
DESCRIPTORS: (*VIBRATIONS, *Absorption).
CARD ALERT: 413, 931

BEHAVIOR OF A NEW TYPE DYNAMIC VIBRATION ABSORBER CONSISTING OF THREE PERMANENT MAGNETS.
Yamakawa, Izumo; Takeda, Sadahiko; Kojima, Hiroyuki
Gunma Univ, Kiryu, Gunma-ken, Jpn
Bull JSME v 20 n 146 Aug 1977 p 947-954 CODEN: BJSEA8
Experimental and analytical studies are presented concerning a new repulsive type dynamic vibration absorber consisting of three permanent magnets of thick disk type. These magnets are arranged in a non-magnetic conductive or non-conductive cylinder so that one magnet can move freely between the two fixed ones. The result showed that: the repulsive force interacting between the two magnets may be assumed to be inversely proportional to the nth power of the center distance between the magnets. This assumption makes the analysis easier, and the results of the experiment show considerable coincidence with those of the analysis; the new absorber may be able to control the resonant amplitude of the vibrating body which weighs several dozen times the free magnet. Further merits of the absorber are an eddy current damping generated in the conductive cylinder and an arbitrary choice of the vibration direction as well as the frequency adjustability. 5 refs.
DESCRIPTORS: (*VIBRATIONS, *Absorption).
IDENTIFIERS: VIBRATION ABSORBERS
CARD ALERT: 931

761152 ID NO.- E1770861152
UNTERSUCHUNG UND BEEINFLUSSUNG DES DYNAMISCHEN VERHALTENS EINES ZUR KRAFTMESSUNG IN EINE ZUGPRUEFMASCHINE EINGEBAUTEN SELBSTABGLEICHENDEN KOMPENSATORS. $left bracket$ Investigation and Control of the Dynamic Behavior of the Automatic Null-Balancing Instrument Incorporated in a Tensile Testing Machine for Measuring the Applied Load $right bracket$
.
Kravcenko, Vasil
Stahlwerke Peine-Salzgitter, Ger
Arch Eisenhuettenwes v 48 n 2 Feb 1977 p 121-126 CODEN: AREIAT
The automatic null-balancing instrument used as part of a 100 kN tensile testing machine showed nonlinear behavior with the feeding-in of the step functions and with undamped natural oscillations. An ac voltage regulator is considered necessary even if the voltage varies much less than $plus or minus$ 10%. The dynamic behavior could be influenced considerably by a change of the amplification of the servoamplifier and by electric feedback and eddy current damping. Differences in load ranges also had an effect. In German.
DESCRIPTORS: (*STEEL TESTING, *Tensile Tests). MATERIALS TESTING APPARATUS.
CARD ALERT: 421, 422, 545

662942 ID NO.- E1760962942
MATHEMATICAL MODEL OF THE MOTION ABOUT THE CENTER OF MASS OF A FLEXIBLE STABILIZED ARTIFICIAL EARTH SATELLITE SEM DASH$ 2.
Kaurov, E. N.
Cosmic Res v 13 n 6 Nov-Dec 1975 p 729-733 CODEN: CSCRA7
Certain questions of the practical use of a mathematical model for the motion about the center of mass of an artificial earth satellite of the Kosmos 215 type, having on board a magnetic damper, intended for decreasing its angular velocity are considered. 7 refs.
DESCRIPTORS: (*SATELLITES, *Stability), MATHEMATICAL MODELS.
CARD ALERT: 655, 921

760911 ID NO.- E1770860911
DRAG FORCE OF AN EDDY CURRENT DAMPER.
Weinberger, M. R.
Fur Space Res & Technol Cent, Noordwijk, Neth
IEEE Trans Aerosp Electron Syst v AES-13 n 2 Mar 1977 p 197-200 CODEN: IEARAX
Closed-form expressions are derived by field calculations for the drag force exerted by spacecraft eddy current dampers. These devices are conducting slabs moving at low speed in a narrow gap between magnets with a rectangular cross section. Finite edge effects of the slab are accounted for. The results can be used for design studies.
DESCRIPTORS: (*SPACECRAFT, *Control), (VIBRATIONS, Absorption).
CARD ALERT: 655

605435 ID NO.- E1760105435
ATTITUDE CAPTURE PROCEDURES FOR GEOS-C.
Lerner, Gerald M.; Coriell, Kathleen P.
Comput Sci Corp, Silver Spring, Md
Am Astron Soc/AIAA Astrodyn Spec Conf, Pap, Nassau, Bahamas, Jul 28-30 1975 Pap AAS 75-029, 28 p. Available from AAS Publ Off, Tarzana, Calif
The satellite utilizes an extendable 6-meter gravity-gradient boom, a momentum flywheel, and an eddy current damper to achieve the requisite stability.. Because l/e libration damping time constants were expected to be in excess of 1 week after boom extension, dynamic studies were undertaken to reduce the 30 to 40 days required to satisfy attitude constraints and begin experimental operations. A three-phase series of maneuvers requiring real-time attitude determination and precise timing resulted from these studies. 7 refs.
DESCRIPTORS: (*SATELLITES, *Control),
CARD ALERT: 655

714034 ID NO.- E1770214034
PASSIVE SECONDARY MAGNETIC DAMPING FOR SUPERCONDUCTING MAGLEV VEHICLES.
Atherton, David L.; Eastham, A. R.; Sturgess, K.
Queen's Univ, Kingston, Ont
J Appl Phys v 47 n 10 Oct 1976 p 4643-4648 CODEN: JAPIAU
A passive magnetic damping scheme for the secondary suspension of a superconducting Maglev vehicle is analyzed. The unsprung levitation or linear synchronous motor magnets are coupled electromagnetically to short-circuited aluminum damper coils mounted on the underside of the sprung mass. Relative motion between the magnets and the passenger compartment causes a time-dependent flux linkage which induces dissipative currents in the coils. Analysis for the typical Canadian Maglev vehicle design shows that a damping factor of 1 sec** $minus$ **1 can be obtained with a typical coil mass of approximately 100 kg, for a secondary/primary suspension stiffness ratio of 0. 2. This scheme appears to offer a design alternative to conventional frictional or hydraulic dampers. 10 refs.
DESCRIPTORS: (*VEHICLES, *Magnetic Levitation),
CARD ALERT: 432, 704

605436 ID NO.- E1760105436
PASSIVE THREE-AXIS STABILIZATION OF THE LONG DURATION EXPOSURE FACILITY.
Huckins, Earle K. III; Breedlove, William J. Jr.; Heinbockel, John D.
Langley Res Cent, Hampton, Va
Am Astron Soc/AIAA Astrodyn Spec Conf, Pap, Nassau, Bahamas, Jul 28-30 1975 Pap AAS 75-030, 32 p. Available from AAS Publ Off, Tarzana, Calif
Analysis of the attitude dynamics of the Long Duration Exposure Facility (LDEF). LDEF is a large cylindrical gravity gradient stabilized Earth satellite (l $equals$ 30 ft, d $equals$ 14 ft, wt. $equals$ 12,600 lbs) which is planned to be delivered to a 270-n. -mi. circular orbit by the space shuttle. The fundamental linear stability, capture requirements, and pitch bias constraints generated by the T. B. Garber instability are discussed. Numerical simulations, based on the full nonlinear equations for the coupled orbital and attitude motion of the vehicle and the viscous magnetic damper, show stable behavior of the spacecraft and a damping time constant of 30 to 70 orbits. 9 refs.
DESCRIPTORS: (*SATELLITES, *Control),
CARD ALERT: 655

535002 ID NO.- EI750535002
MAGNETIC DAMPING FORCE IN INDUCTIVE MAGNETIC LEVITATION SYSTEM FOR HIGH-SPEED TRAINS.
Yamada, T.; Iwamoto, M.; Ito, T.
Mitsubishi Electr Corp, Jpn
Electr Eng Jap v 94 n 1 Jan-Feb 1974 p 80-84 CODEN: EENJAU
It is shown theoretically and experimentally that the superconducting magnetic levitation system is subject to a negative damping force in the medium- and high-speed region ($omega$ tau $greater than$ 1), while it is subject to a positive damping force in the low-speed region ($omega$ tau $less than$ 1). Further, it has been clarified that the negative damping force becomes very small in the extremely high-speed region such that $omega$ tau $greater than$ $greater than$ 1. Since the track loop produces no magnetic damping force, some suitable devices would be indispensable, e. g. , a damper loop aboard the train and a forced damping circuit supplying a damping current to the vehicular loop. 8 refs.
DESCRIPTORS: (*VEHICLES, *Magnetic Suspension), ELECTRIC RAILROADS, SUPERCONDUCTING MAGNETS,
IDENTIFIERS: REPULSIVE MAGNETIC LEVITATION, HIGH SPEED TRAINS
CARD ALERT: 433, 704, 681

533622 ID NO.- EI750533622
RAPID ROTATION OF A SATELLITE WITH A MAGNETIC DAMPER $EM DASH$ 2. MOTION OF THE KINETIC-MOMENT VECTOR IN THE CONSERVATIVE APPROXIMATION.
Sadov, Yu. A.
Cosmic Res v 12 n 4 Jul-Aug 1974 p 474-481 CODEN: CSCRA7
The investigation started in the rotating motion of a satellite with a magnetic damper is continued. The equations of motion are averaged in two approximations, with respect to the spin of the satellite and with respect to the orbital and daily motion. It is shown that on a certain time interval the averaged motion of the satellite under consideration coincides with the motion of a satellite having a constant magnetic moment. Fundamental properties of the motion of the kinetic-moment vector of the system are presented for this case. A simple geometrical picture of this motion is constructed. 4 refs.
DESCRIPTORS: (*SATELLITES, *Control),
CARD ALERT: 655

481867 ID NO.- EI741281867
MAGNETIC DAMPING FORCE IN ELECTRODYNAMICALLY SUSPENDED TRAINS.
Iwamoto, M.; Yamada, T.; Ohno, E.
Mitsubishi Electr Corp, Amagasaki, Hyogo, Jpn
IEEE Trans Magn v MAG-10 n 3 Sep 1974 p 458-461 CODEN: IEMGAQ
The development of a magnetic levitation system utilizing superconducting magnets to be used for a high speed ground vehicle is reported. This paper presents the analysis of the magnetic damping force in a loop track magnetic levitation system; the magnetic damping force is caused by track loops. It is theoretically pointed out that the magnetic damping force is $left double quote$ tau $right double quote$ except in an extremely low velocity [illegible]. The theory is applied to the estimation of the magnetic damping force in a train model of practical interest. [illegible] damping has been also investigated; it is found that [illegible] installed in the levitation cryostat is effective [illegible] operation. It is concluded that rather good [illegible] be obtained by use of the passive damping method. [illegible]
DESCRIPTORS: (*VEHICLES, *Magnetic [illegible], SUPERCONDUCTING DEVICES,
CARD ALERT: 432, 704

469412 ID NO.- EI741169412
STOPPING OSCILLATION IN STEP MOTORS.
Kordik, K. S.; Senica, K. M.
Warner Electr Brake and Clutch Co, Beloit, Wis
Mach Des v 46 n 20 Aug 22 1974 p 97 CODEN: MADEAP
Step motors oscillate when driving an inertial load. This characteristic is most noticeable when the motor is coming to a stop after completing a step or slew motion. You can improve the setting time of step motors by damping $EM DASH$ either mechanically, electronically $EM DASH$ or by altering motor design parameters. Mechanical damping can be provided by viscous-inertia dampers, eddy-current dampers, friction brakes, and other devices. Electronic damping is attained by switching the motor phases. Two common forms are back-phasing and delayed-last-step damping. Inherent motor damping can be achieved by altering the motor design parameters or changing drive operating conditions. Motor design parameters such as slot and tooth shapes as well as the addition of windings can provide improved motor settling. While the variation of these design parameters can provide significantly improved damping characteristics, some form of electronic damping is also required to achieve true deadbeat response.
DESCRIPTORS: *ELECTRIC MOTORS, STEPPING TYPE,
CARD ALERT: 705

528907 ID NO.- E1750528907
USES OF MAGNETIC FLUIDS IN BEARINGS, LUBRICATION AND DAMPING.
Ezekiel, F. D.
Servofio Corp, Lexington, Mass
ASME Pap n 75-DE-5 for Meet Apr 21-24 1975, 5 p CODEN: ASMSA4

applications has emerged during the past few years. This paper focuses on advances in three areas: damping, bearings and lubric, tion. 6 refs.
DESCRIPTORS: (*BEARINGS, *Lubrication), (LIQUIDS, Magnetic Properties).
IDENTIFIERS: MAGNETIC FLUIDS, MAGNETIC LIQUID DAMPING
CARD ALERT: 601, 931, 701

429469 ID NO.- E1740529469
EDD' CURRENT NUTATION DAMPERS FOR DUAL-SPIN SATELLITES.
Haines, Gordon A.; Leondes, Cornelius T.
Hughes Aircr Co, Culver City, Calif
J Astronaut Sci v 21 n 1 Jul-Aug 1973 p 1-25 CODEN: JALSA6

Energy dissipation on the platform, which may be required for stability, can be efficiently achieved by passive eddy current nutation damping in which the nutational forcing function acts to impart relative motion between a permanent magnet and a conducting plate. The drag force on the magnet and resulting energy dissipation through eddy current generation in the conductor yield a dissipation rate per unit damper weight substantially greater than that obtainable by more conventional fluid dampers. Usual y, the requirement that damper pinning occur at or near the spacecraft nutation frequency is automatically satisfied, since damper parameters are adjusted to tune its natural frequency to the nutation frequency. This tuning is the mechanism which yields such efficient use of the damper energy dissipation in damping nutational motion. 21 refs.
DESCRIPTORS: (*SATELLITES, *Stability).
CARD ALERT: 655

107428 ID NO.- E171X007428
Periodic motion of an artificial satellite with magnetic damping in a plane circular orbit
SADOV YUA
Cosmic Research (English translation of Kosmicheskie Issledovaniya) v 7 n 1 Jan-Feb 1969 p 45-53 CODEN: CSCRA

Steady motion o1 a circular orbit of an artificial satellite with a gravitational stabilization system using magnetic damping is investigated. Damping is realized by a permanent magnet oriented along the geomagnetic lines of force and in contact with the body of the satellite through linear isotropic friction. Periodic motion of this system is studied under the assumption that the damping coefficient is small. It is shown that there can be no high- amplitude periodic oscillations. However, periodic rotation can occur with a frequency commensurable with the orbital frequency. 4 refs.
DESCRIPTORS: (*SATELLITES, *Stability), SPECE FLIGHT, (SPACE VEHICLES, Stability), (SATELLITES, Orbits and Trajectories).
CARD ALERT: 655, 656

259921 ID NO.- E172X059921
Stability of circulatory elastic systems in the presence of magnetic damping
SMITH TE; HERRMANN G
Northwestern Univ, Evanston, Ill
Acta Mech v 12 n 3-4 1971 p 175 88 CODEN: AMICA

The effect of a type of magnetic damping upon the stability of some circulatory elastic systems is examined. The results are compared with ose obtained for internal and external viscous damping and the differences and similarities are

029541 ID NO.- E170X029541
Semi- active gravity gradient stabilizatpo system
REDISCH WN; SADROFF AE; WHEELER PC; ZAREMP JG
SAE-Paper 690691 for meeting Oct 6-10 1969, 24 p

Semi- active gravity gradient attitude stabilization system (SAGS) providing active pitch control and semi- passive roll-yaw control has been developed and mounted for flight testing in NASA's Packaged Attitude Control (PAC) system; reaction wheel scanner, including bolometer, optics, inertia wheel, motor and housing are mounted on gimbals that also contain eddy curre.t roll- yaw damper, torsional gimbal support mechanism and caging mechanism. PAC test demonstrates that SAGS has good capability for acquisition and steady- state control despite large disturbance torques. 5 refs.
DESCRIPTORS: (*SPACE VEHICLES, *Stabi lity).
CARD ALERT: 655

APPENDIX II

Finite Element Computer Program and Sample Eddy-Current Problem

APPENDIX II

Finite Element Computer Program and Sample Eddy-Current Problem

A computer program, Eddy 2, was used to calculate the total power loss in an eddy-current damper model. The model was divided into triangular elements (see Figure 1) with the power loss from each element summed to find the total power loss.

The total number of triangular elements (N1) must be input along with the total number of nodes, or corners of the triangular elements (N2). The number of zero boundary points (N3) is the number of nodes in which the elements adjacent to that node have a magnetic field intensity (HO) equal to zero. Each triangular element should consist of only one material, although a given type of material may exist in many different elements throughout the model. N4 is the total number of different materials in the model.

It is also necessary to input the nodes, or vertices [IA(I), JA(I), and MA(I)] and the material number [LA(I)] for each of the N1 elements. Using some reference point as the origin, the X and Y coordinates of each of the N2 nodes, or vertices, must also be input. Additionally, for each of the N3 zero boundary points, input the node or vertex number and the magnetic field intensity at that node.

The final data input is for the material properties. For each of the N4 materials, the relative permeability of the material (XIRON), the magnetic field intensity (HO), and the conductivity (SIGMA) must be added

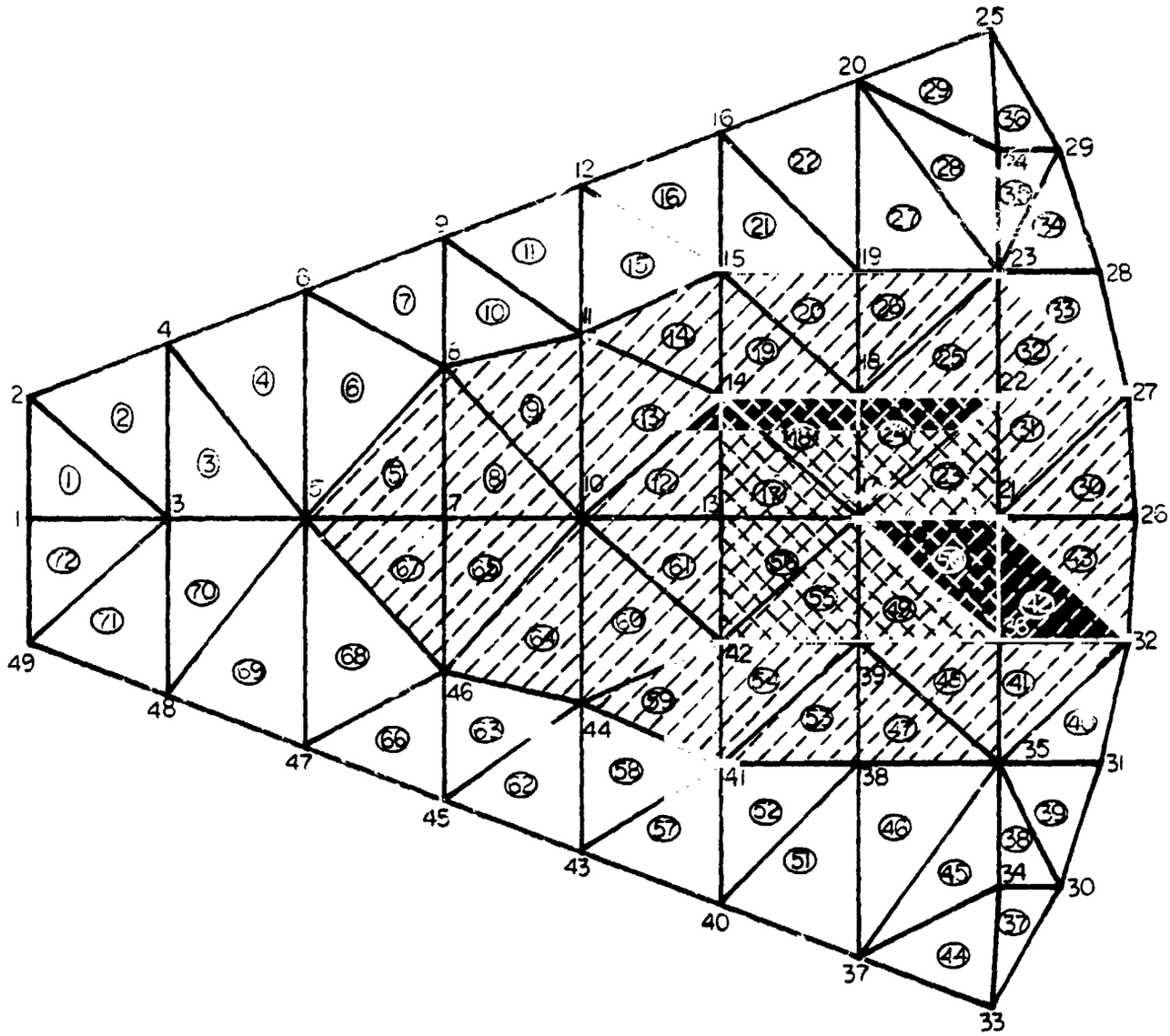

Figure 1. Model of Eddy-Current Damper

to the data input. Note that the magnetic field intensity (HO) is a complex number. For the calculation of the current density (CUR) in the program, the material relative permeability and conductivity has been set to 1.

Additionally, the frequency is read into the program within the program itself, and is currently set equal 60 Hz.

In Figure 1, the model is divided into 72 triangular elements with 49 nodes. Three different sets of material properties are present, with the magnetic field intensity equal to zero in all elements closest to the boundary of the model except elements 30 and 43. Therefore, there are 24 nodes which are not in contact with an element which has a magnetic field intensity greater than zero.

The elements were designated by using the vertices and material type. Using Node 1 as the origin, the normalized X and Y coordinates of each vertex are given using the axis of symmetry as the X-axis. The 24 zero boundary points were all given a magnetic field intensity value of zero. Finally, the material properties are read in using a relative permeability equal to 1.0 and a conductivity equal to 1.0 in all three cases. The magnetic field intensity increases from 0 + 0i in the outer elements, to 6 + 0i in the intermediate elements, and to 10 + 0i in 8 of the central elements. These values are all entered using the MKS system of units.

The listing for the program Eddy 2 along with the printout of the input and output data, which shows the total power loss, is given next.

```
P*
      PROGRAM EDDY(INPUT,OUTPUT,TAPE5=INPUT,TAPE6=OUTPUT)


C                          PROGRAM  EDDY 2
C
C     FIRST ORDER FINITE ELEMENT SOLUTION
C     FOR ELECTROMAGNETIC FIELD PROBLEMS
C     OF X,Y PLANAR GEOMETRIES INCLUDING
C     EDDY CURRENTS IN CONDUCTING PARTS,
C     BUT EXCLUDING THE SOURCE REGION.
C           EVP METHOD
C
C
C     THIS PROGRAM USES ONLY TRIANGULAR FINITE ELEMENTS
C
C     ALL DIMENSIONS AND MATERIAL SPECS
C     ARE IN RATIONALIZED M.K.S. UNITS
C
      COMPLEX S,P,T,CUR,HO
      DIMENSION S(100,100),P(100),T(100),CUR(100),HO(100),DELTAM(100)
      COMPLEX SII,SIJ,SIM,SJJ,SJM,SMM,TT,TI,TJ,TM,FACTOR
      DIMENSION IA(200),JA(200),MA(200),LA(200),XNU(200),PE(100)
      DIMENSION X(100),Y(100),IX(50),XIRON(10),SIGMA(10)
      CHARACTER*80 HEAD1,HEAD2
       POWER=0.0
       AI=BB=BXX=BYY=0.0
C       INITIALIZE ARRAYS
      DO 990 I=1,100
      DO 998 J=1,100
        S(I,J)=(0.0,0.0)
  998 CONTINUE
  990 CONTINUE
      DO 997 I=1,100
       P(I)=(0.0,0.0)
       T(I)=(0.0,0.0)
       CUR(I)=(0.0,0.0)
  997 CONTINUE
      DO 996 I=1 , 200
       IA(I)=0
       JA(I)=0
       MA(I)=0
       LA(I)=0
       XNU(I)=0.0
  996 CONTINUE
      DO 995 I=1 , 100
       X(I)=0.0
       PE(I)=0.0
       DELTAM(I)=0.0
       HO(I)=(0.0,0.0)
         Y(I)=0.0
  995 CONTINUE
      DO 994 I=1,50
       IX(I)=0
  594 CONTINUE
      DO 993 I=1,10
       XIRON(I)=0.0
       SIGMA(I)=0.0
  993 CONTINUE
C
      NOPT=0
C     READ MODEL CONTROL DATA
C
C     IB IS THE FILE LINE NO.
C     N1=TOTAL NO. OF ELEMENTS
```

ORIGINAL PAGE IS
OF POOR QUALITY

```
C      N2=TOTAL NO. OF NODES
C      N3=NO. OF ZERO BOUNDARY PTS.
C      N4=NO. OF MATERIALS
       READ(5,778)HEAD1
       READ(5,778)HEAD2
  778 FORMAT(A80)
C
       READ(5,*)IB,N1,N2,N3,N4
C
C      ELEMENT CONNECTIVITY
C      AND MATERIAL ID NO.
C
C           IA,JA,MA=VERTICES OF TRIANGULAR ELEMENTS
C           LA=MATERIAL ID NUMBER
       DO 12 I=1,N1
   12 READ(5,*)IB,IA(I),JA(I),MA(I),LA(I)
C
C      READ NODE POINTS
C
C            X,Y=COORDINATES OF VERTEX
       DO 13 I=1,N2
   13 READ(5,*)IB,X(I),Y(I)
C
C      BOUNDARY PTS. & BOUNDARY POTENTIALS
C       IX=NODAL NUMBER OF ZERO BOUNDARY POINTS
C
       DO 14 I=1,N3
       READ (5,*)IB,IX(I),TEMP
   14 P(IX(I))=CMPLX(TEMP,0.)
C
C      READ MATERIAL PROPERTIES
C      XIRON=RELATIVE PERMEABILITY
C      HO=MAGNETIC FIELD INTENSITY
C      CUR=CURRENT DENSITY
C      SIGMA=CONDUCTIVITY
C      FREQ=FREQUENCY OF EXCITATION IN HZ
C      OMEGA=ANGULAR FREQUENCY
C
       XMUO=4.*3.14159*(1.0E-7)
       FREQ=60.
       OMEGA=2.*3.14159*FREQ
C
C
       DO 120 I=1,N4
       READ(5,*)IB,XIRON(I),HO(I),SIGMA(I)
        CUR(I)=-CMPLX(0,1)*OMEGA*SIGMA(I)*HO(I)
       IF(XIRON(I).EQ.0)XIRON(I)=1.
       IF(SIGMA(I).EQ.0)SIGMA(I)=1.0E-6
  120 XIRON(I)=1./(XIRON(I)*XMUO)
C
       WRITE(6,778)HEAD1
       WRITE(6,778)HEAD2
       WRITE(6,201)
  201 FORMAT(1H ,//,1X," EDDY$1",/,1X,"ELECTROMAGNETIC FIELD SOLUTION",
     1/,1X," OF X,Y PLANAR GEOMETRIES",/,1X," BY THE FINITE ELEMENT
     2METHOD")
       WRITE(6,102)N1
  102 FORMAT(1H ,2X," TOTAL NO. OF ELEMENTS    =",I4)
       WRITE(6,103)N2
  103 FORMAT(1H ,2X," TOTAL NO. OF NODES       =",I4)
       WRITE(6,104)N3
  104 FORMAT(1H ,2X," NO. OF ZERO BOUNDARY PTS =",I4)
       WRITE(6,105)N4
  105 FORMAT(1H ,2X," NO. OF MATERIALS         =",I4,
     1//,"***********************************************")
       WRITE(6,999)
```

ORIGINAL PAGE IS
OF POOR QUALITY

```
  999 FORMAT(1H ,/////////,"MATERIAL PERMEABILITY,CONDUCTIVITY & SOURCE
     1  CURRENT DENSITY",//)
      DO 1200 I=1,N4
      IB=I
      WRITE(6,1201)IB,XIRON(I),SIGMA(I),CUR(I)
 1201 FORMAT(I5,4E15.4,//)
 1200 CONTINUE
C
C     CONSTRUCT MATRIX
C
      DO 5 I=1,N1
      XNU(I)=XIRON(LA(I))
C
C     FIND GEOMETRIC COEFFICIENTS
C
      BI=Y(JA(I))-Y(MA(I))
      BJ=Y(MA(I))-Y(IA(I))
      BM=Y(IA(I))-Y(JA(I))
      CI=X(MA(I))-X(JA(I))
      CJ=X(IA(I))-X(MA(I))
      CM=X(JA(I))-X(IA(I))
C
      D1=X(JA(I))*Y(MA(I))
      D2=X(MA(I))*Y(JA(I))
      D3=X(IA(I))*BI
      D4=Y(IA(I))*CI
C
C     COMPUTE AREA OF TRIANGLE
C
      DELTA=ABS((D1-D2+D3+D4)/2.)
      DELTAM(I)=DELTA
      FACTOR=CMPLX(0.,1.)*OMEGA*SIGMA(LA(I))*DELTA/12.
C
C     COMPUTE MATRIX ELEMENTS
C
      BB=(BI*BI+CI*CI)/(4.*DELTA)
      BC=(BI*BJ+CI*CJ)/(4.*DELTA)
      BD=(BI*BM+CI*CM)/(4.*DELTA)
      CC=(BJ*BJ+CJ*CJ)/(4.*DELTA)
      CD=(BJ*BM+CJ*CM)/(4.*DELTA)
      DD=(BM*BM+CM*CM)/(4.*DELTA)
C
      SII=2.*FACTOR+BB*XNU(I)
      SIJ=FACTOR+BC*XNU(I)
      SIM=FACTOR+BD*XNU(I)
      SJJ=2.*FACTOR+CC*XNU(I)
      SJM=FACTOR+CD*XNU(I)
      SMM=2.*FACTOR+DD*XNU(I)
C
C     ASSEMBLE MATRIX ELEMENTS
C
      S(IA(I),IA(I))=S(IA(I),IA(I))+SII
      S(IA(I),JA(I))=S(IA(I),JA(I))+SIJ
      S(IA(I),MA(I))=S(IA(I),MA(I))+SIM
      S(JA(I),JA(I))=S(JA(I),JA(I))+SJJ
      S(JA(I),MA(I))=S(JA(I),MA(I))+SJM
      S(MA(I),MA(I))=S(MA(I),MA(I))+SMM
C
      S(JA(I),IA(I))=S(IA(I),JA(I))
      S(MA(I),IA(I))=S(IA(I),MA(I))
      S(MA(I),JA(I))=S(JA(I),MA(I))
C
C     COMPUTE FORCING FUNCTION FOR CURRENT REGION
C
      TT=CUR(LA(I))*DELTA/3.
C
```

ORIGINAL PAGE IS
OF POOR QUALITY

```
C     ASSEMBLE FORCING FUNCTION FOR CURRENT REGION
C
      TI=TT
      TJ=TT
      TM=TT
      T(IA(I))=T(IA(I))+TT
      T(JA(I))=T(JA(I))+TT
      T(MA(I))=T(MA(I))+TT
C
C     PRINT ALL DATA
C
      IF(NOPT.EQ.0)GO TO 5
      WRITE(6,777)I
  777 FORMAT(1H ,/,"ELEMENT NUMBER: ",I2)
      WRITE(6,1000)BI,BJ,BM,CI,CJ,CM
 1000 FORMAT(1H ,//,1X," GEOMETRIC COEFFICIENTS",/,5X,"BI",10X,
     1"BJ",10X,"BM",10X,"CI",10X,"CJ",10X,"CM",/,6E12.4)
      WRITE(6,1001)DELTA
 1001 FORMAT(1H ,//,1X," AREA OF TRIANGLE=",E12.5)
      WRITE(6,1002)BB,BC,BD,CC,CD,DD
 1002 FORMAT(1H ,//,1X," MATRIX ELEMENTS",/,5X,"BB",10X,"BC",10X,"BD",
     110X,"CC",10X,"CD",10X,"DD",/,6E12.4)
      WRITE(6,1003)
 1003 FORMAT(1H ,//,1X," INDIVIDUAL ELEMENT MATRIX")
      WRITE(6,1004)SII,SIJ,SIM
      WRITE(6,1004)SIJ,SJJ,SJM
      WRITE(6,1004)SIM,SJM,SMM
 1004 FORMAT(1X,6E12.4)
      WRITE(6,1005)
 1005 FORMAT(1H ,//,1X," FORCING FUNCTION")
      WRITE(6,1008)TI,TJ,TM
 1008 FORMAT(1X,6F15.4)
      WRITE(6,1006)
 1006 FORMAT(//////)
C
    5 CONTINUE
C
      WRITE(6,1019)
 1019 FORMAT(1H ,//,1X," FULL FORCING FUNCTION")
      DO 1016 K=1,N2
 1016 WRITE(6,3007)K,T(K)
 3007 FORMAT(I5,E12.4,E12.4)
 1050 CONTINUE
C
C     ASSEMBLE FORCING FUNCTION TO INCLUDE
C     APPLIED POTENTIALS - IF ANY
C
      DO 151 IC=1,N3
      DO 151 J=1,N2
  151 T(J)=T(J)-(S(J,IX(IC))*P(IX(IC)))
C
C     MODIFY FORCING FUNCTION ACCORDING TO
C     BOUNDARY CONDITIONS
C
      DO 2000 IC=1,N3
      DO 2000 I=1,N2
      IF(I-IX(IC))2000,2003,2000
 2003 T(I)=P(IX(IC))
C
C     MODIFY [S] MATRIX ACCORDING TO
C     BOUNDARY CONDITIONS
C
      DO 2002 J=1,N2
      S(J,I)=0.
      IF(J.EQ.I)S(I,J)=1.
      S(I,J)=S(J,I)
```

```
 2002 CONTINUE
C
C     SET FORCING FUNCTION ROW =
C     APPLIED POTENTIAL - IF ANY
C
      IF(I.EQ.IX(IC))T(I)=P(IX(IC))
 2000 CONTINUE
C
C     MORE PRINT
C
      WRITE(6,1011)
 1011 FORMAT(1H ,1X," MODIFIED FORCING FUNCTION")
      DO 1012 K=1,N2
 1012 WRITE(6,3007)K,T(K)
C
 1009 CONTINUE
C
      CALL SOLVE(P,T,S,N2)
C
C     WRITE POTENTIALS
C
      WRITE(6,111)
  111 FORMAT(1H ,1X,"ELEMENT #",12X,"COMPLEX FLUX VECTORS",
     + /,2X,78("*"))
      DO 16 I=1,N2
   16   WRITE(6,17) I,P(I)
   17 FORMAT(1H ,5X,I2,9X,"(",E15.6,",",E15.6,")")
C
C     EVALUATE VECTOR POTENTIALS
C
      WRITE(6,1020)
 1020 FORMAT(1H ,17X,"VECTOR POTENTIALS")

 1021 FORMAT(1H ,6X,"BXX",13X,"BYY",13X,"BBB")
      WRITE(6,1022)
 1022 FORMAT(1H ,"**********************************************************
     +*****************")
      WRITE(6,222)
  222 FORMAT(1H ,1X,"ELEMENT #",7X,"JXM",12X,"JYM",12X,"JM",
     +8X,"LOCAL POWER")
C
      DO 8001 I=1,N1
       AI=(X(JA(I))*Y(MA(I))-X(MA(I))*Y(JA(I)))
      BI=(Y(JA(I))-Y(MA(I)))
      CI=(X(MA(I))-X(JA(I)))
      CJ=X(IA(I))-X(MA(I))
      CM=X(JA(I))-X(IA(I))
      BJ=Y(MA(I))-Y(IA(I))
      BM=Y(IA(I))-Y(JA(I))
C
      BYY=REAL(BI*P(IA(I))+BJ*P(JA(I))+BM*P(MA(I)))
      BYY=-BYY/(2.*DELTAM(I))
      BXX=REAL(CI*P(IA(I))+CJ*P(JA(I))+CM*P(MA(I)))
      BXX=BXX/(2.*DELTAM(I))
      BB=(BXX**2+BYY**2)
      PE(I)=BB*DELTAM(I)/SIGMA(LA(I))
      WRITE(6,333)I,BXX,BYY,BB,PE(I)
  333 FORMAT(1H ,4X,I2,4X,4(E15.6))
      POWER=POWER+PE(I)
 8001 CONTINUE
      WRITE(6,888)POWER
  888 FORMAT(1H ,/,49X,29("-"),/,47X,"  TOTAL POWER = ",E15.6)
C
      STOP
      END
C     ------------------------------------------------------------------
```

ORIGINAL PAGE IS
OF POOR QUALITY

```
C
      SUBROUTINE SOLVE(P,T,S,N2)
C
C     SOLVE SIMULTANEOUS EQUATIONS
C     BY GAUSSIAN ELIMINATION METHOD
C
      COMPLEX P,T,S
      DIMENSION P(100),T(100),S(100,100)
      COMPLEX FF,FFX
      FF=(0.0,0.0)
      FFX=(0.0,0.0)
      K=0
      KX=0
C
      DO 111 I=1,N2
      P(I)=T(I)
  111 CONTINUE
C
      M=2
      NN=N2-1
C
      DO 1 I=1,NN
C
      DO 2 J=M,N2
      FF=-S(J,I)/S(I,I)
      P(J)=P(J)+FF*P(I)
C
      DO 3 K=M,N2
    3 S(J,K)=S(J,K)+FF*S(I,K)
C
    2 CONTINUE
    1 M=M+1
C
      P(N2)=P(N2)/S(N2,N2)
      M=N2-1
C
      DO 100 I=2,N2
      J=N2-I+1
      FFX=P(J)
      NN=N2-1
C
      DO 200 K=M,NN
      KX=K+1
  200 FFX=FFX-S(J,KX)*P(KX)
C
      M=M-1
  100 P(J)=FFX/S(J,J)
C
      RETURN
      END
END OF FILE
```

INPUT

2 POLE COBALT - RARE EARTH MAGNET

APPROX. 1 IN. DIA. x .375 IN. HIGH, ASSUME 0.25 IN. GAP; CU DISC 0.20 IN. THICK

0	72	49	24	3
1	2	3	1	1
2	2	4	3	1
3	4	5	3	1
4	4	6	5	1
5	5	8	7	2
6	6	8	5	1
7	6	9	8	1
8	8	10	7	2
9	8	11	10	2
10	9	11	8	1
11	9	12	11	1
12	10	14	13	2
13	11	14	10	2
14	11	15	14	2
15	12	15	11	1
16	12	16	15	1
17	14	17	13	3
18	14	18	17	3
19	15	18	14	2
20	15	19	18	2
21	16	19	15	1
22	16	20	19	1
23	17	22	21	3
24	18	22	17	3
25	18	23	22	3
26	19	23	18	2
27	20	23	19	1
28	20	24	23	1
29	20	25	24	1
30	21	27	26	2
31	22	27	21	2
32	23	27	22	2
33	23	28	27	1
34	23	29	28	1
35	24	29	23	1
36	25	29	24	1
37	34	30	33	1
38	35	30	34	1
39	35	31	30	1
40	35	32	31	1
41	36	32	35	2
42	21	32	36	2
43	21	26	32	2
44	37	34	33	1
45	37	35	34	1
46	38	35	37	1
47	39	35	38	2
48	39	36	35	2
49	17	36	39	3
50	17	21	36	3
51	40	38	37	1
52	41	38	40	1
53	41	39	38	2
54	42	39	41	2
55	42	17	39	3
56	13	17	42	3
57	43	41	40	1

58	44	41	43	1
59	44	42	41	2
60	10	42	44	2
61	10	13	42	2
62	45	44	43	1
63	46	44	45	1
64	46	10	44	2
65	7	10	46	2
66	47	46	45	1
67	5	7	46	2
68	5	46	47	1
69	48	5	47	1
70	3	5	48	1
71	49	3	49	1
72	1	3	49	1

1	0.0	0.0
2	0.0	1.0
3	1.0	0.0
4	1.0	1.42
5	2.0	0.0
6	2.0	1.85
7	3.0	0.0
8	3.0	1.24
9	3.0	2.28
10	4.0	0.0
11	4.0	1.5
12	4.0	2.7
13	5.0	0.0
14	5.0	1.0
15	5.0	2.0
16	5.0	3.13
17	6.0	0.0
18	6.0	1.0
19	6.0	2.0
20	6.0	3.57
21	7.0	0.0
22	7.0	1.0
23	7.0	2.0
24	7.0	3.0
25	6.95	3.98
26	8.0	0.0
27	7.95	1.0
28	7.75	2.0
29	7.45	3.0
30	7.45	-3.0
31	7.75	-2.0
32	7.95	-1.0
33	6.95	-3.98
34	7.0	-3.0
35	7.0	-2.0
36	7.0	-1.0
37	6.0	-3.57
38	6.0	-2.0
39	6.0	-1.0
40	5.0	-3.13
41	5.0	-2.0
42	5.0	-1.0
43	4.0	-2.7
44	4.0	-1.5
45	3.0	-2.28
46	3.0	-1.24
47	2.0	-1.85
48	1.0	-1.42
49	0.0	-1.0

1	1	0.0
2	2	0.0

ORIGINAL PAGE IS
OF POOR QUALITY

```
3   3   0.0
4   4   0.0
5   6   0.0
6   9   0.0
7   12   0.0
8   15   0.0
9   20   0.0
10   24   0.0
11   25   0.0
12   28   0.0
13   29   0.0
14   30   0.0
15   31   0.0
16   33   0.0
17   34   0.0
18   37   0.0
19   40   0.0
20   43   0.0
21   45   0.0
22   47   0.0
23   48   0.0
24   49   0.0
1   1.0   (0.0,0.0)   1.0
2   1.0   (0.0,0.0)   1.0
3   1.0   (10.0,0.0)   1.0
END OF FILE
```

OUTPUT

2 POLE COBALT - RARE EARTH MAGNET

APPROX. 1 IN. DIA. x .375 IN. HIGH, ASSUME 0.25 IN. GAP; CU DISC 0.20 IN. THICK

```
 EDDY$2
ELECTROMAGNETIC FIELD SOLUTION
 OF X,Y PLANAR GEOMETRIES
 BY THE FINITE ELEMENT      METHOD
   TOTAL NO. OF ELEMENTS     =  72
   TOTAL NO. OF NODES        =  49
   NO. OF ZERO BOUNDARY PTS  =  24
   NO. OF MATERIALS          =   3
```

****

MATERIAL	PERMEABILITY	CONDUCTIVITY	SOURCE	CURRENT DENSITY
1	.7958E+06	.1000E+01	0.	0.
2	.7958E+06	.1000E+01	0.	.2262E+04
3	.7958E+06	.1000E+01	0.	-.3770E+04

FULL FORCING FUNCTION

1	0.	0.
2	0.	0.
3	0.	0.
4	0.	0.
5	0.	-.9049E+03
6	0.	0.
7	0.	-.1870E+04
8	0.	-.1500E+04
9	0.	0.
10	0.	-.3951E+04
11	0.	-.1508E+04
12	0.	0.
13	0.	-.2011E+04
14	0.	-.2953E+04
15	0.	-.1131E+04
16	0.	0.
17	0.	-.5027E+04
18	0.	-.2765E+04
19	0.	-.7540E+03
20	0.	0.
21	0.	-.2727E+04
22	0.	-.2350E+04
23	0.	-.1112E+04
24	0.	0.
25	0.	0.
26	0.	-.7540E+03
27	0.	-.1093E+04

```
28  0.          0.
29  0.          0.
30  0.          0.
31  0.          0.
32  0.          -.1093E+04
33  0.          0.
34  0.          0.
35  0.          -.1112E+04
36  0.          -.2350E+04
37  0.          0.
38  0.          -.7540E+03
39  0.          -.2765E+04
40  0.          0.
41  0.          -.1131E+04
42  0.          -.2953E+04
43  0.          0.
44  0.          -.1508E+04
45  0.          0.
46  0.          -.1500E+04
47  0.          0.
48  0.          0.
49  0.          0.
MODIFIED FORCING FUNCTION
 1  0.          0.
 2  0.          0.
 3  0.          0.
 4  0.          0.
 5  0.          -.9349E+03
 6  0.          0.
 7  0.          -.1870E+04
 8  0.          -.1500E+04
 9  0.          0.
10  0.          -.3951E+04
11  0.          -.1508E+04
12  0.          0.
13  0.          -.2011E+04
14  0.          -.2953E+04
15  0.          -.1131E+04
16  0.          0.
17  0.          -.5027E+04
18  0.          -.2765E+04
19  0.          -.7540E+03
20  0.          0.
21  0.          -.2727E+04
22  0.          -.2350E+04
23  0.          -.1112E+04
24  0.          0.
25  0.          0.
26  0.          -.7540E+03
27  0.          -.1093E+04
28  0.          0.
29  0.          0.
30  0.          0.
31  0.          0.
32  0.          -.1093E+04
33  0.          0.
34  0.          0.
35  0.          -.1112E+04
36  0.          -.2350E+04
37  0.          0.
38  0.          -.7540E+03
39  0.          -.2765E+04
40  0.          0.
41  0.          -.1131E+04
42  0.          -.2953E+04
43  0.          0.
```

44	0.	-.1508E+04
45	0.	0.
46	0.	-.1500E+04
47	0.	0.
48	0.	0.
49	0.	0.

ELEMENT #	COMPLEX FLUX VECTORS	
2	(0.	, 0.)
3	(0.	, 0.)
4	(0.	, 0.)
5	(-.238695E-05	, -.218690E-02)
6	(0.	, 0.)
7	(-.479827E-05	, -.467106E-02)
8	(-.327412E-05	, -.307018E-02)
9	(0.	, 0.)
10	(-.783586E-05	, -.734258E-02)
11	(-.491638E-05	, -.442330E-02)
12	(0.	, 0.)
13	(-.959220E-05	, -.891762E-02)
14	(-.834467E-05	, -.769361E-02)
15	(-.470924E-05	, -.411365E-02)
16	(0.	, 0.)
17	(-.111269E-04	, -.104141E-01)
18	(-.916324E-05	, -.843161E-02)
19	(-.505058E-05	, -.436332E-02)
20	(0.	, 0.)
21	(-.106830E-04	, -.955886E-02)
22	(-.865691E-05	, -.778135E-02)
23	(-.352464E-05	, -.303906E-02)
24	(0.	, 0.)
25	(0.	, 0.)
26	(-.101566E-04	, -.883125E-02)
27	(-.820247E-05	, -.710439E-02)
28	(0.	, 0.)
29	(0.	, 0.)
30	(0.	, 0.)
31	(0.	, 0.)
32	(-.820247E-05	, -.710439E-02)
33	(0.	, 0.)
34	(0.	, 0.)
35	(-.352464E-05	, -.303906E-02)
36	(-.865691E-05	, -.778135E-02)
37	(0.	, 0.)
38	(-.505058E-05	, -.436332E-02)
39	(-.916324E-05	, -.843161E-02)
40	(0.	, 0.)
41	(-.470924E-05	, -.411365E-02)
42	(-.834467E-05	, -.769361E-02)
43	(0.	, 0.)
44	(-.491638E-05	, -.442330E-02)
45	(0.	, 0.)
46	(-.327412E-05	, -.307018E-02)
47	(0.	, 0.)
48	(0.	, 0.)
49	(0.	, 0.)

VECTOR POTENTIALS

ELEMENT #	JXM	JYM	JM	LOCAL POWER
1	0.	0.	0.	0.
2	0.	0.	0.	0.
3	0.	-.238695E-05	.569753E-11	.404525E-11
4	-.129024E-05	-.554805E-06	.197254E-11	.182460E-11
5	-.122916E-05	-.241132E-05	.732529E-11	.454168E-11
6	-.129024E-05	-.248707E-05	.785024E-11	.726147E-11
7	-.314819E-05	-.135372E-05	.117437E-10	.61[illegible]671E-11

8	-.122916E-05	-.303759E-05	.107378E-10	.665741E-11
9	-.194632E-05	-.214830E-05	.840337E-11	.630252E-11
10	-.314819E-05	-.246079E-05	.159666E-10	.830263E-11
11	-.409698E-05	-.172073E-05	.197462E-10	.118477E-10
12	-.124753E-05	-.175634E-05	.464107E-11	.232053E-11
13	-.194632E-05	-.245513E-05	.981583E-11	.736187E-11
14	-.363543E-05	-.161058E-05	.158103E-10	.790516E-11
15	-.409698E-05	-.184135E-05	.201758E-10	.121055E-10
16	-.416747E-05	-.179201E-05	.205791E-10	.116272E-10
17	-.124753E-05	-.153472E-05	.391170E-11	.195585E-11
18	-.196368E-05	-.818573E-06	.452610E-11	.226305E-11
19	-.363543E-05	-.818573E-06	.138864E-10	.694321E-11
20	-.411266E-05	-.341344E-06	.170305E-10	.851525E-11
21	-.416747E-05	-.341344E-06	.174843E-10	.987863E-11
22	-.321693E-05	-.141545E-05	.123521E-10	.969644E-11
23	-.202605E-05	.443961E-06	.430197E-11	.215099E-11
24	-.196368E-05	.506330E-06	.411241E-11	.205620E-11
25	-.513228E-05	.506330E-06	.265966E-10	.132983E-10
26	-.411266E-05	.152595E-05	.192425E-10	.962125E-11
27	-.321693E-05	.152595E-05	.126772E-10	.995157E-11
28	-.352464E-05	.200904E-05	.164593E-10	.822966E-11
29	0.	0.	0.	0.
30	-.198048E-05	.526331E-06	.419932E-11	.209966E-11
31	-.202605E-05	.478364E-06	.433770E-11	.205851E-11
32	-.513228E-05	.478364E-06	.265691E-10	.126203E-10
33	-.914237E-05	.469952E-05	.105668E-09	.396256E-10
34	-.140985E-05	.469952E-05	.240731E-10	.902743E-11
35	-.352464E-05	0.	.124231E-10	.279519E-11
36	0.	0.	0.	0.
37	0.	0.	0.	0.
38	.352464E-05	0.	.124231E-10	.279519E-11
39	.140985E-05	.469952E-05	.240731E-10	.902743E-11
40	.914237E-05	.469952E-05	.105668E-09	.396256E-10
41	.513228E-05	.478364E-06	.265691E-10	.126203E-10
42	.202605E-05	.478364E-06	.433370E-11	.205851E-11
43	.198048E-05	.526331E-06	.419932E-11	.209966E-11
44	0.	0.	0.	0.
45	.352464E-05	.200904E-05	.164593E-10	.822966E-11
46	.321693E-05	.152595E-05	.126772E-10	.995157E-11
47	.411266E-05	.152595E-05	.192425E-10	.962125E-11
48	.513228E-05	.506330E-06	.265966E-10	.132983E-10
49	.196368E-05	.506330E-06	.411241E-11	.205620E-11
50	.202605E-05	.443961E-06	.430197E-11	.215099E-11
51	.321693E-05	-.141545E-05	.123521E-10	.969644E-11
52	.416747E-05	-.341344E-06	.174843E-10	.987863E-11
53	.411266E-05	-.341344E-06	.170305E-10	.851525E-11
54	.363543E-05	-.818573E-06	.138864E-10	.694321E-11
55	.196368E-05	-.818573E-06	.452610E-11	.226305E-11
56	.124753E-05	-.153472E-05	.391170E-11	.195585E-11
57	.416747E-05	-.179201E-05	.205791E-10	.116272E-10
58	.409698E-05	-.184135E-05	.201758E-10	.121055E-10
59	.363543E-05	-.161058E-05	.158103E-10	.790516E-11
60	.194632E-05	-.245513E-05	.981583E-11	.736187E-11
61	.124753E-05	-.175634E-05	.464107E-11	.232053E-11
62	.409698E-05	-.172073E-05	.197462E-10	.118477E-10
63	.314819E-05	-.246079E-05	.159666E-10	.830263E-11
64	.194632E-05	-.214830E-05	.840337E-11	.630252E-11
65	.122916E-05	-.303759E-05	.107378E-10	.665741E-11
66	.314819E-05	-.135372E-05	.117437E-10	.610671E-11
67	.122916E-05	-.241132E-05	.732529E-11	.454168E-11
68	.129024E-05	-.248707E-05	.785024E-11	.726147E-11
69	.129024E-05	-.554805E-06	.197254E-11	.182460E-11
70	0.	-.238695E-05	.569753E-11	.404525E-11
71	0.	0.	0.	0.
72	0.	0.	0.	0.

TOTAL POWER = .501995E-09